

Tailored surface and electrode modifications for analytical and biochemical applications

In a u g u r a l d i s s e r t a t i o n

zur

Erlangung des akademischen Grades eines

Doktors der Naturwissenschaften (Dr. rer. nat.)

der

Mathematisch-Naturwissenschaftlichen Fakultät

der

Ernst-Moritz-Arndt-Universität Greifswald

vorgelegt von

Katja Vahl

geboren am 02.02.1983

in Greifswald

Greifswald, 27.05.2013

Dekan: Prof. Dr. rer. nat. Klaus Fesser

1. Gutachter: Prof. Dr. rer. nat. Fritz Scholz

2. Gutachter: PD Dr. rer. nat. Gerd-Uwe Flechsig

Tag der Promotion: 28.08.2013

Table of contents

I	Motivation	1
II	Flow-Injection-Analysis with a pH sensitive graphite/quinhydrone composite electrode	3
1	Introduction	3
2	Theoretical background	5
2.1	Flow-Injection-Analysis (FIA)	5
2.1.1	The concept of FIA	5
2.1.2	FIA titration	7
2.1.3	Detection systems in FIA	8
2.1.3.1	Potentiometry	9
2.1.3.2	The quinhydrone electrode	11
2.1.3.3	Potentiometric pH detectors in FIA systems	14
2.2	Applications of FIA measurements	16
2.2.1	Water hardness	16
2.2.1.1	Definition of water hardness	16
2.2.1.2	Methods for the determination of water hardness	18
2.2.2	Wine	19
2.2.2.1	pH and acidity of wine	19
2.2.2.2	Methods for the determination of titratable acidity of wine	20
3	Experimental	22
3.1	Chemicals	22
3.1.1	Preparation of the pH sensitive layer of the detector cell and preparation of the salt bridge	22
3.1.2	Simple FIA acid-base titrations	22
3.1.3	FIA acid-base titrations in buffered solutions	23
3.1.4	Determination of water hardness	23
3.1.5	Determination of titratable acidity and pH of wine	23
3.2	Instrumentation of the FIA system	24
3.2.1	The detection system	24
3.2.2	FIA configuration	25
3.3	Measurement performance	26
3.3.1	Simple FIA acid-base titrations	26

3.3.2	FIA acid-base titrations in buffered solutions	26
3.3.3	Determination of water hardness	27
3.3.3.1	FIA titration	27
3.3.3.2	Batch titration	27
3.3.4	Determination of titratable acidity and pH of wine	28
3.3.4.1	FIA measurements	28
3.3.4.1.1	Determination of the titratable acidity	28
3.3.4.1.2	pH measurements	28
3.3.4.2	Batch measurements	29
4	Results and discussion	30
4.1	Simple acid-base titrations	30
4.2	FIA acid-base titrations in buffered solutions	33
4.3	Determination of the calcium and magnesium content in aqueous solutions	39
4.3.1	Basic studies concerning the carrier solution	39
4.3.2	Calibration curves	44
4.3.3	pH sensitivity	47
4.3.4	Determination of the detection limit, the dynamic working range and the precision	48
4.3.5	Measuring of sample solutions	50
4.4	Determination of titratable acidity and pH of wine	51
4.4.1	Titratable acidity of wine	51
4.4.1.1	Batch titration	51
4.4.1.2	FIA titration	53
4.4.1.2.1	Matrix simulation of wine	53
4.4.1.2.2	Calibration curves	55
4.4.1.2.3	Measuring of wine samples	56
4.4.1.2.4	Determination of the repeatability	59
4.4.2	pH measurements	59
5	Conclusions	62
III	Modification of gold surfaces for medical applications	64
1	Introduction	64
2	Theoretical background	66
2.1	Free radicals	66
2.2	Oxygen and its derivatives	67

2.3	Reactive oxygen species (ROS)	69
2.3.1	Sources of ROS	69
2.3.1.1	Mitochondrial electron transport chain	70
2.3.1.2	Immune system	70
2.3.1.3	Fenton and Haber–Weiss reaction	71
2.4	Methods to generate oxygen radicals	72
2.5	Impact of $\cdot\text{OH}$ radicals on electrode surfaces, especially on gold surfaces	73
2.6	Circulating tumour cells (CTCs)	74
2.6.1	Methods to detect and analyse circulating tumour cells	76
2.6.1.1	<i>In vivo</i> method based on a functionalized and structured medical wire	77
2.7	Basic principles of the used analytical methods	79
2.7.1	Atomic Force Microscopy (AFM)	79
2.7.2	Inductively Coupled Plasma Atomic Emission Spectroscopy (ICP-AES)	81
2.7.3	Tests for <i>in vitro</i> cytotoxicity of medical products	82
3	Experimental	83
3.1	Chemicals	83
3.2	The impact of $\cdot\text{OH}$ radicals on gold implants	83
3.2.1	Gold preparation	83
3.2.2	Implantation of the gold pieces	84
3.2.3	AFM measurements	84
3.3	Diminishing of the cytotoxicity of the FSMW by treatment with $\cdot\text{OH}$ radicals	84
3.3.1	Wires	84
3.3.2	Washing of the wires	85
3.3.3	Treatment of the gold layer of the wires with $\cdot\text{OH}$ radicals	85
3.3.3.1	Fenton solutions	85
3.3.3.2	UV-photolysis of H_2O_2	86
3.3.4	Electrochemical reduction of the treated gold layer	87
3.3.5	ICP-AES	88
3.3.6	Gamma sterilization	88
3.3.7	Cytotoxicity test	88
3.3.8	AFM measurements	89

4	Results and Discussion	90
4.1	The impact of $\cdot\text{OH}$ radicals on gold implants	90
4.1.1	Variation of the residence time of gold implants in wild type mice and the influence of Lipopolysaccharide (LPS)	90
4.1.2	Implantation of mechanically polished gold and “Fenton-polished” gold plates into wild type mice and knock-out mice	91
4.1.3	Investigation of the roughening effect of the gold surface during implantation in knock-out mice	95
4.2	Diminishing of the cytotoxicity of the FSMW by treatment with $\cdot\text{OH}$ radicals	97
4.2.1	The effect of $\cdot\text{OH}$ radicals generated by Fenton solution	97
4.2.1.1	First experimental series	97
4.2.1.1.1	Cytotoxicity test	98
4.2.1.1.2	ICP-AES	101
4.2.1.1.3	AFM measurements	105
4.2.1.2	Second experimental series	107
4.2.1.2.1	Cytotoxicity test	108
4.2.2	The effect of $\cdot\text{OH}$ radicals generated by UV-photolysis of hydrogen peroxide	110
4.2.2.1	Cytotoxicity test	111
4.2.2.2	ICP-AES	114
4.2.2.3	AFM measurements	115
4.2.3	Comparative discussion of the results obtained with both treatment methods	117
5	Conclusions	118
IV	Summary	120
V	List of references	122
VI	List of abbreviations	135

I Motivation

Surface modifications allow altering the chemical, physical and biological properties of surfaces, such as roughness, surface charge, electrical conductivity, reactivity, reflecting capacity and biocompatibility. These properties can be optimized with respect to the requirements for specific applications. Various physical and (electro-) chemical methods can be employed for surface modifications. Among the physical methods, mechanically polishing and treatment with thermal or ionising irradiation play a major role. Surfaces can be modified by chemical methods, e.g., by treatment with certain reagents or by deposition of certain layers, e.g., gold surfaces by deposition of a self-assembled monolayer (SAM). Electrochemical and chemical treatment can also be applied for changing the redox state of surface layers.

In a similar vein, it is also possible to modify *electrode* materials and *electrode* surfaces. For example, Kahlert et al. have developed a solid composite pH sensor made from quinhydrone, paraffin and graphite powder [1]. To improve the reversibility of the electrodes, the surface of the graphite powder has been modified by chemical oxidation of the graphite resulting in the formation of surface-confined quinhydrone-like redox centres [2]. More recently, Kahlert, Pörksen and Scholz have applied this sensor material, using poly(methyl methacrylate) (PMMA) instead of solid paraffin as binder material, to construct a potentiometric pH detector for Flow-Injection-Analysis (FIA) [3, 4]. This detection system based on the graphite/quinhydrone composite electrode and a common reference electrode fulfils the high demands, which have to be met by flow-through detectors, as low noise, high selectivity, large working range and short response time [5]. In previous investigations the detector has been used successfully for simple FIA pH measurements and FIA acid-base titrations [3, 4].

In the first part of this thesis, these flow-through graphite/quinhydrone composite electrodes could be modified aiming at a more facile handling in the FIA system. A further goal of this thesis was the development of new applications of the FIA system with the modified graphite/quinhydrone composite electrode: (i) to determine the acid or base content in buffered solutions, (ii) to determine water hardness and (iii) to analyse wine samples with respect to titratable acidity and pH.

Beside the application of the modified graphite/quinhydrone electrode in FIA systems, this thesis is also focused on the modification of gold surfaces for medical

applications. Several methods already exist to modify gold surfaces, e.g., mechanically polishing, heating or modification with SAMs. Recently, Nowicka et al. have described the possibility to alter gold surfaces by treatment with $\cdot\text{OH}$ radicals generated in Fenton solutions. They have demonstrated that $\cdot\text{OH}$ radicals smooth a gold surface by dissolution of highly reactive gold atoms [6, 7]. Based on these results, in this thesis the impact of $\cdot\text{OH}$ radicals on gold implants was investigated. Since it is known that medical implants release gold into the surrounding tissue [8, 9], the observations of Nowicka et al. are potentially interesting to shine new light on a possible stabilizing of the surface of gold implants by pre-treatment with $\cdot\text{OH}$ radicals. In this respect it was also interesting to study the effect of $\cdot\text{OH}$ radicals formed by immune reactions *in vivo* on the surface of gold implants.

In medicine, gold is not only used as implant material. Recently, another medical application based on gold surfaces has been developed by a German company named GILUPI GmbH. They have introduced an innovative nanodetector for the *in vivo* isolation of circulating tumour cells (CTCs) from the peripheral blood of cancer patients [10]. CTCs are rare species in the blood stream, which are present in cancer patients in a concentration estimated as one CTC per 10^5 to 10^7 mononuclear cells, or even lower [11–13]. Since CTCs are responsible for the formation of metastases, the detection and analysis of CTCs play a crucial role in the diagnosis and treatment of cancer, e.g., it can be applied as prognostic marker, as a tool to monitor therapy response, and as a method to understand basic tumour characteristics [14]. Several *ex vivo* methods and *in vitro* methods to determine CTCs are described in the literature. However, these methods are often limited by the blood volume obtainable from the patients, and the sensitivity of these analysis systems is usually low [10]. Hence, *in vivo* methods, such as the nanodetector developed by GILUPI GmbH, are required, which offer the isolation of CTCs from the blood stream, and thus from a larger blood volume. The nanodetector is based on a stainless steel wire coated with a gold layer, which is functionalized with an antibody directed to the epithelial cell adhesion molecule (EpCAM), which is present on the surface of most CTCs. For the *in vivo* application, sterility of the nanodetector is essential, which has to be achieved by gamma ray treatment. However, it has been shown that gamma irradiation causes a cytotoxicity of the gold layer of the nanodetector preventing *in vivo* applications. Thus, another goal of this thesis was the modification of the gold layer of the nanodetector by treatment with $\cdot\text{OH}$ radicals aiming at a reduction of the cytotoxicity of the gold layer.

II Flow-Injection-Analysis with a pH sensitive graphite/quinhydrone composite electrode

1 Introduction

The determination of acids and bases ranks among the most frequently performed analyses in research and industrial laboratories, because it plays an important role in various areas of science and technology, e.g., in chemistry, pharmacy, biology, geology, and food industry.

Traditionally, the acid or base content of a sample is determined by classical batch titrations. Classical batch titrations are characterized by a simple and low-cost instrumentation and high reproducibility [15]. However, they also require rather large sample and reagent volumes, and, not at least, they are time and labour intensive. Since — especially in process control — high speed determinations are necessary, the classical titrations are less suitable for such applications. To overcome the drawbacks of classical acid-base titrations, several automated and miniaturized titration systems have been developed [16–20]. Apart from automated and miniaturized pipette and burette systems, titrations based on Flow-Injection-Analysis (FIA) [21] are a well suited alternative to determine the acid and base content of samples. Various optical and electrochemical sensors are applied as detectors in FIA titration systems [5, 22]. Electrochemical sensors are particularly suitable for FIA because of their high sensitivity and linearity. Compared to optical detection systems, electrochemical detectors are not affected by the turbidity and colour of the sample solutions and they are much more simple and less expensive [5, 23].

In the research group of Kahlert and Scholz, pH sensitive composite electrodes based on graphite and quinhydrone have been developed and have been successfully applied for FIA titrations [3, 24, 25]. These electrodes proved to have small time constants and sufficient long term stability. Because of the ring-shaped surface of this potentiometric FIA sensor, the electrode is part of the flow-through system and allows a practically completely undisturbed flow of the solution. The dynamic working range of the detector comprises about 4 orders of magnitude for FIA acid-base titrations. In conjunction with the composite electrodes, the FIA system allows simple, rapid and automated acid-base titrations.

The first aim of this thesis was the modification of the pH sensitive layer to allow an easier handling. The major differences to the previously used electrodes were firstly the use of polysiloxane as binder for the pH sensitive layer instead of poly(methyl methacrylate) (PMMA), and secondly the contact to the reference electrode was established via a gel filled tube acting as a salt bridge. The main advantage of polysiloxane as binder is that a thin replaceable layer can be produced which also provides an excellent sealing. The potentiometric response behaviour with polysiloxane as binder is comparable with that of PMMA-based sensors [26]. It is a further advantage that polysiloxane allows punctuating the pH sensitive layer very easily with a cannula, whereas a driller has to be employed for making a hole through a pH sensitive layer containing PMMA as binder.

After fabrication of the modified electrode, the electrode was tested by performing various acid-base titrations under FIA conditions.

Furthermore a variety of possible applications of the FIA system in conjunction with the graphite/quinhydrone/polysiloxane composite electrode could be demonstrated. As a lot of biological reactions, e.g., enzyme reactions, have to be performed in buffered solutions, the FIA system was adapted to acid-base titrations in buffered solutions. Thus, the performance of the determination of the acid content in buffered solutions allows the determination of enzyme activities of lipases [24].

Another possible application is the determination of water hardness. Schwarzenbach et al. have described the determination of different metal ions by using a small excess of the disodium or trisodium salt of ethylenediaminetetraacetic acid (EDTA) and back titration of the released protons [27, 28]. In this thesis, a FIA titration method for the determination of calcium and magnesium ions could be developed based on the same principle, i.e., determining the released protons by detecting the potential change at the pH sensitive detector surface, when the sample zone passes the electrode. The introduced method has been applied to the analysis of tap water, mineral water and river water.

Last but not least, an application to food analysis could be developed for determining sequentially the titratable acidity and the pH of wine. The determination of these parameters is of great importance, because acidity and pH of wine affects the properties and the quality of wine.

2 Theoretical background

2.1 Flow-Injection-Analysis (FIA)

2.1.1 The concept of FIA

The technique of Flow-Injection-Analysis (FIA) has been developed by Fehér, Nagy, Pungor [29] and Růžicka and Hansen [30]. They have introduced an automated method, which is characterized by a simple configuration, a high sampling frequency, small sample volumes and low reagent consumption [21].

The principle of FIA is shown in Figure II-1. A defined liquid sample volume is injected into a laminar, unsegmented liquid stream of a carrier solution. After injection, the sample is transported by the carrier stream through narrow tubes to the detector. During transport, the sample is mixed in a very defined and reproducible way with the carrier, which can contain reagents. The reagents of the carrier react selectively with the analyte forming a detectable reaction product and a peak shaped signal is recorded at the detector [5, 31, 32]. Height, area and width of the peak are related to the concentration of the analyte and can be used for evaluation of the peak [21].

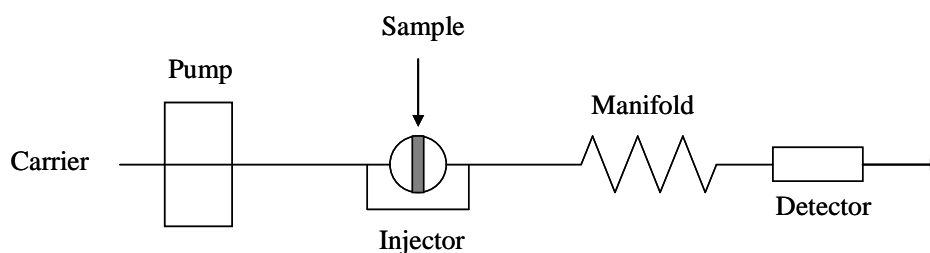


Figure II-1: Scheme of a single line FIA system [32].

Immediately after injection the sample zone is almost rectangular shaped and has still the original concentration c_0 (cf. Figure II-2a). While passing the tubes, the sample solution and the carrier solution are mixed by two phenomena, (i) diffusion and (ii) convection, what results in a dispersion of the primary rectangular sample zone and thus peak shaped signals are recorded at the detector [32, 33]. A concentration gradient is formed, in which no single element of fluid has the same analyte concentration c as its neighbour elements (cf. Figure II-2b) [21].

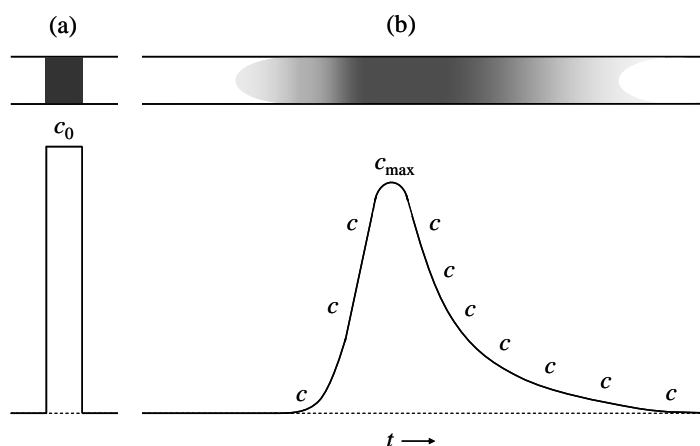


Figure II-2: Concentration–time profiles of the sample zone. **(a)** Rectangular profile of the concentration c_0 before dispersion ($t = 0$). **(b)** Profile with a continuous concentration gradient with maximal concentration c_{\max} caused by dispersion [21, 34].

The degree of dispersion is characterized by the dispersion coefficient D , which is defined as the ratio of the analyte concentration of the injected sample before dispersion (c_0) and the analyte concentration after dispersion has taken place in that element of fluid that yields the analytical readout (c) [35]:

$$D = \frac{c_0}{c}. \quad (\text{II-1})$$

D quantifies the dilution of the sample in the FIA system [36]. The dispersion depends on the distance between injector and detector, on the flow rate and on the sample volume. The higher the flow rate and the longer the distance between injector and detector, the larger is D , whereas an increase of the sample volume decreases D . If sample and carrier are not mixed at all and thus the sample is not diluted, D becomes 1. However, normally a certain dilution of the sample and a reaction between the sample and carrier solution will take place, and is even desired, so that dispersion values higher than 1 are observed. In order to ensure a defined dispersion of the sample zone and thus a controlled reaction between sample and carrier, what permits measurements of high accuracy and reproducibility, flow rate, sample volume, distance between injector and detector and inner diameter of the used tubes have to be adjusted very precisely [5, 32, 33].

In summary, the concept of FIA is based on the following three principles [21, 31]:

- (i) Reproducible injection of well-defined sample volumes into the carrier.

- (ii) Controlled dispersion of the sample zone during transportation from injector to detector.
- (iii) Reproducible timing of the movement of the sample zone from injector to detector.

2.1.2 FIA titration

Titrimetric techniques, which were developed in the late 18th, early 19th century, belong to the oldest methods in the area of quantitative analytical chemistry [15, 37]. During the titration a reagent, which is called titrant (also titrator), is added to the analyte (the titrand) until the latter is quantitatively converted to the reaction product. The point of quantitative conversion of the analyte, which is called equivalence point, is detected by using a colour indicator or a suitable instrumental detector. From the amount of reagent consumed till the equivalence point is reached, the amount of analyte can be calculated by the rules of stoichiometry [38].

Despite new developments in the area of instrumental analysis, titrimetric methods play still an important role in routine analysis, because of the simple, low-cost instrumentation and the high reproducibility [15]. The drawbacks of classical titrations like the large sample and titrant volume and the time demand could be diminished by the development of automated and miniaturized titration systems [16–20]. Furthermore, titrations based on Flow-Injection-Analysis (FIA) were introduced, which allow rapid titrations requiring only small sample volumes and low amounts of reagent.

FIA titration is the oldest approach of gradient techniques in FIA and was described for the first time by Růžicka and Hansen [39]. In principle, a sample, for example, of an acid is injected into a carrier stream of a strong base. Caused by diffusion and convection the sample zone disperses, so that the base of the carrier stream can permeate the sample zone and the neutralisation reaction starts at both sides of the sample zone. If the dispersion coefficient D is higher than one and the concentration of the analyte is larger than the concentration of the titrant, the concentration gradients formed on both sides of the sample zone, which contain a continuum of acid/base ratios, are comparable to conventional titration curves, even though FIA titrations are non-equilibrium titrations. Initially there is an excess of base until the equivalence point is reached. The equivalence point is the volume element of fluid, within which the acid is exactly neutralized by the base. Inside the sample zone, i.e., around and at the peak maximum, an excess of acid exists. At the

tailing zone of the signal the equivalence point is reached for a second time, after which an excess of base is present again. Both equivalence points exhibit the same dispersion coefficient D . The distance between both equivalence points, which is measured as Δt at a constant flow rate, depends on the concentration of the injected acid. If the analyte concentration is smaller than the titrant concentration, instead of equivalence points only inflection points occur on both sides of the peak. In this case the distance of the inflection points is also a function of the analyte concentration [3, 21, 31].

Frequently, mixing chambers are used to mix the sample and the reagent in FIA titrations [21, 31, 39]. Ramsing et al. showed that also simple FIA configurations without a mixing chamber are suitable for FIA titrations, and by this they introduced high-speed titrations based on FIA [31, 40].

2.1.3 Detection systems in FIA

In principle any detection system, which is suitable for flow-through detection, can be coupled to FIA systems. A variety of different detectors are applied in FIA systems: optical detection systems using spectrophotometry (UV/VIS), luminescent detection, refractometry, fluorimetry, atomic spectroscopy (AAS, AES) as well as electrochemical techniques like amperometry, potentiometry, voltammetry, and conductimetry are most commonly used [5, 22].

A number of demands have to be met by detectors employed in FIA: Detectors of low noise characterized by a high selectivity, a large working range and a short response time are required. Furthermore the detector has to be suited for measurements of small sample volumes [5].

Electrochemical detectors are particularly attractive for applications in FIA because of their high sensitivity and good linearity. Contrary to optical detectors, electrochemical detection does not need the addition of supplementary dyes. Further, the instrumentation of an electrochemical detection system is simpler and less expensive [5, 23].

Since in this thesis a FIA system in conjunction with potentiometric pH detection based on a graphite/quinhydrone composite electrode was employed, the following chapter is focused on potentiometric pH detection in FIA systems.

2.1.3.1 Potentiometry

In potentiometry, the cell voltage, i.e., the potential difference between an indicator electrode and a reference electrode in an electrochemical cell is measured (practically) currentless. The potential of the reference electrode is constant, whereas the electrode potential of the indicator electrode is (ideally) directly proportional to the logarithm of the activity of the analyte in the solution [41]. For the reaction



the equilibrium potential of the indicator electrode according to the Nernst equation is as follows:

$$E = E_{\text{Ox/Red}}^{\ominus} + \frac{RT}{zF} \ln \frac{a_{\text{ox}}}{a_{\text{red}}} \quad (\text{II-3})$$

with E : electrode potential

$E_{\text{Ox/Red}}^{\ominus}$: standard potential

R : universal gas constant ($R = 8.314 \text{ J K}^{-1} \text{ mol}^{-1}$)

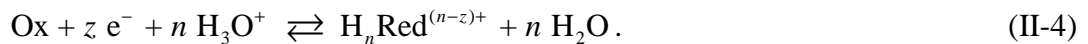
T : absolute temperature

F : Faraday constant ($F = 96485 \text{ C mol}^{-1}$)

z : number of transferred electrons

$a_{\text{Ox}}, a_{\text{Red}}$: chemical activity of the oxidant and reductant.

If hydronium ions are involved in the redox reaction, the potential of the indicator electrode depends not only on the ratio of the activities a_{Ox} and a_{Red} , but also on the pH of the solution:



In that case the equilibrium potential of the indicator electrode can be formulated according to the Nernst equation as:

$$E = E_{\text{Ox/H}_n\text{Red}}^{\ominus(n-z)+} + \frac{RT}{zF} \ln \frac{a_{\text{Ox}}}{a_{\text{H}_n\text{Red}}^{(n-z)+}} + \frac{nRT}{zF} \ln a_{\text{H}_3\text{O}^+}. \quad (\text{II-5})$$

Such redox systems can be used for pH measurements, provided that the ratio a_{Ox} to $a_{\text{H}_n\text{Red}}^{(n-z)+}$ remains constant during the measurement. If this requirement is fulfilled, the potential of the indicator electrode is directly proportional to the pH value of the solution [42].

Potentiometry can be also applied to ion partition equilibria when ions are involved in the establishment of an electrochemical equilibrium [43]. When a membrane, which can accommodate (at least at its surface) the ionic species K, is placed between two electrolyte solutions containing two different activities, a_{K}^{I} and a_{K}^{II} of K, that ionic species K will partition on both sides between the solution and the membrane. Thus, the phase boundary is charged and an electric field is created. When the electrochemical equilibrium is achieved, the electrochemical potentials on both sides of the phase boundary are equal. The potential difference between the two solution phases (across the membrane) is then called a *membrane potential* (also *Donnan potential*) and it follows as:

$$E = \frac{RT}{z_{\text{K}}F} \ln \frac{a_{\text{K}}^{\text{II}}}{a_{\text{K}}^{\text{I}}} \quad [41]. \quad (\text{II-6})$$

The method of potentiometry is very attractive because the equipment is rather simple and inexpensive. Only an indicator electrode and a reference electrode in conjunction with a voltage-measuring instrument with high input impedance are necessary. The potential measurement has to be accomplished almost currentless, because even very low currents would cause a shift of the potential of indicator and reference electrode and thus distort the results. Therefore, today amplifier circuits with input impedance of about $10^{12} \Omega$ are usually applied [41].

A special case of potentiometry is the so-called chronopotentiometry. In chronopotentiometry, the time dependence of the potential of an indicator electrode is measured at a fixed current, which can be also zero. From the potential transient the concentration of an electrochemically oxidizable or reducible analyte can be determined [15].

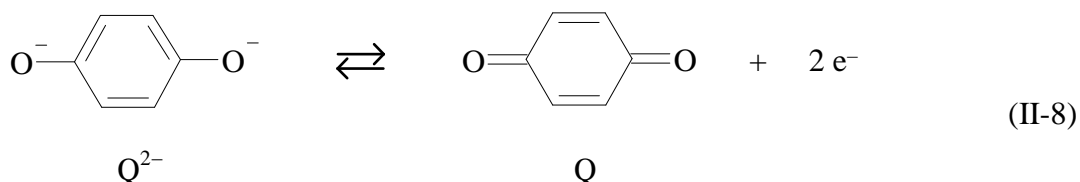
2.1.3.2 The quinhydrone electrode

The quinhydrone electrode as redox electrode for pH measurements was introduced by Biilmann in 1921 [44]. Quinhydrone, which is a charge transfer complex of low solubility consisting of quinone (Q) and hydroquinone (H_2Q) in a 1:1 ratio, is characterized by a pH depended redox potential. The construction of the conventional quinhydrone electrode is quite simple. A platinum wire is immersed into a solution saturated with quinhydrone and the potential of the platinum electrode in that solution is measured versus a reference electrode [42, 45, 46].

In an aqueous solution of quinhydrone the following chemical equilibrium is established:



If a platinum wire is introduced into this solution, an electrochemical equilibrium according to the following electron transfer reaction establishes at the electrode:

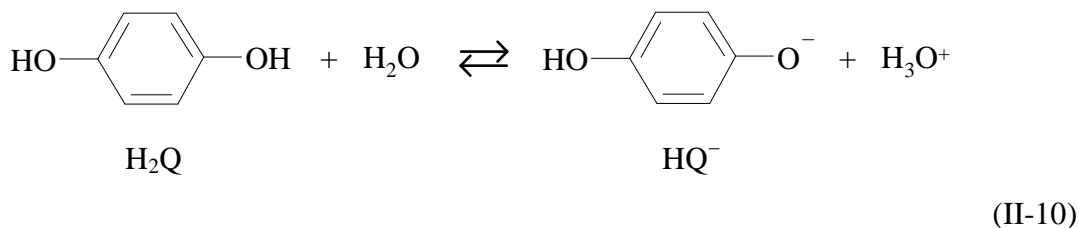


The electrode potential depends on the ratio quinone (Q) to dianion of hydroquinone (Q^{2-}) and can be formulated according to the Nernst equation:

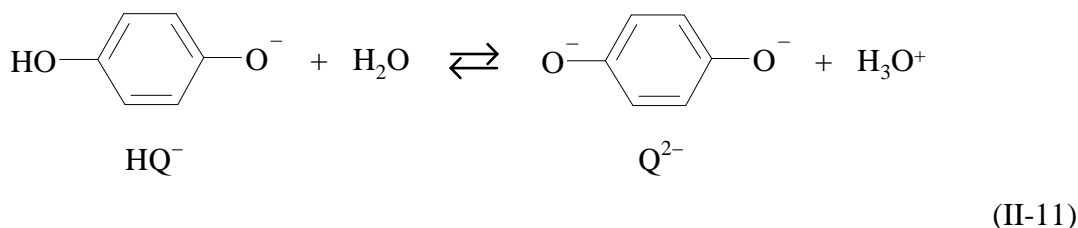
$$E = E_{Q/Q^{2-}}^{\ominus} + \frac{RT}{2F} \ln \frac{a_Q}{a_{Q^{2-}}} \quad (\text{II-9})$$

with $E_{Q/Q^{2-}}^{\ominus}$: standard potential of the system Q and Q^{2-} .

The redox potential depends not only on the ratio Q to Q^{2-} , but also on the pH of the solution because hydroquinone is a dibasic acid with two acidity constants $K_{a,1}$ and $K_{a,2}$:



$$K_{a,1} = \frac{a_{\text{H}_3\text{O}^+} \cdot a_{\text{HQ}^-}}{a_{\text{H}_2\text{Q}}} = 1.41 \cdot 10^{-10}$$



$$K_{a,2} = \frac{a_{\text{H}_3\text{O}^+} \cdot a_{\text{Q}^{2-}}}{a_{\text{HQ}^-}} = 3.98 \cdot 10^{-12}.$$

The activity of hydroquinone (a_{Red} = analytical activity of hydroquinone) can be calculated from the equation of mass balance for hydroquinone using the acidity constants $K_{a,1}$ and $K_{a,2}$:

$$a_{\text{Red}} = a_{\text{H}_2\text{Q}} + a_{\text{HQ}^-} + a_{\text{Q}^{2-}} = a_{\text{Q}^{2-}} \left(\frac{a_{\text{H}_3\text{O}^+}^2}{K_{a,1} \cdot K_{a,2}} + \frac{a_{\text{H}_3\text{O}^+}}{K_{a,2}} + 1 \right). \quad (\text{II-12})$$

By rearranging Equation II-12 for $a_{\text{Q}^{2-}}$ follows:

$$a_{\text{Q}^{2-}} = \frac{a_{\text{Red}} \cdot K_{a,1} \cdot K_{a,2}}{a_{\text{H}_3\text{O}^+}^2 + a_{\text{H}_3\text{O}^+} \cdot K_{a,1} + K_{a,1} \cdot K_{a,2}}. \quad (\text{II-13})$$

Equation II-13 is introduced into Equation II-9 and thus for the potential of the quinhydrone electrode follows:

$$E = E_{\text{Q/Q}^{2-}}^\ominus + \frac{RT}{2F} \ln \frac{a_{\text{Q}}}{a_{\text{Red}}} - \frac{RT}{2F} \ln (K_{a,1} \cdot K_{a,2}) + \frac{RT}{2F} \ln \left(a_{\text{H}_3\text{O}^+}^2 + K_{a,1} \cdot a_{\text{H}_3\text{O}^+} + K_{a,1} \cdot K_{a,2} \right). \quad (\text{II-14})$$

Because of the composition of quinhydrone, the ratio of a_Q to a_{Red} is unity provided that there are no compounds, which react with the constituents of quinhydrone; e.g., strong oxidants and reductants which could change the ratio a_Q to a_{Red} , or in emulsions quinone is preferentially dissolved in the oil phase, so that the ratio a_Q to a_{Red} in the aqueous solution could be also affected.

However, in solutions with $pH < 9.5$, i.e., $a_{H_3O^+}^2 \gg K_{a,1}K_{a,2} + K_{a,1} \cdot a_{H_3O^+}$, and free of compounds, which react with the constituents of quinhydrone, the electrode potential of the quinhydrone electrode can be simplified as:

$$E = E_C^{\ominus'}(\text{quinhydrone}) - 0.059 \cdot pH \quad (\text{for } T = 25 \text{ }^\circ\text{C}) \quad (\text{II-15})$$

with $E_C^{\ominus'}$: formal potential of the quinhydrone electrode at $pH < 9.5$. [41, 45]

At higher pH values it has to be considered that hydroquinone is a dibasic acid, i.e., the dissociation constants $K_{a,1}$ and $K_{a,2}$ affect the electrode potential. Further, in alkaline solutions, hydroquinone is easily oxidized by atmospheric oxygen, and this leads to considerable deviations of measured potentials from those calculated with Equation II-14 [46].

Since the introduction of the glass electrode, the conventional quinhydrone electrode has lost importance for common pH measurements, although this electrode offers a great advantage compared to glass electrodes: Because of the electrochemical reversibility of the electrode, and hence the fixed relation between pH and the redox potential, a calibration of the quinhydrone electrode is not necessary [2, 42]. However, the quinhydrone electrode also possesses some drawbacks and limitations in application: A main disadvantage is that the sample solution has to be contaminated with quinhydrone before the pH measurement [45]. Further, the quinhydrone electrode can only be employed up to pH 8. At higher pH values the hydroquinone is oxidized by atmospheric oxygen [42]. Furthermore the quinhydrone electrode is sensitive towards strong oxidants and reductants, because quinhydrone is a redox system itself [2]. And last but not least the equilibrium of quinone and hydroquinone is affected when the ionic strength exceeds 1 mol L^{-1} [42], so that the so-called salt error is observed [47, 48]. It is also a problem that the quinhydrone electrode is electrochemically reversible only at some noble metals, especially platinum.

To achieve electrochemical reversibility also at carbon electrodes, special surface modifications are needed (see further down in this thesis).

Nevertheless, today the conventional quinhydrone electrode still fills a niche for pH measurements in situations where the glass electrode cannot be used, e.g., in hydrofluoric acid containing solutions or in media, where a glass electrode is easily broken [42].

H. Kahlert et al. developed compact pH electrodes based on quinhydrone, which exhibit the same electrochemically reversibility as the conventional quinhydrone electrode, while being manufactured in such way that no contamination of the sample solutions can happen [45]. These new quinhydrone composite electrodes can be used for pH measurements in emulsion, they can be produced almost of any shape and size, being flexible like rubber or solid like acrylic glass [4]. These composite electrodes consist of quinhydrone, modified graphite and a binder material like paraffin [1, 2], PMMA [3, 4], polysiloxane [26] etc. Various applications of these composite electrodes have been described. They were employed for pH measurements in milk [2], for in situ measurements of soil pH [49] and as detector in FIA measurements [3, 4, 24]. Construction of these composite electrodes was possible because the modified graphite allows the establishment of the reversible quinhydrone electrode potential, allowing applying these sensors without any calibration.

2.1.3.3 Potentiometric pH detectors in FIA systems

FIA potentiometry with ion selective electrodes (ISE) offer several advantages, like a very small dead volume, applicability to a wide concentration range, low-cost instrumentation, and ISEs are not affected by the turbidity and colour of the sample solution [23].

The configurations of electrochemical and thus of potentiometric detector cells for FIA are very versatile, but they all are based on one of the following three principles shown in Figure II-3: (a) annular (wall embedded) sensor, (b) cascade-type sensor, (c) wire-type (end-on) sensor [21, 22]. In case of the annular sensor the sensitive surface is part of the flow system, e.g., the sensor is build up of a cylinder inserted as part of the flow system or it is composed of one or several plates incorporated into the tubing wall. In contrast, the cascade-type sensor is exposed to the flowing stream tangential or frontal. The wire-type sensor is placed in the centre of the stream so that it is spearing the parabolic head of the sample zone. Furthermore, so-called wall-jet electrodes, which are a

combination of cascade-type and wire-type electrodes, are employed as electrochemical cell designs in FIA systems [22].

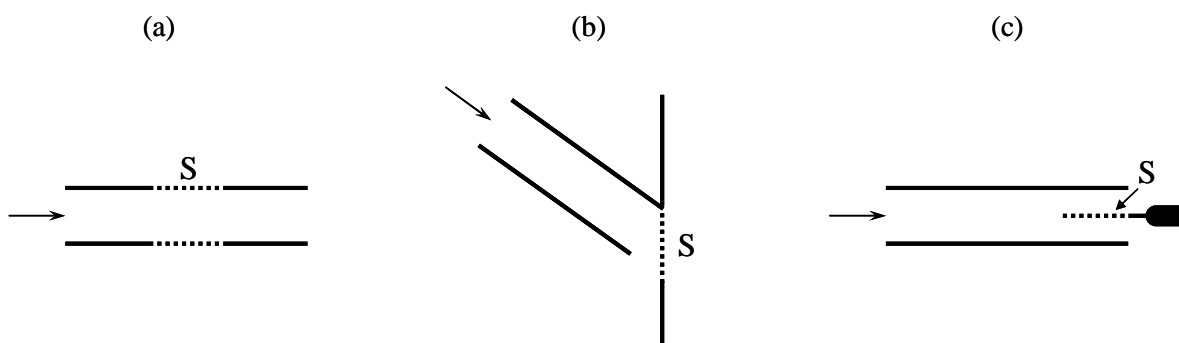


Figure II-3: The basic principles of electrochemical FIA detectors (S: sensitive surface): (a) annular sensor, (b) cascade-type sensor, (c) wire-type sensor [21, 22].

A range of different potentiometric pH detectors for FIA has been described in the literature: glass electrodes [50], PVC or epoxy acrylate membranes [51, 52], pH sensitive electrodes in combination with dialysis tubes [53], metal/metal oxide electrodes [54], pH sensitive ISFET's [55, 56] and stainless steel electrodes [57]. These electrodes are either relative expensive, the cell construction is not simple, response times are rather long, or they suffer from insufficient chemical stability. An ideal potentiometric pH detector for FIA titrations should have the following characteristics: (i) high chemical stability, (ii) short response time (time constants), (iii) large dynamic measuring range, (iv) small influence on the flow profile of the solution. Kahlert et al. developed solid composite electrodes based on quinhydrone in conjunction with a common reference electrode as detectors in FIA acid-base titrations, which fulfil all the required characteristics mentioned before [3, 24]. These detectors proved to have short time constants and sufficient long term stability. The electrodes belong to the annular sensor type. The ring-shaped surface of the composite electrode is exposed to the solution stream resulting in a nearly undisturbed flow of the solution. For the titration of hydrochloric acid and acetic acid by injection of samples (injection volume: 150 μL) into a sodium hydroxide carrier solution the dynamic measuring range of the detector was about 4 orders of magnitude. The detection limit is almost ten times lower than for titrations using colour indicators and spectrophotometric detection [3].

2.2 Applications of FIA measurements

Chemical, environmental, pharmaceutical and biochemical research laboratories as well as industrial control laboratories use FIA systems for the rapid determination of the concentration of various organic and inorganic analytes in diverse sample materials. In dependence on the species to be analysed, different detection systems are employed.

As mentioned before, Kahlert et al. developed a pH detector for flow-injection-potentiometry (cf. Chapter 2.1.3.3). They have already applied this detector to a FIA system for simple acid-base titrations, for pH measurements and even for the determination of enzyme activities [3, 4, 24]. In this thesis, new applications of the FIA system could be developed. Thus, in the following some theoretical aspects of the applications of FIA measurements investigated in this thesis are given.

2.2.1 Water hardness

2.2.1.1 Definition of water hardness

Primarily, water hardness was defined as the capacity of water to precipitate soap, i.e., the precipitation of the calcium and magnesium salts of fatty acids [58]. Actually, the meaning of water hardness is nearly similar to the current definition, because mainly calcium and magnesium ions present in water are responsible for the precipitation of soap.

Nowadays, the term ‘water hardness’ is used to characterize the content of dissolved calcium, magnesium, strontium and barium salts in water. Different terms are used to classify the water hardness. The total concentration of the ions Ca^{2+} , Mg^{2+} , Sr^{2+} and Ba^{2+} is called total hardness. Because water usually does not contain Sr^{2+} and Ba^{2+} , in practice the total hardness is defined as the sum of the ion concentrations of Ca^{2+} and Mg^{2+} :

$$\text{total hardness} = c(\text{Ca}^{2+}) + c(\text{Mg}^{2+}) . \quad (\text{II-16})$$

Normally the total hardness is composed of calcium hardness in the range of 70–85% and magnesium hardness in a range of 15–30% [59].

Given by the behaviour during boiling of the water, carbonate hardness (temporary hardness) and non-carbonate hardness (permanent hardness) are distinguished [60]. The fraction of water hardness, which can be removed by boiling the water, is called carbonate hardness. The hydrogen carbonates dissolved in water form the carbonate hardness:

$$\text{carbonate hardness} = c(\text{HCO}_3^-). \quad (\text{II-17})$$

During boiling, CO_2 evolves from the water and carbonate is formed:



These carbonate ions react with the calcium and magnesium ions dissolved in water, so that hardly soluble calcium and magnesium carbonate precipitates [59]:



These reactions are responsible for the formation of dripstones and for the chemical deposition of boiler scale [61]. Thus high concentrations of Ca^{2+} , Mg^{2+} and HCO_3^- can create severe problems in industry and household as they may precipitate in pipes, boilers etc.

In contrast, the non-carbonate hardness, which is mainly due to the presence of calcium and magnesium sulphate and chloride, cannot be eliminated by boiling the water. The non-carbonate hardness can be described as follows [59]:

$$\text{non-carbonate hardness} = c(\text{Ca}^{2+}) + c(\text{Mg}^{2+}) - c(\text{HCO}_3^-). \quad (\text{II-21})$$

According to § 9 (2) of the German WRMG (= “Wasch- und Reinigungsmittelgesetz” “Gesetz über die Umweltverträglichkeit von Wasch- und Reinigungsmitteln”, i.e., law on the environmental compatibility of washing and cleaning agents) water is classified into different hardness ranges (cf. Table II-1) and has to be expressed as calcium carbonate in mmol L^{-1} [62]. However, in practice the water hardness

is often still expressed in degree of hardness, where one German degree of hardness (1 °dH) is equal to a calcium carbonate concentration of 0.18 mmol L⁻¹ [59].

Table II-1: Ranges of water hardness [62, 63].

Hardness range	$c(\text{CaCO}_3)$ [mmol L ⁻¹]	°dH
Soft	<1.5	<8.4
Moderately hard	1.5–2.5	8.4–14
Hard	>2.5	>14

2.2.1.2 Methods for the determination of water hardness

The determination of water hardness ranks among the most frequently performed analyses of water samples, because too hard water can cause the problems mentioned before (cf. Chapter 2.2.1.1).

Traditionally, the determination of water hardness is performed by complexometric titration using ethylenediaminetetraacetic acid (EDTA) as titrant and Eriochrome black T, murexide or calconcarboxylic acid as indicator [60, 64]. EDTA (H₄Y) is a tetraprotic acid and has a very low solubility in water, so that generally the disodium salt of EDTA (Na₂H₂Y) is used as titrant for complexometric titrations.

For a rapid, but rough estimation of the hardness of water semi-quantitative test strips have been commercialized by various companies, e.g., Aquadur[®] from Macherey-Nagel [65] or MONITOR[™] Water Hardness strips sold by Serim[®] [66]. To overcome the drawbacks of the complexometric titration, like large sample volume, high reagent consumption, high expenditure of time and interference of several other metal ions, different instrumental approaches for the determination of Ca²⁺ and Mg²⁺ ions have been proposed, amongst them AAS [67, 68], AES and ICP-AES [58, 69, 70], polarography [71], ion chromatography [72], various photometric methods [73–75], fluorescent assays [76], optical chemical sensors [77] and ion selective electrodes [78–81]. Instrumental methods are less laborious as they permit direct determinations and they are more sensitive, but they are also more expensive. Optical chemical sensors and ion selective electrodes have good detection limits, but often suffer from long response times and short life times [77]. Approaches to improve the selectivity of ISEs using chemometric data treatment for multivariate sensor arrays have been described by Saurina et al. [82]. Furthermore,

adaptations of these instrumental techniques to flow injection systems have been described in the literature to satisfy the increasing demand for automated, rapid water analysis [83–89].

2.2.2 Wine

2.2.2.1 pH and acidity of wine

In the area of oenology the pH and the acidity of wine play an important role because both parameters influence the properties and the quality of wine. The pH and the acidity affect the colour and the flavour of wine, as well as the microbiological stability and shelf time of a wine [90]. The acids existing in wines are relatively weak organic acids [91], with tartaric acid and malic acid dominating. Wine also contains various other volatile and non-volatile acids in lower concentrations [90].

There are three sources of the organic acid content of wine: (i) The grape itself contains tartaric acid, malic acid and, in much lower concentration, citric acid. (ii) During alcoholic fermentation, several acids are formed as by-products, mainly lactic acid, acetic acid and succinic acid. (iii) Bacteria may produce lactic acid, acetic acid, and occasionally propionic acid and butyric acid. Besides, mould growth on the grape may result in gluconic acid [92].

A criterion for the acid content in wine is the titratable acidity, which is usually expressed as gram tartaric acid per litre. Sometimes the titratable acidity is expressed as contents of other acids, e.g., in France it is expressed as sulphuric acid [91]. In contrast, in Germany the titratable acidity is given in milligram hydronium ions per litre [90].

Often it is necessary to adjust the pH and acidity of wine aiming at producing a well-balanced wine, because too low acid contents and too high pH values cause abnormal colour, flat taste and less microbiological stability [90, 91], whereas too high acidities or too low pH values yield a spicy, less pleasant taste [90]. Therefore different methods for acidity and pH adjustment are employed, amongst them addition of organic acids (commonly tartaric, malic or citric acid), addition of water, sugar or a combination of both; neutralization of the acidity by addition of carbonates (carbonate deacidification), ion exchange of acid anions by hydroxide ions, biological deacidification by malolactic fermentation or by the use of selected yeasts, and blending by combining wines of high

acidity with those of low acidity [92]. Hence, for wine producers the determination of titratable acidity and pH of wine is essential, in order to decide to what extent a correction of the acidity is necessary. Thus, both parameters, titratable acidity and pH, are measured during processing and finishing operations to standardize a wine and to notice unwanted changes caused by bacteria or yeast [91].

2.2.2.2 Methods for the determination of titratable acidity of wine

For the determination of the titratable acidity of wine, different procedures are applied. The European standard method is based on the potentiometric titration with a solution of 0.1 mol L^{-1} sodium hydroxide to an endpoint of pH 7. Alternatively, the acidity is determined by titration with bromothymol blue as indicator, especially in case of white wine [93]. In the USA, pH 8.2 is used as endpoint or phenolphthalein is applied as indicator [91, 92]. However, with these methods the true value of the titratable acidity of wine is not measured, because the endpoint of the acid-base titration is different for each wine. The true endpoint depends on the composition and concentration of the acids present in the wine sample. Since the acids existing in wine are relatively weak, the real endpoint will be more alkaline than pH 7.0. Usually, the endpoint varies between pH 7.8 and pH 8.3 [91]. Furthermore, classical acid-base titrations of wine samples are time-consuming and require quite a large sample and titrant volume.

To overcome the drawbacks of the conventional titrations, alternative methods have been described. Berezin et al. gave a review of different methods for the determination of the titratable acidity in various products [94]. For the determination of the titratable acidity in wine some electrochemical methods have been described. Potentiometric measurements with a copper electrode [95] as well as voltammetric measurements with microelectrodes [95, 96] were suggested. Ohtsuki et al. proposed a method based on the voltammetric reduction of quinone [97]. Recently, Tôrres et al. suggested a digital image-based method using acid-base titrations without any indicator. Here, the pH dependence of the colour change of the anthocyanines present in the wine is exploited for the determination of the titratable acidity [98]. Similar to the classical titrations, there are a few drawbacks of these alternative methods, like large sample and titrant volume, extended analysis time and the requirement of supplementary reagent additions.

To automate the determination of the titratable acidity of wine several flow-through systems have been suggested [99–106]. These methods are less laborious. However, all of

them use photometric detection systems, what can cause a lot of problems especially in case of coloured samples like red wine. Also, such instrumental methods are rather expensive.

3 Experimental

3.1 Chemicals

All chemicals used were of p.a. quality (exceptions are marked in the text) and ultrapure water was used for all solutions (arium[®] 611 UV, Sartorius, Germany).

3.1.1 Preparation of the pH sensitive layer of the detector cell and preparation of the salt bridge

Quinhydrone and graphite powder (fine and extra pure) were purchased from Merck (Germany). For surface modification of the graphite powder concentrated nitric acid (65%) from Merck (Germany) was used. As binder commercially available polysiloxane (“Aquarium Silikon”) from MASTER fix[®] (Austria) was used. For the preparation of the salt bridge potassium chloride and agarose purchased from Merck (Germany) were used.

3.1.2 Simple FIA acid-base titrations

Sodium hydroxide solution (ampoules for 1000 mL, $c(\text{NaOH}) = 0.1 \text{ mol L}^{-1}$ Titrisol[®]) and hydrochloric acid (ampoules for 1000 mL, $c(\text{HCl}) = 0.1 \text{ mol L}^{-1}$ Titrisol[®]), glacial acetic acid, concentrated sulphuric acid (96%, Suprapur[®]), potassium dihydrogen phosphate, concentrated ortho-phosphoric acid (85%), boric acid (Suprapur[®]), citric acid monohydrate, sodium acetate trihydrate, sodium hydroxide pellets, di-sodium DL-malate, borax, dipotassium hydrogen phosphate, disodium oxalate, trisodium citrate dihydrate and potassium chloride were purchased from Merck (Germany). Oxalic acid dihydrate was from Fluka AG, Buchs SG (Switzerland).

3.1.3 FIA acid-base titrations in buffered solutions

Hydrochloric acid (ampoules for 1000 mL, $c(\text{HCl}) = 0.1 \text{ mol L}^{-1}$ Titrisol[®]), glacial acetic acid, potassium dihydrogen phosphate, dipotassium hydrogen phosphate and potassium chloride were purchased from Merck (Germany).

3.1.4 Determination of water hardness

Calcium nitrate tetrahydrate, magnesium nitrate hexahydrate, calcium sulphate dihydrate, magnesium sulphate heptahydrate, calcium chloride, magnesium chloride hexahydrate, potassium chloride, sodium hydroxide, hydrochloric acid, ammoniac, ammonium chloride, Triplex[®] III (ampoules filled with a solution for 1000 mL, $c(\text{Na}_2\text{-EDTA} \cdot 2 \text{ H}_2\text{O}) = 0.1 \text{ mol L}^{-1}$ Titrisol[®], and containing NaOH in an unknown concentration), Eriochrome black T and calconcarbonic acid were from Merck (Germany). Testalon[®] III (ampoules filled with a solid for 1000 mL, $c(\text{Na}_2\text{-EDTA}) = 0.01 \text{ mol L}^{-1}$) was purchased from Feinchemie Sebnitz (Germany). Sodium chloride was from Lancaster (England).

3.1.5 Determination of titratable acidity and pH of wine

DL-malic acid, potassium chloride, boric acid, phosphoric acid, sodium perchlorate, glacial acetic acid, sodium hydroxide solution (ampoules for 1000 mL, $c(\text{NaOH}) = 0.1 \text{ mol L}^{-1}$ Titrisol[®]) and hydrochloric acid (ampoules for 1000 mL, $c(\text{HCl}) = 0.1 \text{ mol L}^{-1}$ Titrisol[®]) were purchased from Merck (Germany). Sodium hydroxide pellets were from Sigma Aldrich (Germany). Wine samples were purchased from local supermarkets.

3.2 Instrumentation of the FIA system

3.2.1 The detection system

Figure II-4 shows schematically the construction of the detector cell.

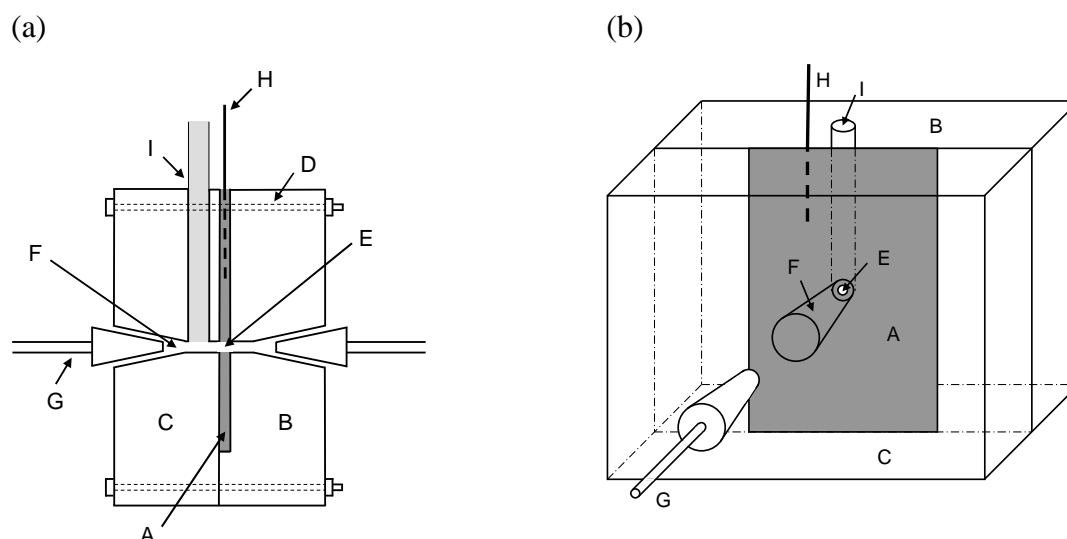


Figure II-4: Scheme of the detector cell. **(a):** lateral view, **(b):** 3D view from the front. A: pH sensitive layer, B and C: Plexiglas plates, D: screws to fix the plates, E: hole punctured through the pH sensitive layer, F: conic holes drilled in the Plexiglas plates, G: tube fittings, H: copper wire for electrical contact, I: hole to house the gel filled tube.

First of all, for the preparation of the pH sensitive layer (A) based on graphite and quinhydrone, surface oxidized graphite powder was prepared to enhance the electrochemical reversibility of quinhydrone on graphite. The surface oxidized powder was obtained by reflux boiling of 15 g milled commercial graphite powder with 150 mL concentrated nitric acid for 2 h. Then, the powder was washed with water until the washing water had a neutral pH. Subsequently, it was washed with ethanol and then with water again. After washing, the powder was dried at 60 °C and milled for 30 minutes. Due to the modification procedure, surface-confined quinhydrone-like redox centres are formed. Because of the similarity of these surface-confined structures and quinhydrone, the electrochemical reversibility of the quinhydrone system on graphite is guaranteed [2]. Without oxidative surface modification of the graphite powder, the quinhydrone on

graphite would be quasi-reversible and thus the slope of the potential versus pH plot would differ from the theoretical slope [1].

The surface oxidized graphite powder was mixed with quinhydrone in the ratio 9:1 in a ball mill. 1 g polysiloxane was added to 1.1 g of the graphite-quinhydrone-mixture, and the resulting paste was carefully mixed before it was pressed to obtain a planar layer of 1 mm thickness. The layer was allowed to polymerise and harden for 2 days. After hardening, the layer was cut into proper squares of an approximate size of 10 mm × 10 mm. One piece was placed in the cavity of the Plexiglas plate (B), and a second plate (C) was fixed on the other side with screws (D). With the help of a cannula, a hole (E) was punctured through the sensitive layer to obtain a flow-through channel with an inner diameter of 0.5 mm. Conic holes in both plates (F) allowed the connection of FIA tube fittings (G). A copper wire (H) was plunged into the sensitive layer to make electrical contact. As reference electrode a KE 10 saturated calomel electrode (Sensortechnik Meinsberg, Germany) with an electrode potential of $E = 244.4$ mV at 25 °C or a saturated Ag/AgCl electrode (DPST Behnert GmbH, Germany) with an electrode potential of $E = 197.0$ at 25 °C was used. The reference electrode was kept in a beaker containing saturated KCl solution. A tube filled with KCl_{sat}-agarose gel was used as salt bridge. One end of the tube was immersed in the beaker with the reference electrode; the other end of the tube was placed in a hole (I) 1 mm downstream of the sensitive layer. The salt bridge was placed as close as possible to the sensitive layer to avoid marked potential drops due to a possible high resistance of solutions with a low ionic strength.

3.2.2 FIA configuration

For all FIA measurements, a single line FIA configuration according to the scheme shown in Figure II-1 (cf. Chapter 2.1.1) was used. A multichannel peristaltic pump (ISMATEC, Switzerland) propelled the carrier stream with a flow rate Q of 1.75 mL min⁻¹. Since the carrier has to provide a stable basic signal at the detector [5], 1·10⁻² mol L⁻¹ KCl was added to each carrier solution. This KCl concentration ensures a sufficient conductivity which provides a smooth baseline and thus a markedly improved signal-to-noise ratio. A 6-port-valve (VICI, USA or Rheodyne, USA) was used to inject a sample volume S_v of 150 µL. The sample loop was filled with a syringe. The pH sensitive detector cell was connected with the injection valve via a 10 cm long Teflon[®] tube with an inner diameter of 0.5 mm. Previously, it has been shown that with this configuration optimal dispersion

coefficients for FIA titrations can be obtained [3]. Chronopotentiometric measurements were recorded using an AUTOLAB with a PSTAT 10 (Eco-Chemie, The Netherlands) in conjunction with a personal computer (IBM compatible). The potential difference between the pH sensitive layer and the reference electrode was measured every 0.2 s. For evaluation of the signals, the peak areas were determined using the Software OriginPro 7.5.

3.3 Measurement performance

3.3.1 Simple FIA acid-base titrations

Solutions of different acids and bases, which contained titratable hydronium ions or titratable alkaline groups in a concentration range from $6 \cdot 10^{-5} \text{ mol L}^{-1}$ to $1.2 \cdot 10^{-2} \text{ mol L}^{-1}$, were prepared. The acids were injected into a carrier solution of $5 \cdot 10^{-3} \text{ mol L}^{-1}$ NaOH and the bases were injected into a carrier solution of $5 \cdot 10^{-3} \text{ mol L}^{-1}$ HCl. All carrier and standard solutions contained $1 \cdot 10^{-2} \text{ mol L}^{-1}$ KCl to improve the conductivity.

3.3.2 FIA acid-base titrations in buffered solutions

Acetic acid was used as analyte in a concentration range from $1 \cdot 10^{-4} \text{ mol L}^{-1}$ to $1 \cdot 10^{-1} \text{ mol L}^{-1}$ dissolved in buffer solutions (pH = 7.12). The following buffer compositions were tested: 6.25 mM KH_2PO_4 + 6.25 mM K_2HPO_4 (12.5 mM buffer); 12.5 mM KH_2PO_4 + 12.5 mM K_2HPO_4 (25 mM buffer); 25 mM KH_2PO_4 + 25 mM K_2HPO_4 (50 mM buffer); 50 mM KH_2PO_4 + 50 mM K_2HPO_4 (100 mM buffer); 100 mM KH_2PO_4 + 100 mM K_2HPO_4 (200 mM buffer). Solutions of hydrochloric acid in a concentration range from $5 \cdot 10^{-4} \text{ mol L}^{-1}$ to $5 \cdot 10^{-2} \text{ mol L}^{-1}$ were used as carrier solution. All analyte solutions and all carrier solutions contained $1 \cdot 10^{-2} \text{ mol L}^{-1}$ KCl to ensure a sufficient conductivity.

Conventional pH measurements were performed using a pH meter set Qph 70 including a glass electrode in conjunction with a pH meter (VWR International GmbH, Germany).

3.3.3 Determination of water hardness

3.3.3.1 FIA titration

As carrier, two different EDTA solutions were tested. Carrier solution 1 contained 0.01 mol L^{-1} of the disodium salt of EDTA (Testalon[®] III ampoule, Feinchemie Sebnitz), and carrier solution 2 was prepared by dissolving a Titrisol[®] ampoule (Merck) in 5 L ultrapure water as to obtain a 0.02 mol L^{-1} solution. As mentioned before, the KCl concentration in both carrier solutions was $1 \cdot 10^{-2} \text{ mol L}^{-1}$ (cf. Chapter 3.2.2). The EDTA concentrations were chosen to obtain a large working range.

The FIA system was calibrated using calcium and magnesium salts in different concentrations. In order to improve the conductivity $1 \cdot 10^{-2} \text{ mol L}^{-1}$ KCl were added to all standard solutions.

For the determination of the sum of calcium and magnesium ions the water samples were injected into the FIA system without any pre-treatment, whereas for the determination of the calcium ion content separately the samples were pre-treated in the following way: 40 mL of the water sample were put in a 50 mL measuring flask and 5 mL of 1 mol L^{-1} NaOH were added in order to precipitate magnesium ions as magnesium hydroxide in the sample solution. The volume was adjusted to 50 mL in the measuring flask using ultrapure water. The magnesium hydroxide was then filtered off by using a syringe filter (pore size: $0.45 \mu\text{m}$). To 25 mL of the filtrate, hydrochloric acid was added to adjust the solution pH to 6 and the volume was adjusted to 50 mL. This solution was injected into the FIA system.

3.3.3.2 Batch titration

Conventional complexometric titrations of calcium and magnesium ions were performed for the sake of comparison.

For the determination of the total hardness, i.e., the sum of calcium and magnesium ions 50 mL of the sample were used and 10 mL $\text{NH}_3/\text{NH}_4\text{Cl}$ buffer solution ($c(\text{NH}_3) = 5 \text{ mol L}^{-1}$, $c(\text{NH}_4\text{Cl}) = 1 \text{ mol L}^{-1}$, pH = 10) were added. Eriochrome black T (mixed with sodium chloride in a ratio 1:99 in a mortar) was added as indicator. The solution was

titrated using a 0.02 mol L^{-1} EDTA solution (Merck) as reagent until the colour change of the indicator from violet to blue appeared.

Also, for the determination of the calcium concentration 50 mL sample were used. However, here 5 mL NaOH solution ($c(\text{NaOH}) = 1 \text{ mol L}^{-1}$) were added so that a pH value of 12 was achieved. Under these conditions magnesium ions precipitate as magnesium hydroxide, so that only the calcium content is measured. As indicator calconcarbonic acid (mixed with sodium chloride in a ratio 1:99 in a mortar) was used and as reagent a 0.02 mol L^{-1} EDTA solution (Merck) was employed. The colour change of calconcarbonic acid at the equivalence point occurs from pink to blue.

3.3.4 Determination of titratable acidity and pH of wine

3.3.4.1 FIA measurements

3.3.4.1.1 Determination of the titratable acidity

A solution of $5 \cdot 10^{-3} \text{ mol L}^{-1}$ sodium hydroxide (+ $1 \cdot 10^{-2} \text{ mol L}^{-1}$ KCl; cf. Chapter 3.2.2) was used as carrier solution. The sodium hydroxide concentration was chosen to obtain a convenient dynamic working range.

Solutions of DL-malic acid in a concentration range from $5 \cdot 10^{-4} \text{ mol L}^{-1}$ to $1.25 \cdot 10^{-2} \text{ mol L}^{-1}$ were used to calibrate the FIA system. Malic acid was used as it is one of the main acids in wine [90]. To all calibration solutions $1 \cdot 10^{-2} \text{ mol L}^{-1}$ KCl was added to ensure a satisfactory conductivity.

The wine samples were purged with nitrogen for approximately 10 minutes in order to eliminate carbon dioxide before they were diluted and injected into the FIA system.

3.3.4.1.2 pH measurements

As carrier a solution of $1 \cdot 10^{-2} \text{ mol L}^{-1}$ hydrochloric acid and $1 \cdot 10^{-2} \text{ mol L}^{-1}$ KCl was used. The FIA system was calibrated using Britton–Robinson buffer solutions in a pH range from 2 to 8. The Britton–Robinson buffer solutions were prepared as described in [107].

Because of the high ionic strength of the buffer solutions, what ensures a sufficiently high conductivity, no KCl was added to the standard solutions. The wine samples were injected into the FIA system without any pre-treatment.

3.3.4.2 Batch measurements

Conventional pH measurements and potentiometric titrations were performed using the pH meter set Qph 70 (VWR International GmbH, Germany) including a glass electrode in conjunction with a pH meter. All batch titrations of wine samples were performed as follows: At first the wine sample was purged with nitrogen for 10 minutes to eliminate carbon dioxide. After the purging procedure, 10 mL wine were titrated using a solution of 0.1 mol L^{-1} NaOH as reagent, and the pH was measured after each addition of NaOH to the wine sample.

For redox potential measurements, a platinum electrode was used as working electrode and an Ag/AgCl electrode in 3 M KCl (Metrohm, Switzerland) with an electrode potential of $E = 207.0 \text{ mV}$ at 25°C served as reference electrode. Before redox potential measurements 40 mL of sample solution were purged with nitrogen for 30 minutes. Then, a solution of 0.5 mol L^{-1} NaOH was added to the sample solution successively and the redox potential was measured after each addition, respectively. During the whole procedure the sample solution and also the 0.5 mol L^{-1} NaOH solution were purged with nitrogen to exclude the influence of oxygen on the redox potential.

4 Results and discussion

4.1 Simple acid-base titrations

In a first experiment, the composite electrode based on graphite and quinhydrone in conjunction with polysiloxane as binder was tested by the titration of different acids and bases. In Table II-2 the applied acids as well as their associated pK_a values are given, and in Table II-3 the applied bases as well as their pK_b values are given.

Table II-2: pK_a values of the titrated acids ($T = 25\text{ }^{\circ}\text{C}$, exceptions: H_3BO_3 $T = 20\text{ }^{\circ}\text{C}$ and $\text{C}_6\text{H}_8\text{O}_7$ $T = 18\text{ }^{\circ}\text{C}$).

Acid	pK_{a1}	pK_{a2}	pK_{a3}
HCl	-7^{**}	-	-
CH_3COOH	4.75^*	-	-
NH_4^+	9.25^*	-	-
H_2SO_4	-3^{**}	1.92^{**}	-
$\text{C}_2\text{H}_2\text{O}_4$	1.23^*	4.19^*	-
H_2PO_4^-	7.12^{**}	12.32^{**}	-
H_3PO_4	1.96^{**}	7.12^{**}	12.32^{**}
H_3BO_3	9.14^*	12.74^*	13.80^*
$\text{C}_6\text{H}_8\text{O}_7$	3.08^*	4.74^*	5.40^*

* [108], ** [109]

Table II-3: pK_b values of the titrated bases ($T = 25\text{ }^{\circ}\text{C}$, exception: $\text{C}_6\text{H}_5\text{O}_7^{3-}$ $T = 18\text{ }^{\circ}\text{C}$).

Base	pK_{b1}	pK_{b2}	pK_{b3}
CH_3COO^-	9.25^*	-	-
OH^-	-1.74^*	-	-
$\text{C}_4\text{H}_4\text{O}_5^{2-}$	8.90^{***}	10.54^{***}	-
$\text{B}_4\text{O}_7^{2-}$	0.20^*	1.26^*	4.86^*
HPO_4^{2-}	6.88^{**}	12.04^{**}	-
$\text{C}_2\text{O}_4^{2-}$	9.81^*	12.77^*	-
$\text{C}_6\text{H}_5\text{O}_7^{3-}$	8.60^*	9.26^*	10.92^*

* [108], ** [109], *** [110]

Solutions containing different concentrations of acids or bases were injected into the FIA system. In the FIA titrations typical asymmetric peak shaped signals were recorded and the peak areas A_p were determined. The obtained peak areas were plotted against the concentration of titratable hydronium ions or against the concentration of titratable alkaline groups, respectively (cf. Figure II-5 and II-6).

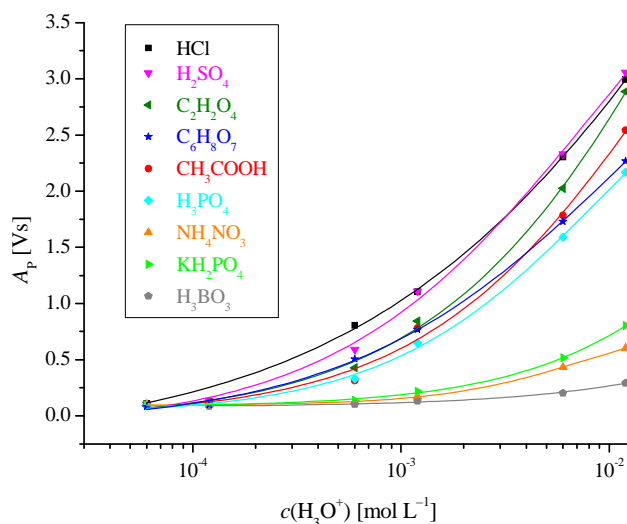


Figure II-5: Dependence of the peak area A_p on the hydronium ion concentration $c(\text{H}_3\text{O}^+)$ obtained for FIA titration of different acids (carrier solution: $5 \cdot 10^{-3}$ mol L⁻¹ NaOH + $1 \cdot 10^{-2}$ mol L⁻¹ KCl, injection volume: 150 μL , flow rate: 1.75 mL min⁻¹).

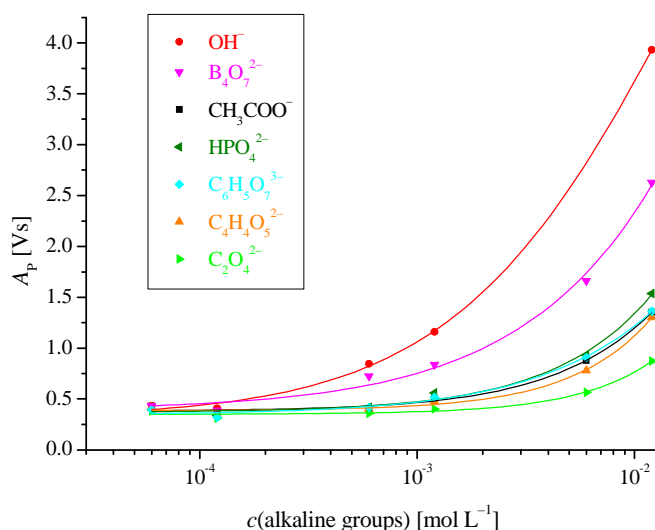


Figure II-6: Dependence of the peak area A_p on the concentration of titratable alkaline groups obtained for FIA titration of different bases (carrier solution: $5 \cdot 10^{-3}$ mol L⁻¹ HCl + $1 \cdot 10^{-2}$ mol L⁻¹ KCl, injection volume: 150 μL , flow rate: 1.75 mL min⁻¹).

As can be seen in Figure II-5 and II-6, non-linear calibration curves were obtained. The calibration curves can be fitted best by sigmoidal relations according to the following type of function:

$$y = \frac{A_1 - A_2}{1 + (x/x_0)^p} + A_2 \quad (\text{II-22})$$

with A_1 : initial y-value

A_2 : final y-value

p : power

x_0 : centre (x-value of the inflection point of the sigmoidal curve).

Furthermore, it was found that the peak size and thus the shape of the calibration curve depended on the pK_a value of the acid or the pK_b value of the base, respectively. The lower the pK_a or pK_b value was (i.e., the stronger the acid or base is), the larger were the peak areas and the higher was the increase of the peak area with increasing concentration of hydronium ions or alkaline groups. If a polyprotic acid or base was measured, the peak size and increase of the peak area with increasing concentration of hydronium ions or alkaline groups depended not only on the pK_{a1} or pK_{b1} value of the respective acid or base; in contrast all pK_a or pK_b values of the respective acid or base played an important role. In fact, the mean of all pK_a or pK_b values of the respective acid or base affected the peak sizes and the shapes of the calibration curves. For example, phosphoric acid ($pK_{a1} = 1.96$) is a stronger acid than acetic acid ($pK_a = 4.75$). However, in the FIA titration phosphoric acid (mean of all pK_a values = 7.13) appears as a weaker acid than acetic acid. This can be explained by the fact that FIA titration is a dynamic, non-equilibrium titration method.

In summary, it follows that the calibration curves of different acids (or bases) resemble each other, if the pK_a values of the acids (and the pK_b values of the bases) are similar. In contrast, if the pK_a or pK_b values differ strongly, also the calibration curves are different. That means that for the determination of the acid or base content of a sample it is essential to know the pK_a or pK_b values of the acids or bases in the sample, because it is essential to calibrate the FIA system with an acid or base of a pK_a or pK_b value similar to the pK_a or pK_b value of the analysing acid or base. That is the only way to calibrate the FIA system exactly so that an accurate measurement is guaranteed.

4.2 FIA acid-base titrations in buffered solutions

The determination of the acid content in buffered solutions plays an important role especially in biological issues. For example a number of enzymes (e.g., lipases, carboxylesterases, amidases, peptidases, nitrilases, etc.) convert substrates with formation of acids [111, 112]. Thus, the activity of these enzymes can be determined by measuring the change of the acid content in the medium during the enzymatic reaction. Because enzymes are only active in a proper pH range, the enzyme reaction has to be performed in a buffered medium.

Previously, it has been shown that the FIA system in conjunction with a graphite quinhydrone composite electrode is suitable for acid-base titrations in buffered solutions and for the determination of enzyme activities of lipase type B from *Candida antarctica* [24].

Now, the FIA system with the modified composite electrode (containing polysiloxane instead of PMMA as binder) had to be tested for the suitability of acid-base titrations in buffered solutions, and the titration in buffered solutions had to be optimized concerning buffer concentration and concentration of the carrier solution.

At first, a calibration curve for acetic acid in buffer solution of $0.025 \text{ mol L}^{-1} \text{ KH}_2\text{PO}_4 + 0.025 \text{ mol L}^{-1} \text{ K}_2\text{HPO}_4$ was recorded by injecting the sample solutions into the carrier solution of $1 \cdot 10^{-2} \text{ mol L}^{-1} \text{ HCl}$. The FIA titration yielded asymmetric peak shaped signals as expected for moderate dispersion. The peak area was used for calibration and non-linear calibration curves resulted. As can be seen in Figure II-7, the peak area decreased exponentially with increasing acetic acid concentration. In fact, using an acid as carrier solution the concentration change of the base component of the buffer caused by the acid addition is titrated. The higher the acid concentration was, the more pronounced was the decrease of the concentration of the base component of the buffer and the smaller was the potentiometric signal.

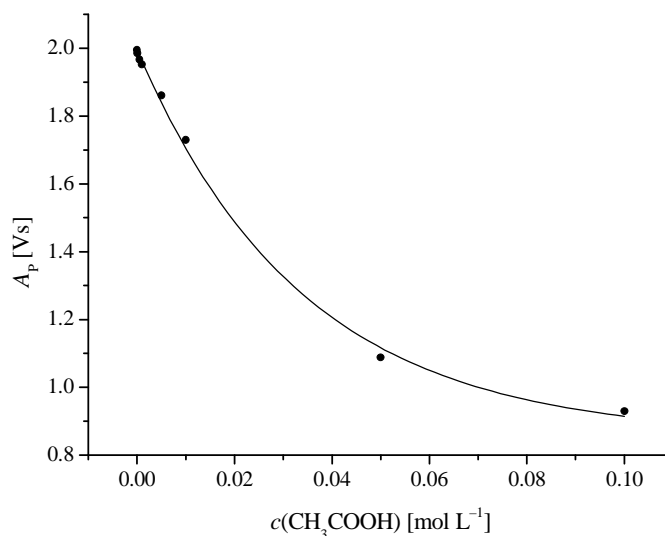


Figure II-7: Dependence of peak area A_p on acetic acid concentration in buffer solution of $0.025 \text{ mol L}^{-1} \text{KH}_2\text{PO}_4 + 0.025 \text{ mol L}^{-1} \text{K}_2\text{HPO}_4$ (carrier solution: $1 \cdot 10^{-2} \text{ mol L}^{-1} \text{HCl} + 1 \cdot 10^{-2} \text{ mol L}^{-1} \text{KCl}$, injection volume: $150 \mu\text{L}$, flow rate: 1.75 mL min^{-1}).

To investigate the influence of the buffer concentration on the calibration curve of acetic acid, standard solutions of acetic acid with different buffer concentrations were prepared and injected into the carrier solution ($1 \cdot 10^{-2} \text{ mol L}^{-1} \text{HCl}$). The peak area was used for evaluation and was plotted against the acetic acid concentration. Furthermore the lowest detection limits were determined by injection of blank solutions (proper buffer solutions without acetic acid) ten times, respectively. The mean values of the peak areas and the standard deviations were determined and by using the proper calibration functions the lowest detection limits (3σ) were calculated. Figure II-8 shows the obtained calibration curves. In Table II-4 the functions of the calibration curves, the mean values and standard deviations (s_r) of the peak areas obtained for the blank injections and the lowest detection limits (LODs) are given.

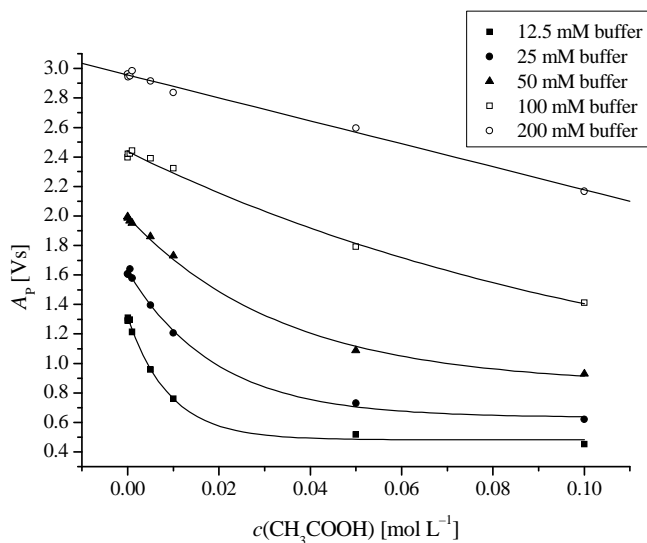


Figure II-8: Dependence of peak area A_P on acetic acid concentration in buffer solutions with different concentrations (carrier solution: $1 \cdot 10^{-2} \text{ mol L}^{-1} \text{ HCl} + 1 \cdot 10^{-2} \text{ mol L}^{-1} \text{ KCl}$, injection volume: $150 \mu\text{L}$, flow rate: 1.75 mL min^{-1}).

Table II-4: Calibration functions of acetic acid in different buffer compositions obtained with FIA titration; mean and standard deviation of peak area A_P , and lowest detection limits (LODs) for acetic acid determined with FIA titration for 10 repeated injections of different buffer compositions respectively.

$c(\text{buffer})$ [mmol L ⁻¹]	Calibration function	A_P		LOD [mol L ⁻¹]
		Mean [Vs]	s_r [%]	
12.5	$y = 0.83 \cdot e^{(-x/0.009)} + 0.48$	1.28 ± 0.02	1.6	$1.0 \cdot 10^{-3}$
25	$y = 0.99 \cdot e^{(-x/0.019)} + 0.63$	1.61 ± 0.02	1.2	$1.4 \cdot 10^{-3}$
50	$y = 1.14 \cdot e^{(-x/0.034)} + 0.85$	2.01 ± 0.01	0.5	$3.0 \cdot 10^{-4}$
100	$y = 1.81 \cdot e^{(-x/0.119)} + 0.62$	2.39 ± 0.03	1.3	$8.9 \cdot 10^{-3}$
200	$y = 2.96 - 7.79x$	2.95 ± 0.03	1.0	$1.3 \cdot 10^{-2}$

In case of the lower concentrated buffer solutions, an exponential dependence of the peak area on the acetic acid concentration occurs. With increasing buffer concentrations, the dependence approaches more and more a straight line resulting in a linear calibration curve in case of a buffer solution consisting of $1 \cdot 10^{-1} \text{ mol L}^{-1} \text{ KH}_2\text{PO}_4$ and $1 \cdot 10^{-1} \text{ mol L}^{-1} \text{ K}_2\text{HPO}_4$.

As expected, the lower the buffer concentration, the smaller is the peak area. With increasing buffer concentration the concentration of the base component increases. Hence,

the amount of base component, which reacts with the titrant, increases and the peak size increases. An advantage of a small peak size and thus of a lower buffer concentration lies in the more rapid signal formation. Besides, at lower buffer concentrations the sensitivity for low acetic acid concentrations is higher and the lowest detection limit (LOD) is smaller (cf. Table II-4). The smallest LOD is obtained for a buffer concentration of 50 mmol L⁻¹. However, if high acetic acid concentrations in the sample are expected, a high buffer concentration should be chosen, because in case of a lower concentrated buffer the peak area changes only slightly in the range of high acetic acid concentrations. That means that for high acetic acid concentrations the sensitivity increases with increasing buffer concentration. Furthermore, in case of buffer solutions containing equimolar amounts of acid and corresponding base, of course the buffering capacity is the higher the higher the concentration of the buffer is (cf. Table II-5).

Table II-5: pH values of solutions containing acetic acid and phosphate buffer in different concentrations measured with a glass electrode.

$c(\text{CH}_3\text{COOH}) [\text{mol L}^{-1}]$	pH				
	12.5 mM buffer	25 mM buffer	50 mM buffer	100 mM buffer	200 mM buffer
0	6.96	6.93	6.89	6.84	6.76
$1 \cdot 10^{-4}$	6.88	6.90	6.87	6.81	6.75
$5 \cdot 10^{-4}$	6.84	6.85	6.84	6.80	6.79
$1 \cdot 10^{-3}$	6.74	6.80	6.82	6.80	6.73
$5 \cdot 10^{-3}$	5.91	6.49	6.68	6.70	6.70
$1 \cdot 10^{-2}$	4.77	5.92	6.51	6.62	6.65
$5 \cdot 10^{-2}$	3.82	4.17	4.62	5.45	6.22
$1 \cdot 10^{-1}$	3.54	3.87	4.20	4.62	5.45

Moreover, the dependence of the calibration curve of acetic acid on the concentration of the carrier solution was investigated. Therefore, solutions of acetic acid in a concentration range from $1 \cdot 10^{-3} \text{ mol L}^{-1}$ to $1 \cdot 10^{-1} \text{ mol L}^{-1}$ in buffer solutions of $2.5 \cdot 10^{-2} \text{ mol L}^{-1} \text{ KH}_2\text{PO}_4$ and $2.5 \cdot 10^{-2} \text{ mol L}^{-1} \text{ K}_2\text{HPO}_4$ were injected into hydrochloric acid solutions of different concentrations. In Figure II-9, the peak shaped signals obtained for a $5 \cdot 10^{-3} \text{ mol L}^{-1}$ acetic acid solution injected into the different carrier solutions of hydrochloric acid are shown, and in Figure II-10 the obtained calibration curves of acetic acid for the different solutions of hydrochloric acid are given.

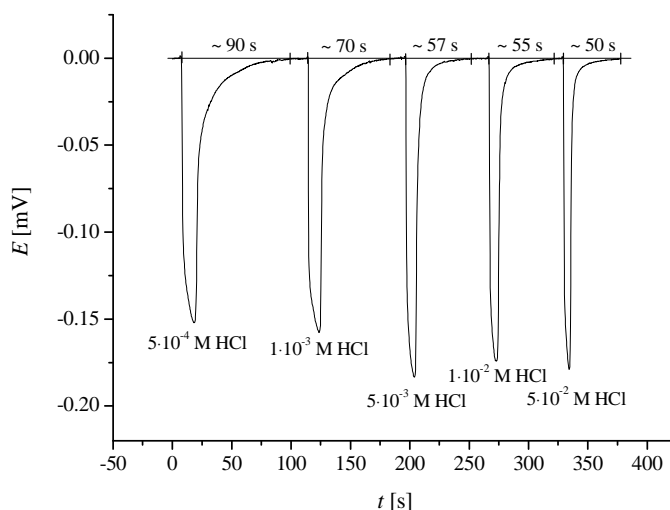


Figure II-9: Potentiometric peaks and the corresponding time of peak formation obtained for a solution of $5 \cdot 10^{-3} \text{ mol L}^{-1}$ acetic acid injected into different carrier solutions containing hydrochloric acid in different concentrations (injection volume: $150 \mu\text{L}$, flow rate: 1.75 mL min^{-1}). The baseline is related to zero.

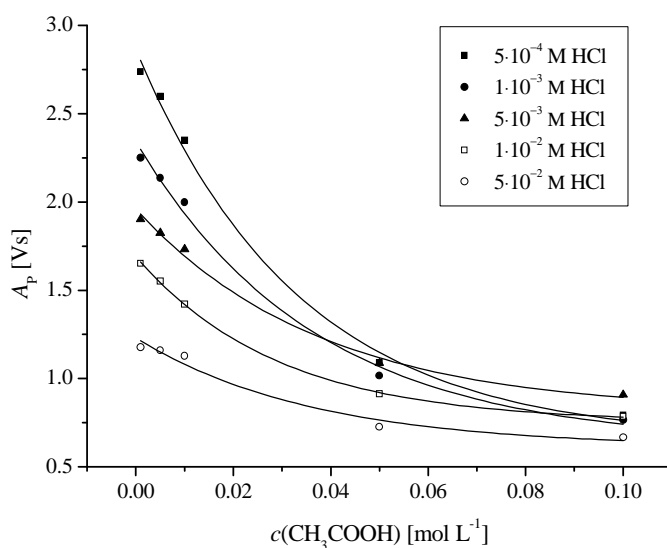


Figure II-10: Dependence of the peak area A_P on the acetic acid concentration in 50 mM buffer solution injected into HCl solutions of different concentrations (injection volume: $150 \mu\text{L}$, flow rate: 1.75 mL min^{-1}).

Figure II-9 and Figure II-10 clearly show that the lower the hydrochloric acid concentration of the carrier was the larger were the peak areas, i.e., the slower was the signal formation and the lower was the sampling frequency. However, the higher

sensitivity especially for lower acetic acid concentration is advantageous in case of using a lower concentration of hydrochloric acid as carrier. If a solution of $5 \cdot 10^{-2} \text{ mol L}^{-1}$ hydrochloric acid was used as carrier the signal formation was rapid, but the sensitivity was low.

The calibration curves obtained with $5 \cdot 10^{-4} \text{ mol L}^{-1}$ and $1 \cdot 10^{-3} \text{ mol L}^{-1}$ hydrochloric acid as well as the calibration curves obtained with $5 \cdot 10^{-3} \text{ mol L}^{-1}$ and $1 \cdot 10^{-2} \text{ mol L}^{-1}$ hydrochloric acid as carrier solution showed the same shape respectively, but they were shifted along the ordinate. That means that the peak areas obtained with $1 \cdot 10^{-3} \text{ mol L}^{-1}$ hydrochloric acid as carrier were smaller than the peak areas obtained with $5 \cdot 10^{-4} \text{ mol L}^{-1}$ hydrochloric acid, and thus the signal formation was more rapid. Similarly, the peak formation was more rapid for a $1 \cdot 10^{-2} \text{ mol L}^{-1}$ hydrochloric acid solution than for a $5 \cdot 10^{-3} \text{ mol L}^{-1}$ hydrochloric acid solution.

To choose the most suitable hydrochloric acid concentration of the carrier solution, the required sensitivity as well as the required sampling frequency has to be considered. If a high sensitivity is required, a carrier solution containing $1 \cdot 10^{-3} \text{ mol L}^{-1}$ hydrochloric acid should be applied. If a high sampling frequency is requested and a lower sensitivity is sufficient, a solution of $1 \cdot 10^{-2} \text{ mol L}^{-1}$ hydrochloric acid is suggested as carrier solution.

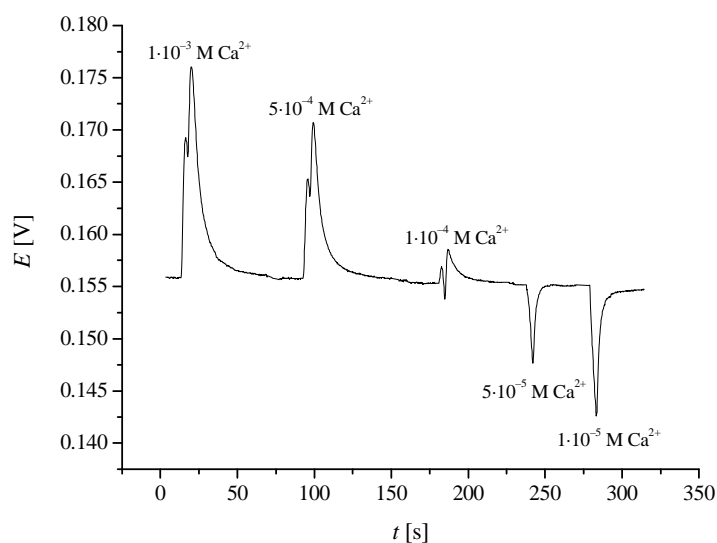
4.3 Determination of the calcium and magnesium content in aqueous solutions

4.3.1 Basic studies concerning the carrier solution

Two carrier solutions, one containing $0.01 \text{ mol L}^{-1} \text{ H}_2\text{Y}^{2-}$ and one containing $0.02 \text{ mol L}^{-1} \text{ HY}^{3-}$, were tested with respect to the detection limits obtainable for calcium ions. Carrier solution 1 (prepared from the disodium salt of EDTA, cf. Chapter 3.3.3.1) had a pH value of 4.5 at 23°C . At this pH value H_2Y^{2-} is the dominant species. In contrast, the pH of carrier solution 2 (prepared from a Titrisol[®] ampoule, cf. Chapter 3.3.3.1) was determined to be 9, meaning that HY^{3-} is the dominant species in this solution.

With both carrier solutions smooth baselines were obtained. In order to ascertain which of both carrier solutions is more suitable for the determination of water hardness, solutions of calcium nitrate in a concentration range from $1 \cdot 10^{-5} \text{ mol L}^{-1}$ to $1 \cdot 10^{-3} \text{ mol L}^{-1}$ were injected into both carrier solutions, respectively. $0.01 \text{ mol L}^{-1} \text{ KCl}$ was added to all calcium solutions for improving the conductivity, and the pH values of the calcium solutions were adjusted to 6. In Figure II-11 typical potentiometric peaks obtained for the calcium ion solutions injected into carrier solution 1 (cf. Figure II-11a) and into carrier solution 2 (cf. Figure II-11b) are shown.

(a)



(b)

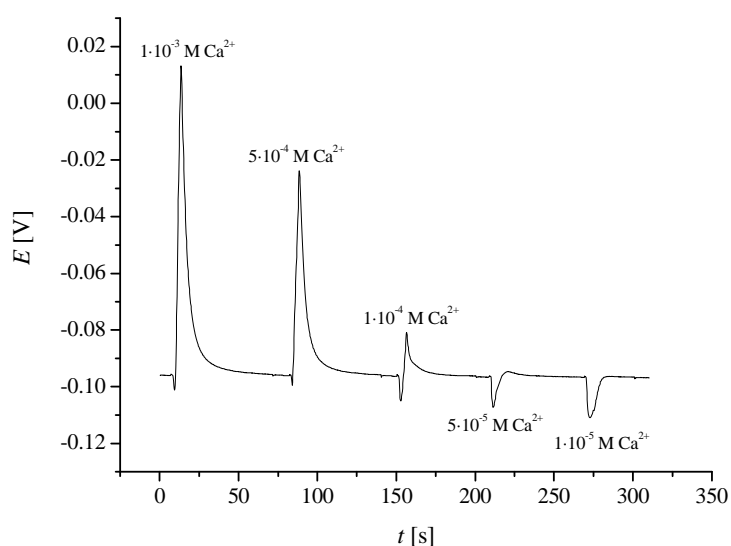
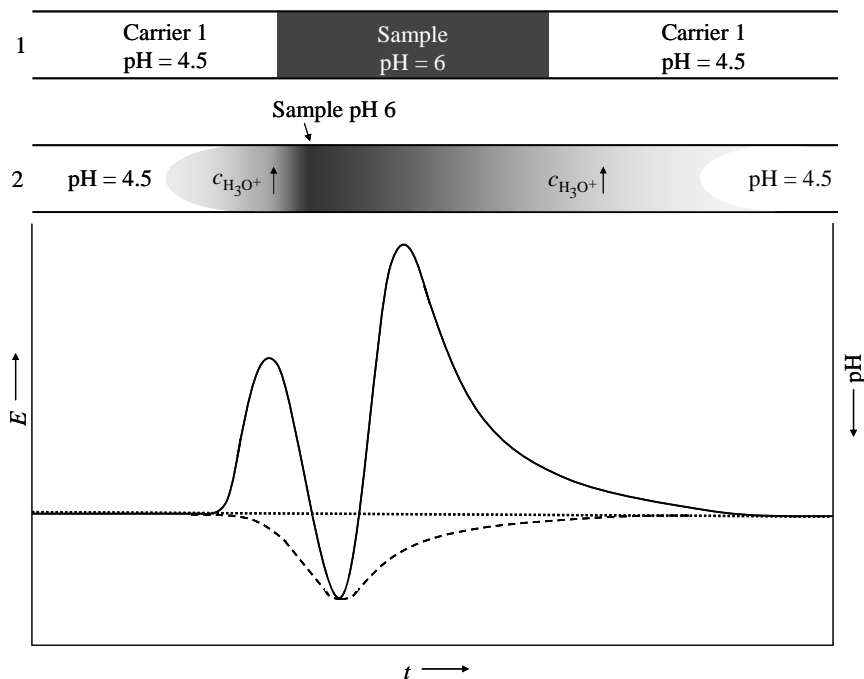


Figure II-11: Potentiometric peaks obtained for calcium ion solutions injected into (a) carrier solution 1 and (b) carrier solution 2 (injection volume: 150 μL , flow rate: 1.75 mL min^{-1}).

In general, an increase in potential means a decrease in pH according to the function of the quinhydrone electrode (cf. Chapter 2.1.3.2). Obviously, the peaks of the same calcium concentration obtained in case of carrier solution 1 were smaller than in case of carrier solution 2. Furthermore, the peak shape obtained in case of carrier solution 1 was more complex than in case of carrier solution 2. In case of carrier solution 2 single peaks

occurred, whereas in case of carrier solution 1 double peaks appeared. A schematic explanation for the peak shape is given in Figure II-12a and II-12b.

(a)



(b)

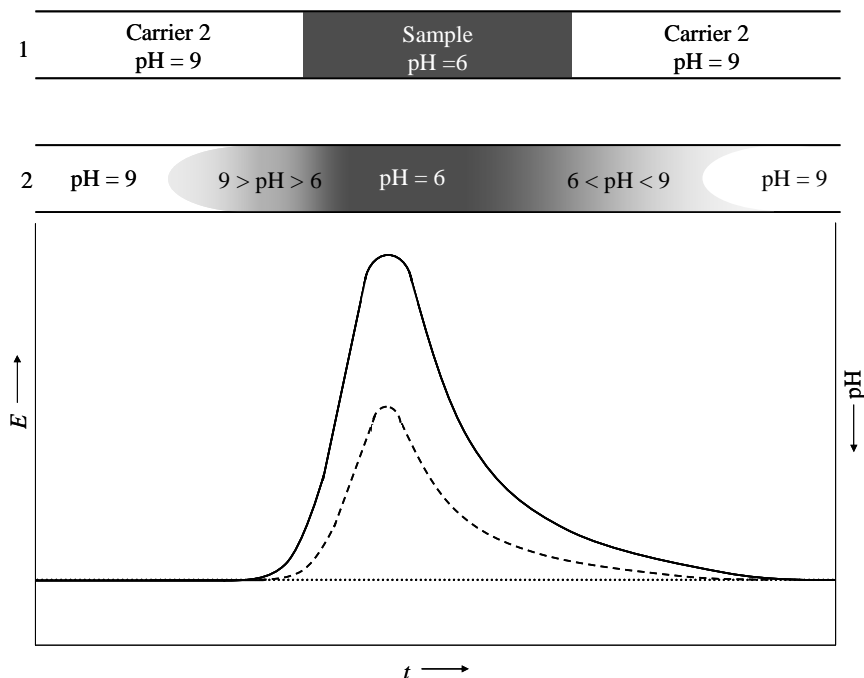


Figure II-12: Schematic explanation of the obtained peak shape (a) in case of carrier solution 1 and (b) in case of carrier solution 2. Dotted line: baseline without sample injection, dashed line: injection of a sample without calcium or magnesium ions, full line: injection of a sample with calcium or magnesium ions.

The pH of carrier solution 1 (pH = 4.5) is slightly lower than the pH of the calcium containing solutions (pH = 6). If no reaction would occur between the carrier solution and the sample, one had to expect that the potential will slightly decrease when the sample passes the detector and it will slightly increase when the carrier passes the detector, respectively. That means that a negative peak will appear (cf. dashed line in Figure II-12a). However, after injection of the calcium solution into the carrier solution a dispersion zone is formed on both sides of the sample solution. In the dispersion zone, a complex is formed between the calcium ions of the sample solution and the EDTA of the carrier solution according to the following reaction:



Due to the proton release by the complexation, the pH in the dispersion zone decreases and thus the potential of the quinhydrone electrode increases depending on the proton release and hence on the concentration of calcium ions. In the centre of the sample zone, the concentration of reagent (EDTA) diminishes and hence the proton release decreases. Because of the higher pH of the sample solution the pH increases and the potential decreases. The extent to which the potential decreases in the centre of the sample zone depends on the concentration of calcium ions. Then, the pH decreases and thus the potential increases again, when the backside of the dispersion zone passes the detector, before the potential decreases again to the baseline potential (cf. full line in Figure II-12a). The appearance of double peaks during FIA titrations has already been described in the literature and has been traced back to the lack of reagent in the centre of the injected sample zone [21].

In case of carrier solution 2, the EDTA has a higher pH value than the sample solution (cf. Figure II-12b). The difference of the pH values is about 3. If no reaction would occur between the carrier solution and the sample, one had to expect that the potential increases when the sample passes the detector according to the lower pH of the sample (cf. dashed line in Figure II-12b). However, after injection of the calcium containing sample solution, the mixing of sample and carrier solution starts in the dispersion zone, and thus a complexation of calcium ions with EDTA takes place according to the following reaction:



While the complexation reaction occurs in the dispersion zones, protons are released and the slope of the increasing potential must depend on the amount of released protons and hence on the calcium ion concentration (cf. full line in Figure II-12b). The higher the calcium ion concentration, the more calcium ions can react with EDTA, and hence the more protons can be released and the steeper the slope will be. This holds true for the backside of the dispersion zone, too. This means that the peak area depends on the extent of reaction II-24 and hence on the calcium ion concentration. Whereas the concentration of protons increases in the dispersion zones, the pH value of the sample zone is lower than in the dispersion zones and hence a decrease in potential in the centre of the sample zone is not observable and no double peaks appear.

At very low calcium concentrations (lower than $1 \cdot 10^{-4} \text{ mol L}^{-1}$), negative peaks were observed also in case of carrier solution 2. This was somewhat surprising. To explain this phenomenon 25 mL of the carrier solution 2 were successively diluted in a beaker and the pH was measured with a glass electrode after each dilution step (cf. Table II-6).

Table II-6: Dependence of the pH of carrier solution 2 ($0.02 \text{ mol L}^{-1} \text{ HY}^{3-}$, Merck) on its dilution with ultrapure water.

$V(\text{H}_2\text{O})_{\text{add}}$ [mL]	pH
0	8.94
5	8.96
10	9.04
15	9.08
20	9.12
25	9.14

Table II-6 clearly shows that when diluting carrier solution 2 in a beaker an increase in the pH of the solution was observed, too; i.e., the appearance of negative peaks could be caused by a simple dilution of the carrier solution in the sample zone. Besides, at low calcium concentration the amount of proton release in the dispersion zones is too small to compensate the dilution effect and thus no increase of the potential can be observed.

Since the peaks obtained with carrier solution 2 were less complex and better quantifiable, this carrier solution was used for further experiments.

4.3.2 Calibration curves

In a first series of experiments, the dependence of the peak area on the calcium ion concentration had to be investigated. Therefore, solutions of calcium chloride in a concentration range from $1 \cdot 10^{-5} \text{ mol L}^{-1}$ to $5 \cdot 10^{-2} \text{ mol L}^{-1}$ were prepared. All standard solutions contained 0.01 mol L^{-1} KCl and the pH of all standard solutions was adjusted to 6. The standard solutions were injected into carrier solution 2 (Merck) and potentiometric measurements were performed. The peak areas of the recorded peaks were determined and they were plotted against the calcium ion concentrations. A typical calibration curve is given in Figure II-13.

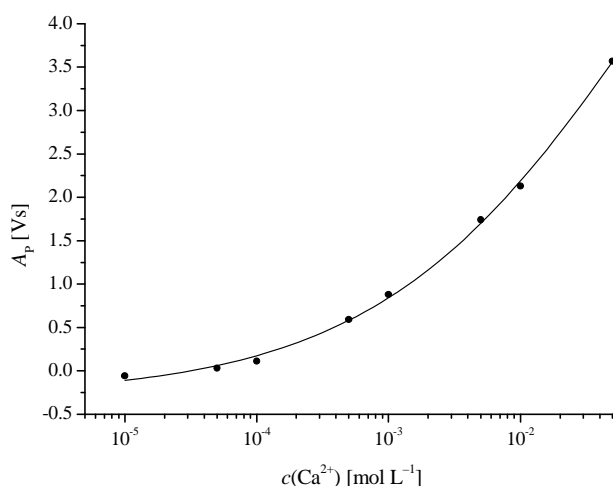


Figure II-13: Dependence of the peak area A_p on the concentration of calcium ions in solutions (by using CaCl_2) in case of carrier solution 2 (injection volume: $150 \mu\text{L}$, flow rate: 1.75 mL min^{-1}).

As Figure II-13 shows, a non-linear calibration curve was obtained. In fact, the calibration curve could be fitted best by a sigmoidal growth function of the type:

$$y = \frac{A_1 - A_2}{1 + (x/x_0)^p} + A_2 \quad (\text{II-25})$$

with A_1 : initial y-value

A_2 : final y-value

p : power

x_0 : centre (x -value of the inflection point of the sigmoidal curve).

Furthermore, it had to be studied, if there is a difference of the peak areas obtained with calcium ions containing solutions and the peak areas obtained with magnesium ions containing solutions. Also, the effect of the anion of the calcium and magnesium salts on the peak area was investigated. Therefore, calibration curves were recorded with different magnesium and calcium salts in a concentration range from $1 \cdot 10^{-5} \text{ mol L}^{-1}$ to $1 \cdot 10^{-2} \text{ mol L}^{-1}$, in the same way as described before for the case of calcium chloride. Beside calcium chloride, the following other calcium and magnesium salts were used: calcium sulphate, calcium nitrate, magnesium chloride, magnesium sulphate and magnesium nitrate. In Figure II-14 the calibration curves obtained for the different calcium and magnesium salts are shown.

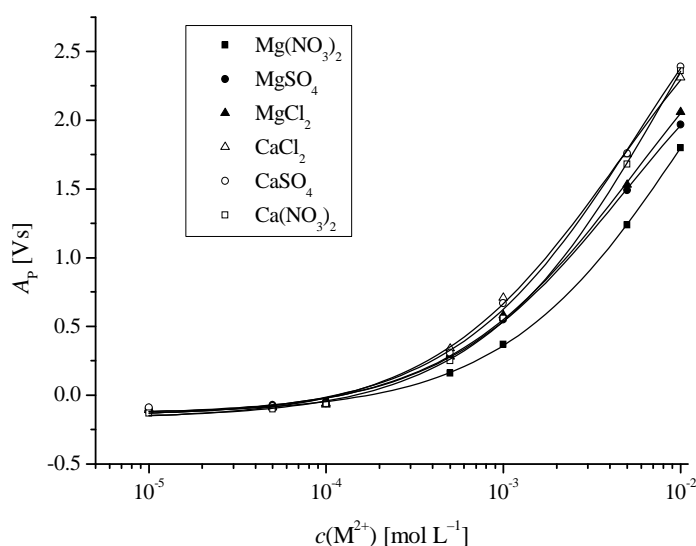


Figure II-14: Dependence of the peak area A_p on the concentration of calcium and magnesium ions in solutions of different calcium and magnesium salts (carrier solution 2, injection volume: $150 \mu\text{L}$, flow rate: 1.75 mL min^{-1}).

Again, it was established that a sigmoidal growth function according to Equation II-25 is most suitable to describe the shape of the calibration curves. The parameters of the function for the calibration curves of the different calcium and magnesium salts are shown in Table II-7.

Table II-7: Parameters for calibration curves with different calcium and magnesium salts.

	A_1	A_2	x_0	p
Ca(NO₃)₂	-0.17	4.66	0.009	0.81
CaSO₄	-0.15	4.02	0.006	0.83
CaCl₂	-0.17	3.55	0.004	0.83
Mg(NO₃)₂	-0.13	4.05	0.012	0.81
MgSO₄	-0.14	3.12	0.005	0.84
MgCl₂	-0.15	3.45	0.006	0.81

It is not only that Equation II-25 gave the best fit of the experimental data, but also some calibration curves really showed at the highest concentrations a decrease of slope as it is expected for a sigmoidal curve, so that the choice of Equation II-25 is additionally supported. Further, at calcium concentrations exceeding the concentration of EDTA salt, the signal must become constant for reasons of stoichiometry.

As expected, the kind of anion has no influence on the calibration curve (cf. Figure II-14 and Table II-7). However, small differences of the calibration curves for calcium and magnesium ions are observed. At concentrations higher than $1 \cdot 10^{-4} \text{ mol L}^{-1}$, the peak areas obtained for calcium salts were slightly larger than the peak areas obtained for magnesium salts of the same concentration. This small differences of the calibration curves were most probably due to different conventional stability constants of the EDTA complex of magnesium ions ($\log K(\text{Mg}^{2+}) = 8.79$ for $I = 0.1$ at 20°C [113]) and of the EDTA complex of calcium ions ($\log K(\text{Ca}^{2+}) = 10.69$ for $I = 0.1$ at 20°C [113]). The higher the conventional stability constant, the larger is the extend of complex formation and thus the more hydronium ions are released, which cause an increase of the potential. Because of the higher stability constant of the Ca^{2+} -EDTA-complex compared to the Mg^{2+} -EDTA-complex, the production of hydronium ions was higher in case of calcium solutions, and hence the signals obtained with calcium solutions were slightly larger than the signals obtained with magnesium solutions.

Consequently, for the determination of the total hardness the calibration had to be performed with solutions containing a mixture of calcium and magnesium ions, whereas for the determination of the calcium hardness, solutions which only contain calcium ions had to be used to calibrate the system. An unknown concentration of the mixture of calcium and magnesium ions or an unknown concentration of only calcium ions can be calculated with Equation II-25 by using the fitting parameters from the respective calibration curve.

4.3.3 pH sensitivity

For automatic real sample analysis it is interesting, how sensitive the method is with respect to sample pH. Therefore, solutions of calcium nitrate using three different concentrations were prepared ($c_1(\text{Ca}^{2+}) = 1 \cdot 10^{-3} \text{ mol L}^{-1}$, $c_2(\text{Ca}^{2+}) = 5 \cdot 10^{-3} \text{ mol L}^{-1}$, $c_3(\text{Ca}^{2+}) = 1 \cdot 10^{-2} \text{ mol L}^{-1}$) and the pH values of each solution was varied between 3 and 9. The FIA system was calibrated with calcium nitrate solutions in a concentration range from $1 \cdot 10^{-5} \text{ mol L}^{-1}$ to $1 \cdot 10^{-2} \text{ mol L}^{-1}$. The pH of all standard solutions was adjusted to 6. All standard solutions and all sample solutions contained $1 \cdot 10^{-2} \text{ mol L}^{-1}$ KCl. Table II-8 gives the determined calcium ion concentrations depending on the pH.

Table II-8: Measured calcium ion concentration depending on the pH of the sample solution (carrier solution 2).

$c(\text{Ca}^{2+})_{\text{given}} = 0.01 \text{ mol L}^{-1}$		$c(\text{Ca}^{2+})_{\text{given}} = 0.005 \text{ mol L}^{-1}$		$c(\text{Ca}^{2+})_{\text{given}} = 0.001 \text{ mol L}^{-1}$	
pH	$c(\text{Ca}^{2+})_{\text{exp}} [\text{mol L}^{-1}]$	pH	$c(\text{Ca}^{2+})_{\text{exp}} [\text{mol L}^{-1}]$	pH	$c(\text{Ca}^{2+})_{\text{exp}} [\text{mol L}^{-1}]$
3.06	0.160	3.06	0.0079	3.02	0.0030
4.09	0.010	4.04	0.0052	3.97	0.0011
4.91	0.010	4.88	0.0050	4.87	0.0010
5.40	0.010	5.63	0.0050	5.34	0.0010
6.02	0.010	6.38	0.0051	5.89	0.0010
7.09	0.010	6.80	0.0050	6.98	0.0010
8.11	0.010	7.90	0.0047	7.84	0.0010
9.19	0.011	9.09	0.0048	9.19	0.0009

Interestingly, the influence of sample pH was negligible over a large range, namely from pH 4.5 to 7.0. To explain this, two effects have to be considered, which influence the peak area in FIA titrations: On one side, the peak area depends on the acidity of the sample solution and on the other side the effective stability constant and thus the complexation in the dispersion zone depends on the pH of the solution. If no complexation would take place, the peak area would increase with decreasing pH of the sample solution. However, in complexation reactions the effective stability constant plays an important role. The effective stability constant is the lower, the lower the pH of the sample solution is, i.e., with decreasing pH values less amounts of complex are formed and thus less hydronium ions are released during complexation. In case of more alkaline sample solutions, the peak areas caused only by the pH of the sample solution would be smaller, but the effective

stability constants increase, and hence more protons are released, so that the peak areas are increasing.

For practical applications, the pH independence of the peak area in the range from pH 4.5 to pH 7 is very convenient, because the pH of many water samples lies in that range, i.e., the pH of such sample solutions has not to be adjusted. Only if the pH of the sample solution is out of the mentioned range, the pH has to be adjusted.

4.3.4 Determination of the detection limit, the dynamic working range and the precision

For the determination of the detection limits for calcium and the sum of calcium and magnesium ions, calibration curves were recorded. Therefore solutions were prepared, which contained on one side calcium ions only and on the other side equimolar amounts of calcium and magnesium ions in a concentration range ($c(M^{2+})$) from $1 \cdot 10^{-5} \text{ mol L}^{-1}$ to $5 \cdot 10^{-1} \text{ mol L}^{-1}$. $1 \cdot 10^{-2} \text{ mol L}^{-1}$ KCl was added to all standard solutions. In Figure II-15, the obtained sigmoidal calibration curves are given.

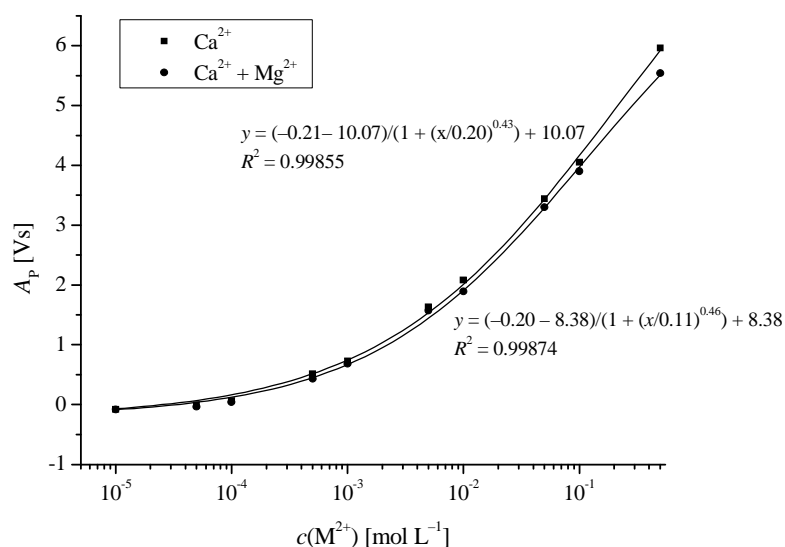


Figure II-15: Dependence of the peak area A_p on the concentration of calcium ions and on the concentration of the sum of calcium and magnesium ions respectively (carrier solution 2, injection volume: $150 \mu\text{L}$, flow rate: 1.75 mL min^{-1}).

Afterwards, a blank solution, i.e., ultrapure water with $1 \cdot 10^{-2} \text{ mol L}^{-1} \text{ KCl}$, was injected into the carrier solution 2 ten times. Figure II-16 shows the obtained peaks.

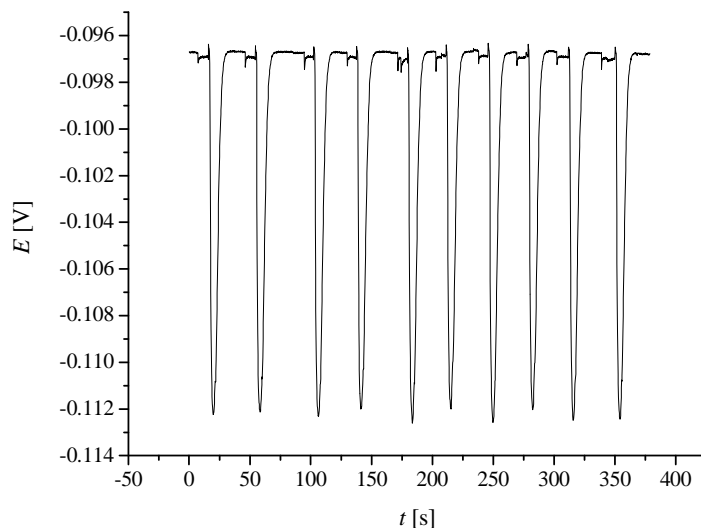


Figure II-16: Potentiometric peaks obtained for the blank solution (ultrapure water with $1 \cdot 10^{-2} \text{ mol L}^{-1} \text{ KCl}$) injected into carrier solution 2 ten times (injection volume: $150 \mu\text{L}$, flow rate: 1.75 mL min^{-1}).

The mean and standard deviation of the obtained peak areas was calculated as follows:

$$\text{mean} = -0.095 \text{ Vs}$$

$$\text{standard deviation} = -0.002 \text{ Vs } (\sim 2\%).$$

Using this values and the functions of the calibration curves, the lowest detection limits (3σ) were calculated as $7 \cdot 10^{-6} \text{ mol L}^{-1}$ for calcium and as $9 \cdot 10^{-6} \text{ mol L}^{-1}$ for the sum of calcium and magnesium ions, respectively. By means of the obtained calibration curves and the tenfold injections of the blank solution, it was found that for calcium and the sum of calcium and magnesium ions the dynamic working range extends to at least four orders of magnitude with a standard deviation of 2% (maximum deviation for small concentrations). Of course, the precision depends on the fitting parameters of the calibration curve (cf. Chapter 4.3.2). The larger the difference between A_1 and A_2 , the larger p and the better the unknown concentration approaches x_0 , the better is the precision.

4.3.5 Measuring of sample solutions

Different water samples were analysed with respect to the content of the sum of calcium and magnesium ions and with respect to the content of calcium ions separately, using the FIA system. In parallel, also batch titrations were performed for the sake of comparison.

To determine the sum of calcium and magnesium ions, the FIA system was calibrated with equimolar calcium nitrate and magnesium nitrate solutions in a concentration range from $5 \cdot 10^{-6} \text{ mol L}^{-1}$ to $2.5 \cdot 10^{-2} \text{ mol L}^{-1}$, respectively. The mixture of both ions was used to eliminate slight deviations due to slight differences in the calibration curves of separate calcium and magnesium ion solutions (cf. Chapter 4.3.2). After addition of 0.01 mol L^{-1} KCl, the water samples were injected in the FIA system without any further pre-treatment, and the sum of calcium and magnesium ions was determined.

To determine the calcium ion content separately, the FIA system was calibrated by using calcium ion solutions in a concentrations range from $1 \cdot 10^{-5} \text{ mol L}^{-1}$ to $5 \cdot 10^{-2} \text{ mol L}^{-1}$. After removing magnesium ions (cf. Chapter 3.3.3.1) and addition of $1 \cdot 10^{-2} \text{ mol L}^{-1}$ KCl, the water samples were injected in the FIA system, and the calcium ion concentration was determined. The results of FIA and batch titrations for synthetic water sample, mineral water, river water and drinking water are compared in Table II-9.

Table II-9: Comparison of the results of different water samples obtained with batch titrations and FIA titrations (number of replication is 3).

	$c(\text{Ca}^{2+} + \text{Mg}^{2+}) [\text{mmol L}^{-1}]$		$c(\text{Ca}^{2+}) [\text{mmol L}^{-1}]$	
	Batch	FIA	Batch	FIA
Synthetic water	4.49 ± 0.01	4.52 ± 0.05	2.03 ± 0.01	1.90 ± 0.01
Drinking water	3.28 ± 0.04	3.44 ± 0.14	2.59 ± 0.02	2.35 ± 0.10
Mineral water	2.94 ± 0.02	3.16 ± 0.02	1.52 ± 0.06	1.30 ± 0.01
River water	3.37 ± 0.01	3.52 ± 0.08	1.75 ± 0.13	2.32 ± 0.07

Table II-9 shows that a rather good agreement could be achieved between the FIA results and batch titrations. By applying a student's *t*-test it was confirmed that there is no statistically significant difference of the results obtained by FIA and batch titrations ($p = 0.95$).

4.4 Determination of titratable acidity and pH of wine

4.4.1 Titratable acidity of wine

4.4.1.1 Batch titration

Conventional potentiometric batch titrations of different wine samples were performed for the sake of comparison. Typical titration curves were obtained (cf. Figure II-17).

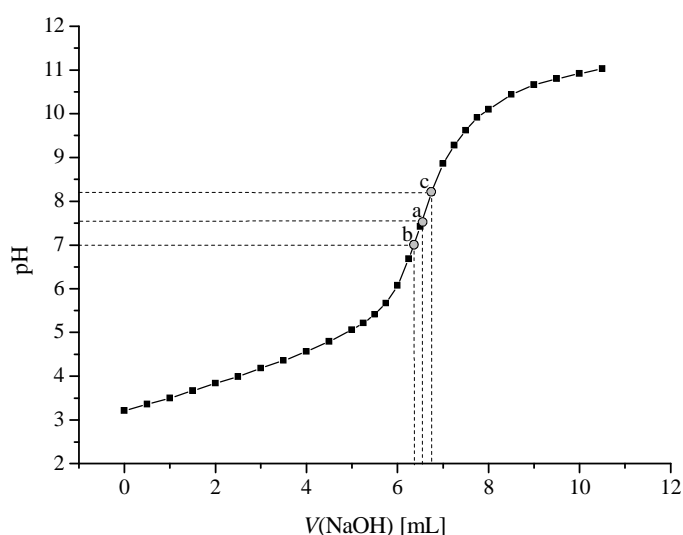


Figure II-17: Titration curve obtained for a classical acid-base titration of a white wine using a solution of 0.1 mol L^{-1} NaOH as titrant (volume of sample solution: 10 mL); **(a)**: equivalence point determined from the zero crossing of the second derivative of the titration curve, **(b)**: pH 7 is used as endpoint of the titration, **(c)**: pH 8.2 is used as endpoint of the titration.

The equivalence point was determined from the zero crossing of the second derivative plot of the titration curve, and from the consumption of sodium hydroxide the titratable hydronium ion concentration $c(\text{H}_3\text{O}^+)$ in the wine sample was evaluated. Figure II-17a shows the determined equivalence point in the titration curve. Furthermore, the endpoint obtained for the titration up to pH 7 and the endpoint for the titration up to pH 8.2 are marked in Figure II-17. To calculate the titratable acidity expressed as

g L^{-1} tartaric acid, the following formula was applied ($150.09 \text{ g mol}^{-1}$ is the molar mass of tartaric acid [107]):

$$\text{titratable acidity } [\text{g L}^{-1} \text{ tartaric acid}] = c(\text{H}_3\text{O}^+) \cdot \frac{150.09 \text{ g mol}^{-1}}{2}. \quad (\text{II-26})$$

For each wine sample, three batch titrations were executed. The results are shown in Table II-10. The table shows the results of batch titrations (i) for titration until the real equivalence point, (ii) for the titration up to pH 7.0, (iii) for the titration up to pH 8.2.

Table II-10: Comparison of the results of different wine samples obtained for titration until the real equivalence point (EP), for the titration up to pH 7.0 and for the titration up to pH 8.2.

	Titratable acidity in $\text{mmol L}^{-1} \text{H}_3\text{O}^+$ (and in brackets in g L^{-1} tartaric acid)		
	EP	pH 7	pH 8.2
Red wine 1	68.0 (5.10)	66.2 (4.97)	72.0 (5.40)
Red wine 2	63.3 (4.75)	62.6 (4.70)	67.4 (5.06)
Red wine 3	73.8 (5.54)	69.7 (5.23)	75.9 (5.70)
Red wine 4	74.2 (5.57)	71.9 (5.40)	75.8 (5.69)
White wine 1	65.7 (4.93)	63.9 (4.80)	67.6 (5.07)
White wine 2	67.8 (5.09)	65.1 (4.89)	69.1 (5.19)
White wine 3	82.8 (6.21)	78.5 (5.89)	83.2 (6.24)
White wine 4	81.5 (6.12)	78.9 (5.92)	82.6 (6.20)
Rosé wine	63.1 (4.74)	59.6 (4.47)	63.9 (4.80)

It is shown that for all three methods of endpoint determination, different values of the titratable acidity were obtained. Neither by titration up to pH 7 nor by titration up to pH 8.2, the true value of titratable acidity is determined; in fact, the pH of the true endpoint was different for each wine and was between pH 7 and pH 8 [91]. By analysing the zero crossing of the second derivative plot of the titration curve to determine the endpoint, a good approximation to the true endpoint was obtained.

4.4.1.2 FIA titration

4.4.1.2.1 Matrix simulation of wine

In preliminary experiments with water as solvent, very well reproducible peaks were obtained, but a systematic and highly reproducible deviation between the results obtained with FIA and batch titrations were observed. The main reason for that lies in the fact that wine is a very complex matrix containing constituents which obviously interfere in the sensor response.

One of the main redox systems in wine are phenols. In Table II-11, further examples of typical redox systems in wine and their standard potentials E^\ominus are given [92].

Table II-11: Typical redox systems found in wine and the corresponding standard potentials E^\ominus at pH 3.5 [92].

Reaction	E^\ominus in V
$1/2 \text{O}_2 + 2 \text{H}^+ + 2 \text{e}^- \rightleftharpoons \text{H}_2\text{O}$	1.022
$\text{Fe}^{3+} + \text{e}^- \rightleftharpoons \text{Fe}^{2+}$	0.771
$\text{O}_2 + 2 \text{H}^+ + 2 \text{e}^- \rightleftharpoons \text{H}_2\text{O}_2$	0.475
Dehydroascorbate + $2 \text{H}^+ + 2 \text{e}^- \rightleftharpoons$ ascorbate	0.267
Fumarate + $2 \text{H}^+ + 2 \text{e}^- \rightleftharpoons$ succinate	0.237
$\text{Cu}^{2+} + \text{e}^- \rightleftharpoons \text{Cu}^+$	0.158
Oxaloacetate + $2 \text{H}^+ + 2 \text{e}^- \rightleftharpoons$ malate	0.105
Acetaldehyde + $2 \text{H}^+ + 2 \text{e}^- \rightleftharpoons$ ethanol	0.044
Pyruvate + $2 \text{H}^+ + 2 \text{e}^- \rightleftharpoons$ lactate	0.027
Acetyl-CoA + $2 \text{H}^+ + 2 \text{e}^- \rightleftharpoons$ acetaldehyde + CoA	-0.203
$\text{SO}_4^{2-} + 4 \text{H}^+ + 2 \text{e}^- \rightleftharpoons \text{H}_2\text{SO}_3 + \text{H}_2\text{O}$	-0.244
Acetate + $2 \text{H}^+ + 2 \text{e}^- \rightleftharpoons$ acetaldehyde	-0.390

Of course, redox systems can disturb the response of the used graphite/quinhydrone/polysiloxane composite electrode since quinhydrone is a redox system itself. To confirm this assumption a white wine sample, an aqueous solution of DL-malic acid and a solution of DL-malic acid dissolved in a white wine titrated to the equivalence point were titrated with 0.5 mol L^{-1} NaOH and the redox potential E_{redox} was measured after each NaOH addition using a platinum electrode in conjunction with a common reference electrode (cf. Figure II-18). The hydronium ion concentration of the DL-

malic acid solutions was similar to the hydronium ion concentration in the wine. The redox potential in such a malic acid solution must change after NaOH addition, because malic acid is in chemical equilibrium with malate and malate/oxaloacetate is a redox system, the potential of which is dependent on the pH of the solution (hydronium ions are involved in the electrochemical equilibrium).

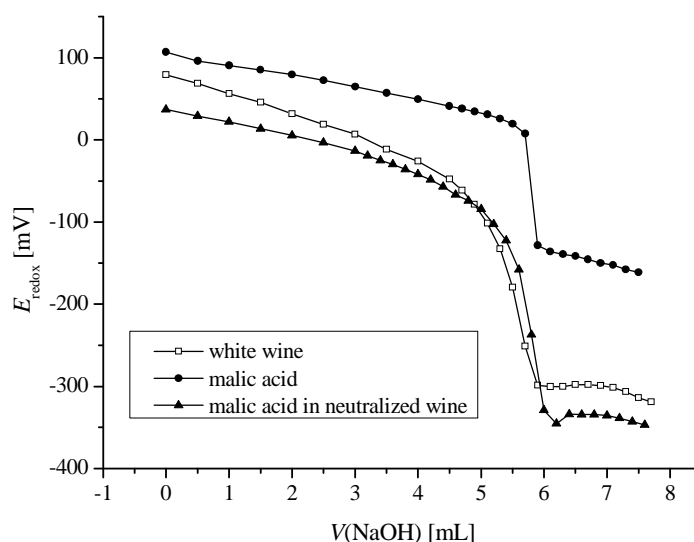


Figure II-18: Dependence of the redox potential E_{redox} vs. Ag/AgCl (3 M KCl) on the volume of 0.5 mol L^{-1} NaOH added to (i) aqueous solution of DL-malic acid, (ii) DL-malic acid dissolved in wine titrated to equivalence point and (iii) wine (volume of sample solution: 40 mL).

In Figure II-18, it is shown that the curves of the aqueous solution of DL-malic acid and wine had similar shape, but the redox potential in dependence of the added NaOH volume was shifted. In case of the wine sample, the potential jump at the equivalence point was larger than in case of the aqueous DL-malic acid solution. The differences of the redox potential indicated that additional redox systems were present in wine, which affected the quinhydrone response of the sensor. When DL-malic acid was dissolved in white wine titrated to the equivalence point, the titration curve approached the titration curve of the wine (cf. Figure II-18).

Consequently, the matrix of the standard solutions used to calibrate the FIA system has to be similar to the wine matrix. To simulate the matrix of wine, a solution of 4 mol L^{-1} sodium hydroxide was added successively to a wine until the pH of the wine was equal to the pH of its equivalence point (pH ~ 7.5). This wine titrated to the endpoint was

used as solvent for all calibration solutions and as solvent for the dilution of all wine samples.

4.4.1.2.2 Calibration curves

Calibration curves were recorded with solutions of DL-malic acid in a concentration range from $5 \cdot 10^{-4} \text{ mol L}^{-1}$ to $1.25 \cdot 10^{-2} \text{ mol L}^{-1}$. This range corresponds to hydronium ion concentrations between $1 \cdot 10^{-3} \text{ mol L}^{-1}$ and $2.5 \cdot 10^{-2} \text{ mol L}^{-1}$, because malic acid is a dibasic acid. All standard solutions contained $1 \cdot 10^{-2} \text{ mol L}^{-1}$ KCl. As solvents, white wines as well as red wines titrated to the equivalence point were used, respectively. Asymmetric peak shaped signals, which are typical for FIA titrations, were recorded (cf. Figure II-19).

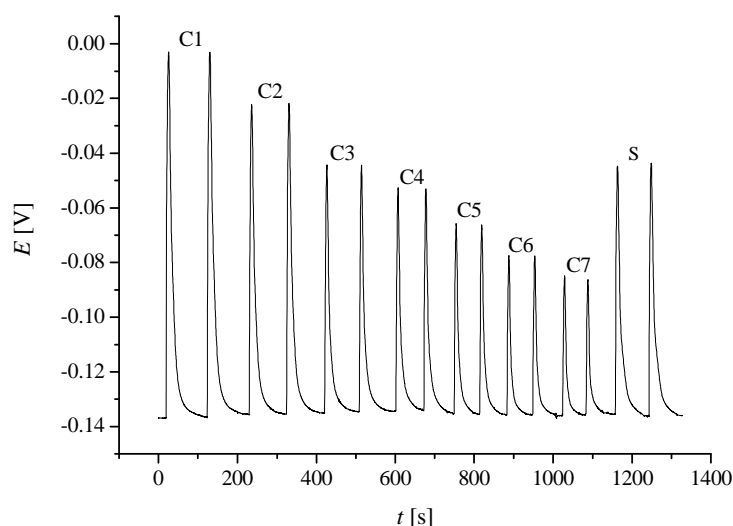


Figure II-19: Potentiometric peaks obtained for calibration solutions (C1 to C7) and wine sample solutions (S) injected into the carrier solution ($5 \cdot 10^{-3} \text{ mol L}^{-1}$ NaOH + $1 \cdot 10^{-2} \text{ mol L}^{-1}$ KCl) (injection volume: $150 \mu\text{L}$, flow rate: 1.75 mL min^{-1}). C1: $1.25 \cdot 10^{-2} \text{ M}$ DL-malic acid, C2: $8.75 \cdot 10^{-3} \text{ M}$ DL-malic acid, C3: $5 \cdot 10^{-3} \text{ M}$ DL-malic acid, C4: $3.75 \cdot 10^{-3} \text{ M}$ DL-malic acid, C5: $2.5 \cdot 10^{-3} \text{ M}$ DL-malic acid, C6: $1.25 \cdot 10^{-3} \text{ M}$ DL-malic acid, C7: $5 \cdot 10^{-4} \text{ M}$ DL-malic acid.

The peak area A_P was used for calibration. With both solvents, comparable calibration curves were obtained: linear dependencies of A_P on the hydronium ion concentration were observed (cf. Figure II-20).

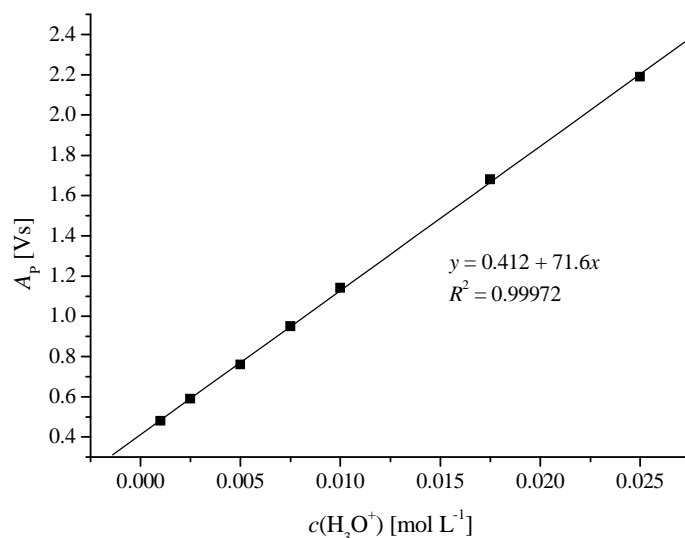


Figure II-20: Dependence of peak area A_p on the concentration of hydronium ions in the solution. White wine adjusted to pH 7.5 was used as solvent (carrier solution: $5 \cdot 10^{-3} \text{ mol L}^{-1} \text{ NaOH} + 1 \cdot 10^{-2} \text{ mol L}^{-1} \text{ KCl}$, injection volume: $150 \mu\text{L}$, flow rate: 1.75 mL min^{-1}).

4.4.1.2.3 Measuring of wine samples

After purging with nitrogen, the wine samples were diluted by a factor of 5 in a volume flask using the same white wine titrated to the EP as solvent as for the calibration solutions. The diluted wine solutions were injected into the FIA system and the hydronium ion concentration was calculated using the calibration equation and taking into account the dilution of the wine. Equation II-26 (cf. Chapter 4.4.1.1) was applied to calculate the titratable acidity expressed as g L^{-1} tartaric acid. In Table II-12, the results of FIA titration and batch titration until the real equivalence point for different wine samples are compared.

Table II-12: Comparison of the results of different wine samples obtained with FIA titrations and batch titrations until the real equivalence point (number of replication is 3).

	Titratable acidity in mmol L ⁻¹ H ₃ O ⁺ (and in brackets in g L ⁻¹ tartaric acid)	
	FIA	Batch
Red wine 1	64.8 (4.86)	68.0 (5.10)
Red wine 2	63.6 (4.77)	63.3 (4.75)
Red wine 3	73.3 (5.50)	73.8 (5.54)
Red wine 4	75.9 (5.70)	74.2 (5.57)
White wine 1	67.5 (5.07)	65.7 (4.93)
White wine 2	68.9 (5.17)	67.8 (5.09)
White wine 3	83.3 (6.25)	82.8 (6.21)
White wine 4	79.6 (5.97)	81.5 (6.12)
Rosé wine	66.6 (5.00)	63.1 (4.74)

The results of FIA titrations were in good agreement with the results obtained with batch titrations until the equivalence point. By applying a paired *t*-test, it could be established that for the different wine samples the titratable acidity determined with FIA titration and batch titration to the equivalence point do not differ significantly ($p = 0.98$). Furthermore, the *Organisation Internationale de la Vigne et du Vin* (OIV) requires a reproducibility of 0.3 g L⁻¹ tartaric acid for white and rosé wines and a reproducibility of 0.4 g L⁻¹ tartaric acid for red wines [93]. That means that the differences of the results obtained with FIA titration and batch titration until the real equivalence point were within the specified range for all the wine samples.

However, the legal requirements in the US and Europe require titrations up to pH 8.2 and 7.0, respectively. Thus, the results obtained by FIA titration have to be corrected. Therefore, a solution of DL-malic acid dissolved in white wine titrated to the equivalence point was titrated with NaOH and the pH was measured after each NaOH addition. The consumption of NaOH up to pH 7 and up to pH 8.2 was determined and compared to the NaOH consumption until the real equivalence point, respectively. With respect to the NaOH addition until the real equivalence point, the added NaOH volume amounts to 96.2% in case of titration up to pH 7 and 100.5% in case of titration up to pH 8.2. These correction factors were applied to the FIA titration by multiplying the DL-malic acid concentrations of the calibration curves with 0.962 or 1.005 to determine the titratable acidity of wine samples up to pH 7 or up to pH 8.2, respectively. In Table II-13, the titratable acidity of the wine samples determined by correction of the FIA results and determined by batch titration up to pH 7 and pH 8.2 respectively are compared.

Table II-13: Comparison of the results of different wine samples obtained with FIA titration after multiplication with a correction factor and batch titrations up to pH 7 and pH 8 (number of replication is 3).

	Titratable acidity in mmol L ⁻¹ H ₃ O ⁺ (and in brackets in g L ⁻¹ tartaric acid)			
	Titration to pH 7		Titration to pH 8.2	
	FIA	Batch	FIA	Batch
Red wine 1	62.2 (4.67)	66.2 (4.97)	65.0 (4.88)	72.0 (5.40)
Red wine 2	61.1 (4.59)	62.6 (4.70)	63.8 (4.79)	67.4 (5.06)
Red wine 3	70.6 (5.30)	69.7 (5.23)	73.7 (5.53)	75.9 (5.70)
Red wine 4	72.8 (5.46)	71.9 (5.40)	76.2 (5.72)	75.8 (5.69)
White wine 1	64.8 (4.86)	63.9 (4.80)	67.8 (5.09)	67.6 (5.07)
White wine 2	66.2 (4.97)	65.1 (4.89)	69.1 (5.19)	69.1 (5.19)
White wine 3	79.9 (6.00)	78.5 (5.89)	83.6 (6.27)	83.2 (6.24)
White wine 4	76.4 (5.73)	78.9 (5.92)	80.0 (6.00)	82.6 (6.20)
Rosé wine	63.9 (4.80)	59.6 (4.47)	66.9 (5.02)	63.9 (4.80)

By using the correction values, the FIA results are in good accordance with the results of batch titration up to pH 7 and pH 8.2. The differences were within the range specified by the OIV for nearly all wine samples. Only in case of the titration of red wine 1 up to pH 8.2 and the titration of rosé wine up to pH 7, the differences of the results determined with FIA and batch titrations were outside the required range. While the obtained deviation for the rosé wine was only marginally outside the required range (0.33 g L⁻¹, while only a difference of 0.3 g L⁻¹ is allowed), the deviation for red wine 1 was larger; here, the values determined with FIA titration and batch titration up to pH 8.2 differed by around 0.52 g L⁻¹ tartaric acid, while only a difference of 0.4 g L⁻¹ is allowed according to the requirements of the OIV.

4.4.1.2.4 Determination of the repeatability

The repeatability of the determination of titratable acidity of wine with FIA titrations was studied using a red wine. Four samples of the wine were prepared by purging the wine with nitrogen and diluting the wine using a white wine titrated to the equivalence point as solvent. Each sample was injected into the FIA system three times and the titratable acidity was determined (cf. Table II-14).

Table II-14: Investigation of the repeatability of the determination of titratable acidity of wine by FIA titration. Four samples of one red wine were prepared and injected three times.

	Titratable acidity in mmol L ⁻¹ H ₃ O ⁺ (and in brackets in g L ⁻¹ tartaric acid)			
	Injection 1	Injection 2	Injection 3	Mean
Sample 1	67.9 (5.10)	66.9 (5.02)	67.5 (5.07)	67.4 (5.06)
Sample 2	70.7 (5.31)	70.4 (5.28)	66.2 (4.97)	69.1 (5.19)
Sample 3	66.0 (4.95)	68.3 (5.13)	-*	67.2 (5.04)
Sample 4	67.8 (5.09)	70.4 (5.28)	68.0 (5.10)	68.7 (5.16)

* sample 3 could be injected only twice

Using the mean values of the four samples the titratable acidity of the studied red wine was determined to be 0.0681 ± 0.0009 mol L⁻¹ H₃O⁺ (5.11 ± 0.07 g L⁻¹ tartaric acid), i.e., the standard deviation for the determination of the titratable acidity of wine via FIA titration was less than 1.5%. The obtained deviation fulfilled the requirements of the OIV, which requires a repeatability of 0.07 g L⁻¹ tartaric acid [93].

4.4.2 pH measurements

The pH values of different wine samples were measured under FIA conditions, and the data were compared with pH measurements using a conventional glass electrode.

The FIA system was calibrated using Britton–Robinson buffer solutions in the pH range 2 to 8. Peak shaped signals typical for FIA were obtained and the peak height ΔE_p was used for calibration. By plotting ΔE_p versus pH of the injected buffer solution, a linear dependence with a satisfactory slope of $-51.1 \text{ mV} \cdot (\text{pH})^{-1}$ was observed in a pH range 2 to 6 (cf. Figure II-21).

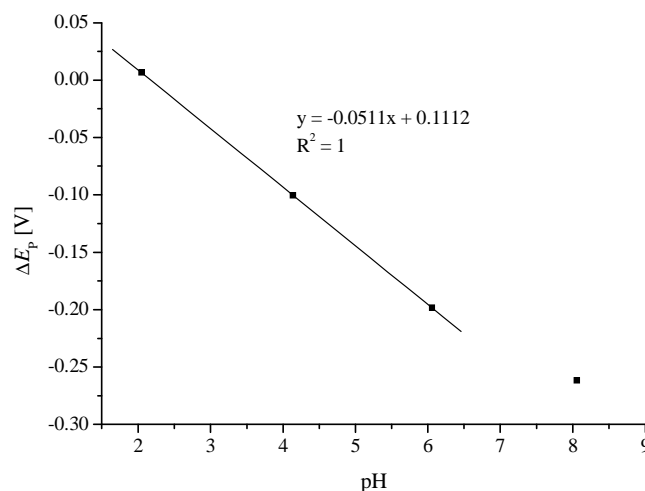


Figure II-21: Dependence of peak height ΔE_P on the pH of the Britton–Robinson buffer solution (carrier solution: $1 \cdot 10^{-2} \text{ mol L}^{-1} \text{ HCl} + 1 \cdot 10^{-2} \text{ mol L}^{-1} \text{ KCl}$, injection volume: $150 \text{ }\mu\text{L}$, flow rate: 1.75 mL min^{-1}).

The obtained slope is smaller than the theoretical value of $-59.2 \text{ mV} \cdot (\text{pH})^{-1}$ (for $T = 25 \text{ }^\circ\text{C}$), because steady state signals were not obtained under the measurement conditions (injection volume: $150 \text{ }\mu\text{L}$) allowing rapid determinations of small sample volumes. As could be shown, for the pH measurements of the wine samples, no steady signals are necessary.

In more alkaline regions, the pH dependence of ΔE_P deviated from the linear behaviour due to the oxidation of the hydroquinone of the graphite/quinhydrone/polysiloxane composite electrode by atmospheric oxygen (cf. Chapter 2.1.3.2) [46]. However, the linear part of the calibration curve can be used for evaluation, because the pH value of wine usually ranges between 2.9 and 4.2 [90]. After injection of the calibration buffers, the samples were injected into the FIA system without any pre-treatment and ΔE_P was determined. The pH values of the wine samples were calculated using the calibration data (cf. Table II-15).

Table II-15: Comparison of the pH values of different wine samples determined with the FIA system and the glass electrode (number of replication is 3).

	pH	
	FIA	Glass electrode
Red wine 1	3.32 ± 0.01	3.32
Red wine 2	3.58 ± 0.04	3.55
Red wine 3	3.71 ± 0.03	3.73
White wine 1	3.26 ± 0.01	3.34
White wine 2	3.23 ± 0.02	3.17

Table II-15 shows that there was a good agreement between the FIA measurements and the batch determinations using a glass electrode (no statistically difference, paired t -test, $p = 0.98$). In Table II-15, also the standard deviations of the threefold pH measurements of the wine samples with the FIA system are given. For most of the studied wines, the standard deviation of the pH values determined with the FIA system was less than 1%, i.e., the pH measurements deviated less than about 0.05 pH units. According to the OIV, a determination within ± 0.05 pH units is necessary, so that the repeatability obtained with the FIA system fulfilled also that requirement of the OIV [93].

5 Conclusions

A flow-through composite electrode based on graphite and quinhydrone was improved by using polysiloxane as binder and was successfully implemented in a FIA system. Compared with electrodes, in which PMMA was used as binder, the polysiloxane electrodes were much easier to handle, whereas the potentiometric response behaviour was comparable with that obtained with PMMA. By using polysiloxane as binder, a hole through the pH sensitive layer can be punctured very easily with the help of a cannula, whereas a drill is has to be employed for making a hole through a pH sensitive layer with PMMA as binder. This is an important advantage for routine analytical use. Further, the pH sensitive layer with polysiloxane as binder is replaceable, so that no new detector cell has to be fabricated when new electrode surfaces are needed.

The modified electrode proved to be a very useful potentiometric detector for FIA acid-base titrations of aqueous solutions. The titration of several acids and bases showed that the calibration curves depend on the pK_a values of the acids or on the pK_b values of the bases, respectively: For the determination of the acid or base content of a sample, it is essential to calibrate the FIA system with an acid or base of a pK_a or pK_b value similar to the pK_a or pK_b value of the analysed acid or base. That is the only way to ensure accurate measurements.

Furthermore, it was demonstrated that the FIA system in conjunction with the graphite/quinhydrone/polysiloxane composite electrode is a useful tool for acid-base titrations in *buffer solutions*. This offers the opportunity to measure activities of enzymes, which produce acids during the enzymatic reaction, in the same way as described already in [24].

New applications of the flow injection system with the graphite/quinhydrone/polysiloxane composite electrode were developed in the area of *water analysis* and *food analysis*. The FIA system was applied to determine the calcium and magnesium content in aqueous solutions (water hardness) by measuring the hydronium ion release during the complexometric reaction between EDTA and calcium or magnesium ions. The method was employed successfully to the analysis of mineral water, drinking water and river water.

Further, a method was established to determine sequentially the titratable acidity and the pH of wine. White wine, red wine as well as rosé wine were analysed. The obtained results were in good agreement with those obtained by classical potentiometric

titrations or by pH measurements using a conventional glass electrode. The new FIA methods fulfil the official requirements of the *Organisation Internationale de la Vigne et du Vin* with respect to reproducibility and repeatability. The developed titration method to determine the acidity of wine can be easily adjusted to the legal requirements in the USA and Europe, which require titrations up to pH 8.2 and 7.0, by introducing a multiplication factor. It is expected that the described methods to determine pH and titratable acidity of wine are easily adaptable to other aqueous drinks like tea, coffee or juice.

The main advantage of the described FIA system with the potentiometric detector based on graphite and quinhydrone lies in the fact that for all the different applications one and same FIA configuration can be used, without changing the detector system. Only different carrier solutions are necessary and can be provided by a proper stream selector. In this thesis, it could be successfully shown that the FIA system in conjunction with the graphite/quinhydrone/polysiloxane composite electrode allows simple, rapid and automated determinations of small sample volumes in the areas of water analysis, food analysis or even biochemical analysis, provided that hydronium ions are involved.

III Modification of gold surfaces for medical applications

1 Introduction

Gold is one of the most important materials in electronic devices [114], for optics [115], in medicine as implants [116] and as electrode material [117, 118] due to its physical and chemical properties as high conductivity, excellent corrosion resistance and high reflecting capacity for infrared radiation.

In electrochemistry, gold electrodes are often used as substrate for various modified electrodes, e.g., gold electrodes modified with self-assembled monolayers (SAMs). It is known that $\cdot\text{OH}$ radicals generated in Fenton solutions dissolve such rather stable SAMs of alkyl thiols on gold. López de Lara Gonzales, Hilgemann and Scholz have used this destructive interaction to detect radicals and radical scavengers [119, 120].

In further studies, Nowicka et al. have investigated the impact of $\cdot\text{OH}$ radicals on mechanically polished gold surfaces. Unexpectedly, they have found that $\cdot\text{OH}$ radicals generated in Fenton solutions smooth mechanically polished gold surfaces by dissolution of the asperities of the gold surface [6]. The smoothing of the surface goes along with a selective knock-out of the electrocatalytically active sites [7]. Since gold is known as a chemically inert metal, the obtained results were all the more surprising. Especially for medical gold implants, the attack of gold by $\cdot\text{OH}$ radicals may play an important role, as it is known that such implants release gold into the surrounding tissue, which is most likely attributed to an immune reaction in which free oxygen radicals are formed [8, 9]. Thus, one aim of this thesis was to investigate, if there is an analogue effect between the exposure of gold to Fenton solutions and the exposure of gold to immune reactions. Furthermore it was an aim to examine, if the release of gold from implants can be reduced by chemical polishing of gold implants with $\cdot\text{OH}$ radicals of Fenton solutions. Therefore, mechanically polished gold pieces and “Fenton-polished” gold pieces were implanted into the peritoneal cavity of mice and the impact on the gold surfaces was analysed by atomic force microscopy (AFM). The animal experiments have been performed by the co-workers of Prof. Jack in the Institute of Immunology and Transfusion Medicine, Greifswald University.

Beside the application to gold implants, the polishing of gold surfaces with $\cdot\text{OH}$ radicals was employed to another medical device based on gold, which has been recently developed by the German company GILUPI GmbH. This company has introduced a functionalized and structured medical wire (FSMW) for the *in vivo* isolation of circulating tumour cells (CTCs) from the peripheral blood of cancer patients [10]. The wire is coated with a gold layer before it is functionalized with an antibody directed to the epithelial cell adhesion molecule (EpCAM), which is present on the surface of most CTCs. For catching CTCs from the blood stream, the FSMW is inserted through a standard venous cannula into the cubital vein of the patient. For such an *in vivo* method, a high sterility of the intravenous device is indispensable. Since autoclaving would partially destroy the hydrogel layer, the FSMW has to be sterilized by gamma irradiation. However, in previous investigations undertaken by GILUPI GmbH, it has been shown that the gold layer is cytotoxic after irradiation with gamma rays. Thus, it is essential to find a method, which diminishes the cytotoxicity of the gold layer below an acceptable level. Only if this goal is achieved, the FSMW can be used for catching specific cells *in vivo*.

As mentioned before, the investigations of Nowicka et al. have clearly shown that highly reactive gold atoms can be dissolved from a gold surface. These reactive gold atoms are most probably responsible for the cytotoxicity of gold. Furthermore, it has been shown that the dissolution of the reactive gold atoms by treatment with Fenton solutions results in a more inert gold surface, from which almost no more gold atoms are dissolved [6].

Hence, a further aim of this thesis was the modification of the gold layer of the FSMW by treating with $\cdot\text{OH}$ radicals purposing no cytotoxicity of the gold layer after gamma irradiation. Two methods of radical generation, namely the Fenton reaction and the UV-photolysis of hydrogen peroxide, were applied and optimized. After treating the gold layer with $\cdot\text{OH}$ radicals, the FSMWs were sterilized by gamma irradiation and the cytotoxicity was determined. In addition, the impact of the $\cdot\text{OH}$ radicals on the gold surface was investigated applying atomic force microscopy (AFM), and the solutions used for the treatment of the FSMWs were analysed by inductively coupled plasma atomic emission spectroscopy (ICP-AES) determining the gold content.

2 Theoretical background

2.1 Free radicals

The term “free radical” cannot be strictly defined; however, one may use this term as denoting any species having an unpaired electron and existing for a certain time period so that it can interact with other chemical species [121, 122]. The simplest, although highly reactive radical is atomic hydrogen (^1H), which contains only one electron and thus the electron must be unpaired.

Free radicals can be formed, e.g., by homolysis or by redox reactions [121, 123]. In case of homolysis, a covalent bond is broken and two radicals are formed from one molecule:



The required energy to dissociate the chemical bond can be provided by heat (thermolysis) or by electromagnetic radiation (photolysis).

Radicals can also be generated by one-electron transfer reactions, e.g., a one-electron oxidation:



or a one-electron reduction:



Because of the unpaired electron, free radicals are paramagnetic and usually highly reactive. They tend to loose the free electron, or to gain another electron for electron pair formation. The latter may also result from dimerization of radicals. The high reactivity of free radicals normally results in very short life times. Only the careful exclusion of reaction partners may be used to increase their life time. Dimerization can be decreased only by dilution of the free radicals. Some free radicals are chemically rather stable and hence quite

unreactive. The stability of these radicals may result from steric protection of the paramagnetic centre by bulky groups or from delocalization of the unpaired electron over many conjugated or aromatic chemical bonds [122].

2.2 Oxygen and its derivatives

Molecular oxygen in its ground state, i.e., triplet oxygen ($^3\Sigma_g^-O_2$), is a radical. It possesses two free electrons with parallel spins, which are located in different antibonding orbitals ($\pi^* 2p$) (cf. Figure III-1). Due to the parallel spin configuration, triplet oxygen is quite unreactive and only a weak oxidant. The oxidation of another atom or molecule by triplet oxygen would be only feasible, if both electrons, which have to be accepted, would have antiparallel spins so that they can pair with the two electrons in the $\pi^* 2p$ orbital of oxygen. However, due to Pauli's principle a pair of electrons in one orbital will not comply with this requirement, because they would have opposite spins [121]. That is the reason why a spin conversion is required for simultaneous two-electron reactions. Since a spin conversion is rather slow [124], most of the reactions involving triplet oxygen are one-electron reactions [125]. This contributes to explain the low reactivity of oxygen with many non-radicals.

However, triplet oxygen can be activated physically by energy-transfer or chemically by electron-transfer, and hence more reactive derivatives of oxygen are formed [126]. The physical activation does not change the number of electrons, but the electron spin is reversed from parallel to antiparallel and an excited state of oxygen results, which is called singlet oxygen [127]. Two forms of singlet oxygen are known, namely delta ($^1\Delta_g O_2$) and sigma ($^1\Sigma_g^+ O_2$). In case of the delta form both electrons occupy the same orbital, while in case of sigma singlet oxygen the electrons are placed in different orbitals (cf. Figure III-1) [124]. Since in both forms of singlet oxygen the spin restriction is eliminated, the oxidizing ability of oxygen is greatly enhanced.

Oxygen can be activated chemically in different ways, namely (i) by the successive addition of electrons to triplet oxygen to form a series of intermediates, (ii) by the reaction of carbon-centred radicals with oxygen, or (iii) by the complexation of oxygen with transition metals, which also contain unpaired electrons.

In a first step of oxygen activation by electron addition the superoxide radical anion ($O_2^{\cdot-}$) is formed via a one-electron reduction process. By addition of a further electron to

the π^* 2p orbital, the peroxide ion (O_2^{2-}) is formed. As Figure III-1 shows, the peroxide ion is not a radical because two electrons have been added to the ground state oxygen [121]. Hydrogen peroxide (H_2O_2) is formed via two-electron reduction of triplet oxygen. If another electron is added to hydrogen peroxide the highly reactive hydroxyl radical ($\cdot\text{OH}$) is generated (cf. Figure III-1) [124].

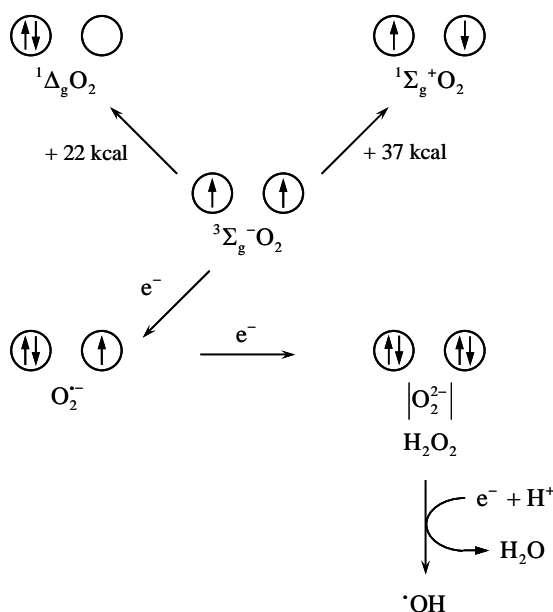


Figure III-1: Spin-orbital diagram of the electron configuration of oxygen and its activated derivatives in the antibonding molecular orbital (π^* 2p) [124, 127].

Water is formed when four electrons are transferred to triplet oxygen (cf. Figure III-2):



This four-electron reduction of oxygen is one of the most important biochemical reactions.

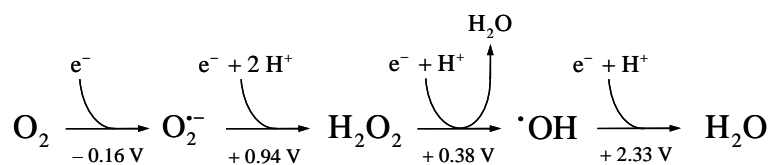


Figure III-2: Reduction of molecular oxygen to water [128].

2.3 Reactive oxygen species (ROS)

The activated oxygen species mentioned before (cf. Chapter 2.2), e.g., singlet oxygen and the intermediates generated during the reduction of oxygen to water, belong to the group of reactive oxygen species (ROS). The term reactive oxygen species is a collective term including oxygen radicals and also non-radical derivatives of oxygen (cf. Table III-1) [121].

Table III-1: Reactive oxygen species [121].

Radicals	Non-radicals
Superoxide anion radical ($\text{O}_2^{\cdot-}$)	Hydrogen peroxide (H_2O_2)
Hydroxyl radical ($\cdot\text{OH}$)	Hypochlorous acid (HOCl)
Peroxyl radical (RO_2^{\cdot})	Ozone (O_3)
Alkoxyl radical (RO^{\cdot})	Singlet oxygen ($^1\Delta_g\text{O}_2$)
Hydroperoxyl radical (HO_2^{\cdot})	Peroxynitrite (ONOO^-)

ROS play an important role in several biological processes, like inflammation, ageing and cancerogenesis. Due to the permanent ROS exposure, aerobic organisms would be damaged continuously. But in the course of evolution the organisms developed several enzymatic or non-enzymatic antioxidant defence systems, which make the life under permanent oxygen exposure possible. However, if the defence systems are strongly perturbed, toxic effects may occur. The oxidative damage caused by reactive oxygen species is called oxidative stress [124].

However, ROS have also positive effects: They play an essential role in immune defence as they can destroy invading microorganisms and activate leucocytes.

2.3.1 Sources of ROS

Various internal and external sources exist contributing to the cellular steady-state concentration of ROS in aerobic organisms: ROS are formed *in vivo* by aerobic metabolic processes in electron transfer chains and by certain enzymes. ROS are also produced in response to stimuli by certain reactions; e.g., oxygen radicals are formed during the respiratory burst. In addition to these internal sources, ROS are formed in the environment

by air pollution, photochemical smog, industrial chemicals and ionising radiation [126]. In the following some internal sources are discussed in more detail.

2.3.1.1 Mitochondrial electron transport chain

In vivo, $O_2^{\bullet -}$ is mainly formed as by-product of the mitochondrial electron flow of the respiratory chain [121, 129]. More than 95% of the oxygen, which is breathed by human organisms, is converted to water via the four-electron reduction process (cf. Chapter 2.2) catalysed by cytochrome oxidase of complex IV in the mitochondrial electron transport chain [130]. However, it has been found that some earlier components of the mitochondrial electron transport chain do leak a few electrons, which react with molecular oxygen and generate $O_2^{\bullet -}$ [121, 130]. The major source of $O_2^{\bullet -}$ within mitochondria *in vivo* is complex I, but also at complex III ROS production occurs [129, 131]. It is estimated that 1–2% of the oxygen consumed during the respiratory chain may be converted to $O_2^{\bullet -}$ [129, 130].

2.3.1.2 Immune system

Phagocytes produce large amount of ROS to kill invading microorganisms during infection defence. Phagocytosis is accompanied by an increased O_2 uptake and consumption by the phagocytes. This phenomenon is called respiratory burst [121]. The respiratory burst observed during phagocytosis results in oxygen activation and formation of reactive species [124]. The initial reaction, in which the additional oxygen of the respiratory burst is converted to $O_2^{\bullet -}$, is catalysed by NADPH oxidase [124, 132]:



The formed $O_2^{\bullet -}$ is converted into H_2O_2 , which undergoes a series of reactions generating HOCl, $\cdot OH$, and 1O_2 [132, 133]. The reactive oxygen species released during phagocytosis can attack macromolecular substances inside the phagocytic vacuole or outside the cell. This way the formed ROS contribute to anti-bacterial, anti-parasitic and

anti-tumour functions. Beside bacteria, also several endogenous substances and xenobiotics can operate as stimulators [124].

ROS serve not only as weapons against invading bacteria, but also as signalling species for leucocytes. By the release of ROS, leucocytes are activated and provided at the source of infection [124].

2.3.1.3 Fenton and Haber–Weiss reaction

Transition metal ions, especially iron and copper ions, play an important role for *in vivo* ROS generation as they catalyse several free-radical reactions [121]. The archetype of such reactions is the so-called Fenton reaction, which was reported firstly by Henry John Horstman Fenton (1854–1929) at the end of the 19th century [134]. The Fenton reaction is based on the decomposition of H₂O₂ by Fe²⁺ under generation of the highly reactive [•]OH radicals:



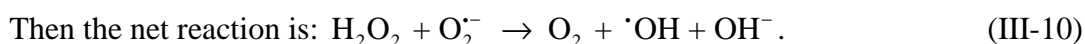
In cells, various forms of iron complexes (chelates) exist (e.g., haem or ADP) facilitating the Fenton reaction *in vivo* [125]. The Fenton reaction is the main source of [•]OH radicals in biological systems. Since the formed [•]OH radical is a non-selective and highly reactive oxidant, it will not diffuse far away from its locus of formation until it attacks almost all organic molecules and can directly damage most biomolecules. Thus, DNA is a particularly favoured target of [•]OH radicals abstracting electrons from the sugar or base moieties as well as transferring electrons to unsaturated bases [128].

Another reaction to produce [•]OH radicals was suggested by Fritz Haber and Richard Willstätter in 1931 [135] and Fritz Haber and Joseph Joshua Weiss in 1932 [136]:



This reaction is now referred to as the Haber–Weiss reaction. Instead of O₂^{•−} these authors wrote HO₂, i.e., the protonated form, but this is nothing essential. The rate constant of the Haber–Weiss reaction in aqueous solution is very small, but can be increased by

employing transition metal ions as catalysts (e.g., Fe^{3+}) [121, 124]. *In vivo* the non-catalytic Haber–Weiss reaction is irrelevant, because of the very low intracellular $\text{O}_2^{\bullet-}$ concentration ($\sim 10^{-10} \text{ mol L}^{-1}$ [137]) [128]. The catalysed Haber–Weiss reaction can be formulated as follows; here with iron ions as catalyst:



2.4 Methods to generate oxygen radicals

Oxygen radicals can be generated by various chemical, physical or enzymatic reactions. Some of the main methods to produce radicals are listed below:

Fenton reaction (cf. Equation III-6)

UV-Photolysis of hydrogen peroxide [138]



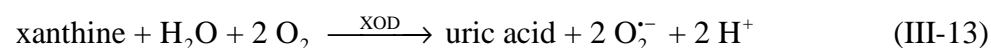
(at $\lambda = 200\text{--}280 \text{ nm}$ [139])

Radiolysis of water [138]



(at ionising radiation, e.g., x-rays, gamma rays [140])

Enzymatic reaction [141, 142]



2.5 Impact of $\cdot\text{OH}$ radicals on electrode surfaces, especially on gold surfaces

Recently, Nowicka et al. have started to investigate the impact of $\cdot\text{OH}$ radicals generated in Fenton solutions on gold surfaces. Although gold is known to be a chemical rather inert metal [61], the results obtained by Nowicka et al. have shown that $\cdot\text{OH}$ radicals attack mechanically polished gold surfaces and dissolve the asperities [6, 143]. The dissolution stops after removal of the asperities. This means that the effect of the Fenton solution upon the gold surface is selective with respect to the asperities, and the smooth gold surface remains unaffected. In further studies, these authors have found that the smoothing of the gold surface goes along with a selective knock-out of the electrocatalytically active sites of gold [7, 143]. These active sites are obviously associated with the asperities, since the removal of the asperities by Fenton solutions renders the gold surface catalytically inactive; i.e., the electron transfer rates (k_s) of electrochemical reactions having radical intermediates are slowed down (cf. Figure III-3).

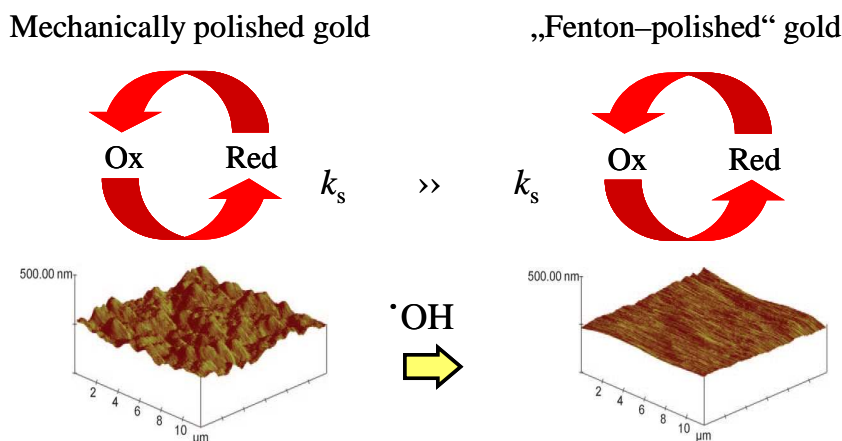


Figure III-3: Scheme of the effect of $\cdot\text{OH}$ radical attack on a gold surface [7].

In additional investigations, Sievers et al. could demonstrate that not only the number of electrocatalytically active sites is diminished by treatment with Fenton solutions, but also the number of active sites for platinum nucleation [144].

Dutta et al. were inspired by the results of Nowicka et al. to study the effect of Fenton solutions on gold nanoparticles (AuNPs) [145]. They have shown that the electrocatalytic activity of AuNPs is also decreased after treatment with $\cdot\text{OH}$ radicals, although no surface alterations were observed.

Feng et al. confirmed the smoothing of a gold surface by radicals in the framework of a study about different pre-treatment methods of a gold electrode, as they observed a decreasing of the roughness factor of a gold surface after treatment with UV and O₃ [146].

Meanwhile, Nowicka et al. extended their studies on the interaction of $\cdot\text{OH}$ radicals with materials to silver, palladium, platinum and glassy carbon. In case of silver, they observed similar effects as in the case of gold [147]. The treatment of glassy carbon electrodes with Fenton solutions led to a loss of activity, although a surface roughening was observed [148]. In contrast, in case of palladium the surface became smoother, while the activity did not change by Fenton treatment [147]. For platinum, no significant changes in roughness and electrochemical activity were obtained after exposure to Fenton solutions [147].

2.6 Circulating tumour cells (CTCs)

Circulating tumour cells (CTCs) discovered by Ashworth in 1869 [149] are malignant cells which are detached from the primary tumour or metastatic sites, circulating freely in the peripheral blood [14, 150]. CTCs can be detected during all tumour stages, including early-stage diseases, in which distant metastases are not yet diagnosable, whereas no CTCs could be detected in healthy persons [10]. If CTCs are present in the blood, their number is usually extremely low. Estimates range from one CTC per 10⁵ to one CTC per 10⁷ mononuclear cells, or even lower in patients with early-stage disease [11–13].

Tumour cells reach the systemic circulation via normal neighbouring vessels, or through newly formed capillaries by tumour-induced angiogenesis [14]. The presence of CTCs in the peripheral blood is in good accordance with the “seed and soil” theory of metastases formation, which was firstly described by Paget in 1889 [151, 152]: After detaching from the primary tumour, tumour cells enter the blood circulation and migrate to distant organs, where they can implant themselves and provoke metastasis formation [11]. During the process of epithelial-mesenchymal transition (EMT) the phenotype of cancer cells changes, what enables their detachment from the primary tumour and transformation into mobile and invasive cells. These mobile cells can invade through the basement membrane and so intravasate into the blood circulation. In the blood circulation, the cells survive intact, come to rest, and then enter the tissue of a secondary organ by extravasation. It is hypothesized that the reverse process called mesenchymal-epithelial

transition (MET) facilitates the adhesion of these tumour cells to the new tissue and the development of the tumour cells into a distant metastasis (cf. Figure III-4) [12, 14].

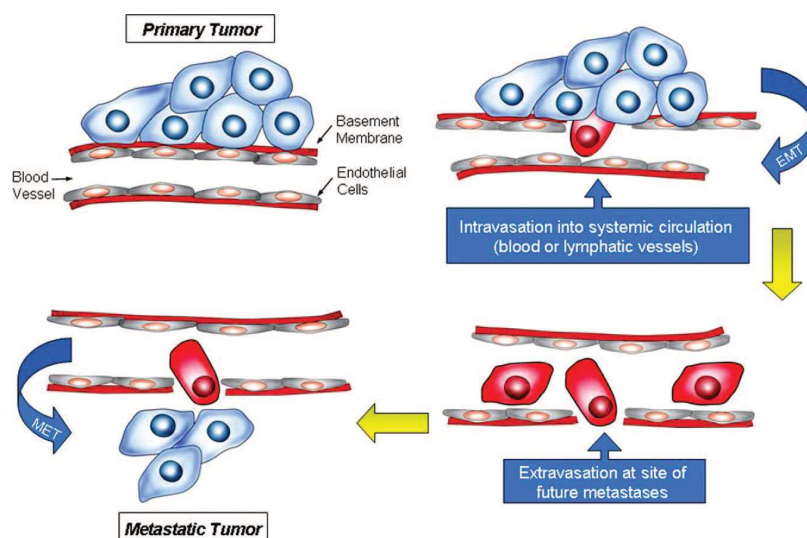


Figure III-4: Schema of the metastatic process [14].

Cells in the peripheral blood possessing the phenotype of cancer are called CTCs [14] and play a crucial role in the metastatic cascade. This is the reason why the detection and analysis of CTCs offers several crucial applications in the field of oncology, e.g., as prognostic marker, as a tool to monitor therapy response, and as a method to understand basic tumour characteristics [14] (cf. Table III-2).

Table III-2: Potential applications of circulating tumour cell analysis [153].

Enumeration of CTCs	Molecular characterisation of CTCs
<ul style="list-style-type: none"> • Guide prognosis • Assist in measuring response to anticancer therapy (predictive and/or pharmacodynamic biomarker) • May lead to more accurate prognosis when added to existing staging classification • Select patients for adjuvant chemotherapy • Detect recurrent disease • Aid diagnostic process 	<ul style="list-style-type: none"> • Surrogate for biological activity of underlying tumour ("real-time biopsy") • Elucidate prognostic and predictive molecular features • Detection of treatment-resistant profiles (ease of serial sampling) • Improve understanding of mechanisms of biological processes • Discover and identify new targets for therapeutic manipulation

For example, the survival prognosis of cancer patients depends strongly on the number of CTCs in the peripheral blood. To point out the correlation between the number of CTCs and the survival in cancer, Cristofanilli et al. performed a multicentre study with breast cancer patients [154]. They demonstrated that patients with 5 or more CTCs per 7.5 mL of blood had a shorter progression-free survival (2.7 months vs. 7.0 months) and shorter overall survival (10.1 months vs. > 18 months) than patients with less than 5 CTCs per 7.5 mL of blood.

2.6.1 Methods to detect and analyse circulating tumour cells

Tumour cells are released in the early-stage of the disease and can be found in the blood before metastases are diagnosed. About 30–40% of the patients afflicted with a localised disease have occult metastases, which are probably originating from CTCs [11]. Thus, the detection and analysis of CTCs play a crucial role in the diagnosis and treatment of cancer. Due to the very low numbers of CTCs in the blood CTC analysis is a very demanding task. High sensitivity and specificity are required [150]. In the last years a lot of new methods have been developed to improve the analysis of CTCs. In the following a short overview is given about the main methods applied for CTC isolation and detection. Several *in vitro* methods for CTC detection are based on the technique of polymerase chain reaction (PCR) [155–157]. Furthermore, image-based immunological approaches [158–160] and flow cytometric techniques [161, 162] were reported. Nagrath et al. described the identification and measurement of CTCs in cancer patients using a microfluidic chip technology [163]. Currently, many *ex vivo* tests to quantify CTCs in the blood of cancer patients use an antibody-coated magnetic particle isolation system targeting the EpCAM, which is present on the surface of most CTCs [154, 164–167]. However, all *ex vivo* methods are limited by the blood volume obtainable from the patients, and the sensitivity of these analysis systems is usually relatively low [10]. Thus, *in vivo* methods are needed, which offer the detection of CTCs in a larger blood volume. In the last decade some *in vivo* methods were described using the principle of flow cytometry with photoacoustic [168, 169] or fluorescent detection systems [170, 171].

2.6.1.1 *In vivo* method based on a functionalized and structured medical wire

Recently, Lücke and co-workers have developed a new method for the *in vivo* isolation of CTCs from peripheral blood using a functionalized and structured medical wire (FSMW) [10]. In Figure III-5 the constitution of the wire and the principle of the method is shown.

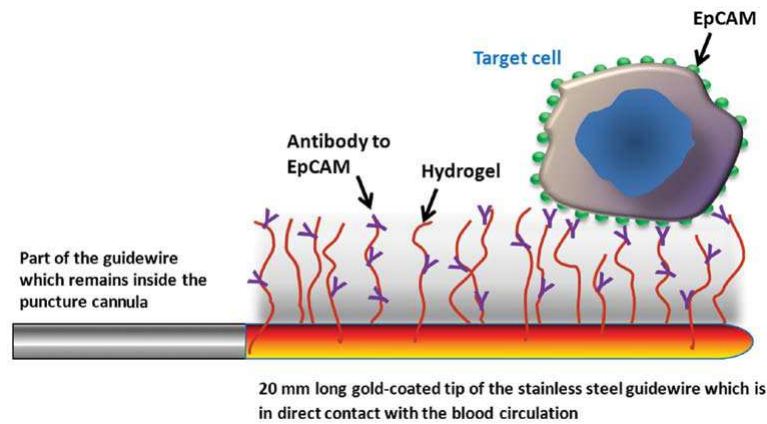


Figure III-5: Schematic drawing of the functionalized tip of the FSMW [10].

The FSMW is based on a stainless steel Seldinger guide wire [172], which is normally employed for diverse diagnostic and therapeutic applications, in which safe access to blood vessels and other organic cavities is required, e.g., for angiography, insertion of chest drains, and central venous catheters [10, 173]. One tip of the wire is preliminarily coated with gold, and then a hydrogel layer consisting of a linear, synthetic polycarboxylate is attached to the gold layer. The carboxyl groups of the hydrogel layer are activated with 1-ethyl-3-(3-dimethylaminopropyl)carbodiimide (EDC) and 1-hydroxy-2,5-pyrrolidinedione (NHS), allowing the covalent coupling of an antibody via a primary amino group. The used chimeric antibody is directed to the EpCAM, which is present on the surface of most CTCs. In that way, CTCs can be caught and enriched from blood using the FSMW by inserting the FSMW through a standard venous cannula into the cubital vein of the patient for 30 minutes. The FSMW is slowly pushed forward into the cannula until the functionalized tip is exposed to the blood flow within the lumen of the cubital vein. A mark on the FSMW, which is not inserted into the cannula, indicates the correct length of insertion. Using an IN-Stopper the FSMW is fixed securely to the intravenous cannula (cf. Figure III-6).

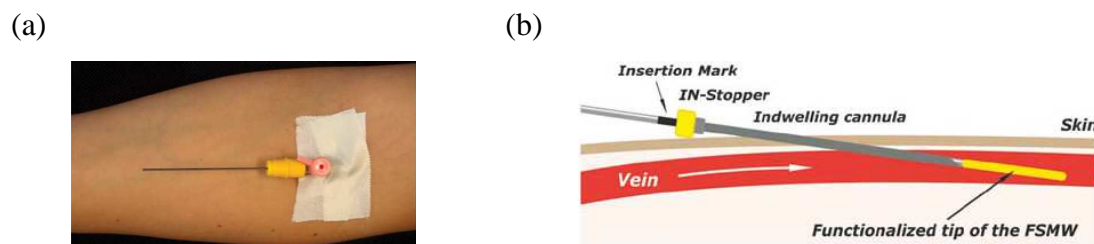


Figure III-6: Insertion of the FSMW into the cubital vein. **(a):** Arm bend with the inserted FSMW; **(b):** Principle of the insertion of the FSMW into the vein [10].

After removing the FSMW from the vein, the CTCs can be identified by immunocytochemical staining of EpCAM or cytokeratins and staining of their nuclei, before the CTCs can be counted.

Compared to *ex vivo* CTC enrichment technologies, the main advantage of this method is the large volume of blood, which comes in contact with the FSMW during the application period, and thus a higher number of CTCs can be caught and detected. The total blood volume amounts to approximately 1.5 to 3 L [10, 174], while *ex vivo* methods allow the detection of CTCs only in a few millilitres blood, that can be obtained from the patients or handled by the detection system [10, 12, 175–177].

Besides trapping CTCs, also non-tumour cells can be detected with the FSMW by attaching other cell surface-directed antibodies to the hydrogel. In fact, the FSMW functionalized with an antibody directed to a trophoblast surface antigen was used to trap circulating trophoblasts from peripheral blood of pregnant women in order to test the trophoblasts with respect to genetic foetal abnormalities [10].

2.7 Basic principles of the used analytical methods

2.7.1 Atomic Force Microscopy (AFM)

Atomic Force Microscopy (AFM) is a special, high-resolution type of scanning probe microscopy (SPM), in which the force acting between sample and probe is used for imaging [178]. Binnig, Quate and Gerber developed the first atomic force microscope (AFM) in 1986 [179].

The operating principle of a typical AFM is shown in Figure III-7. A sharp tip (probe), which is located at the end of a cantilever, is scanned over a sample surface in a distance of less than a few nanometres or in mechanical contact. For scanning, either the sample moves against the fixed tip, or the tip moves against the fixed sample. The moving element is usually mounted on a piezo scanner consisting of piezoelectric crystals, which change their dimensions in dependence of the applied voltage and thus allow the systematic movement of the sample or tip in three directions [180]. While scanning, the cantilever is deflected caused by the forces between sample and tip. The deflection of the cantilever is measured and thus a topographic image of the surface can be obtained [181]. Nowadays, the deflection measurements are usually realized by an optical detection system collimating a laser beam onto the back of the cantilever and determining the reflected laser beam using a position-sensitive photodiode [182].

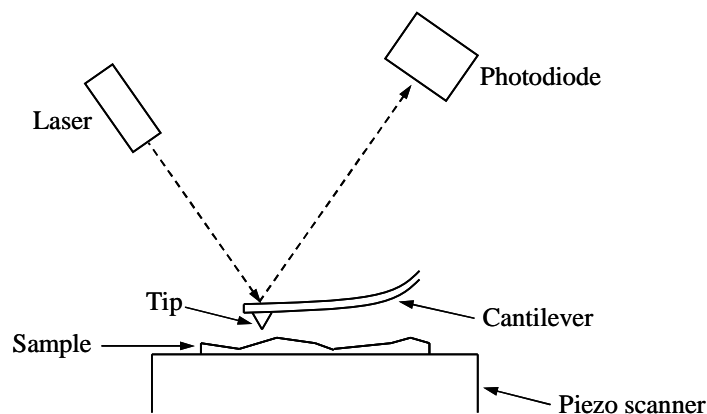


Figure III-7: Schematic illustration of atomic force microscopy.

AFM measurements can be performed in different modes depending on the kind of interaction. Two imaging modes of AFM can be distinguished: (i) the static (contact)

mode, and (ii) the dynamic (non-contact or tapping) mode. In the contact mode, the tip touches the sample surface during the whole measurement, what causes a strong electrostatic repulsion between the sample surface and the tip provoking a deflection of the cantilever. The deflection of the cantilever can be used to measure the contours of the surface directly. In the dynamic modes, the tip is oscillating at or close to its resonance frequency. Due to force interactions between tip and sample the oscillation amplitude, the phase, and the resonance frequency of the vibrated cantilever are modified [180]. These changes in oscillation, which provide information about the characteristics of the sample surface, are measured in the dynamic mode of AFM. In non-contact mode the oscillating cantilever tip is moved slightly away from the sample surface, while in tapping mode the tip impacts the sample surface for a minimal amount of time, i.e., the tip is intermittently in contact with the sample surface. So, the tapping mode combines qualities of both the contact and non-contact modes [183].

The interaction forces between sample and tip in the three modes can be identified on a force–distance curve (cf. Figure III-8).

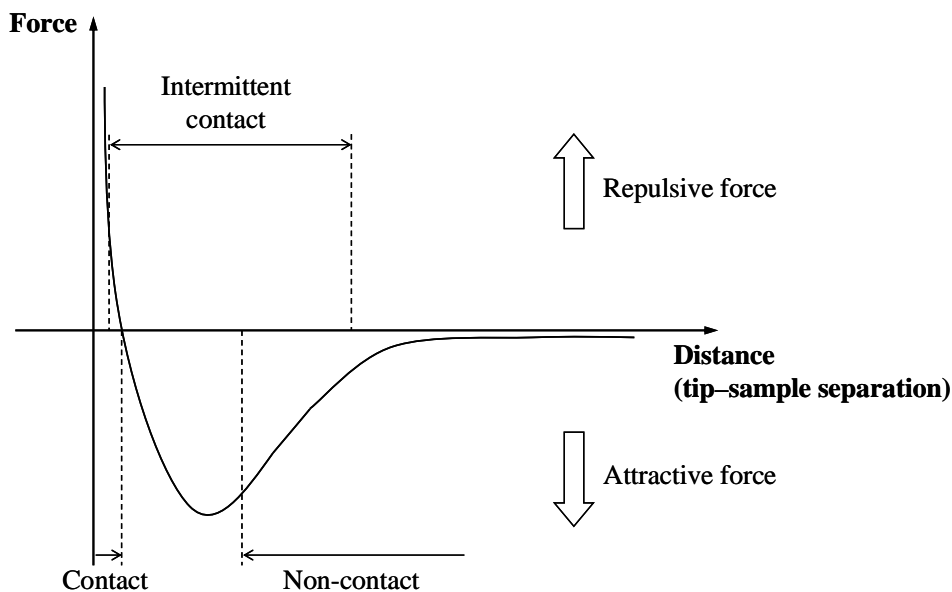


Figure III-8: Interatomic force variation versus distance between AFM tip and sample [183].

If the cantilever tip is far away from the sample surface, no force is measured. Approaching the tip to the sample, weak attractive forces between the atoms of sample and tip occur. These attractive van der Waals forces are detected in the non-contact mode. By further approach, the atoms are gradually brought closer to each other. Hence, the

attractive forces between tip and sample increase until the atoms become so close that the electron clouds start to repel each other electrostatically. Decreasing the tip-sample distance, the repulsive force between the atoms damps the attractive forces progressively until the interaction force becomes zero. At this point, the distance of the atoms reaches a couple of Ångströms. When the atoms are in contact, i.e., in contact mode, the interaction force becomes completely repulsive [183].

2.7.2 Inductively Coupled Plasma Atomic Emission Spectroscopy (ICP-AES)

Atomic emission spectroscopy (AES) is based on the measurement of the element-specific radiation emitted during the relaxation of thermally excited valence electrons of the atoms [5]. AES is an analytical tool for the quantitative determination of elements in a sample.

For AES measurements, a common optical spectrometer consisting of a radiation source, a monochromator and a detection system can be used. Different methods, like flame, arc or plasma, can be employed to excite atoms and to act as radiation sources [32].

When inductively coupled plasma (ICP) is used for the excitation of atoms, the method is called Inductively Coupled Plasma Atomic Emission Spectroscopy (ICP-AES). It allows the simultaneous determination of several elements because of its excellent exciting conditions [5]. In the following, the principle of ICP is described briefly: The plasma torch consists of three concentric quartz glass tubes through which argon flows. The top of the plasma torch is surrounded by the coil of a high frequency (HF) generator. The argon gas flowing through the torch is ignited by a Tesla discharge resulting in a partial ionisation of the argon and in free charge carriers. Subsequently, a HF current is induced in the conducting gas causing further ionisation. This generates a stable high temperature plasma in which temperatures of 6000–10000 K are achieved [32]. The analyte is introduced as an aerosol through the inner quartz glass tube. First, the analyte is dried in the plasma, then the solid particles are melted, evaporated, and finally the molecules dissociate and free atoms and also ions are formed. Both the atoms and ions are thermally excited.

The relative long residence time of the atoms in the plasma as well as the high plasma temperature ensure ideal conditions of atomisation, ionisation and excitation. The effective sample input allows the determination of very small amounts of analyte; for some elements detection limits in the range of ng L^{-1} can be obtained using ICP-AES [32].

2.7.3 Tests for *in vitro* cytotoxicity of medical products

In vitro cytotoxicity tests for the biological evaluation of medical products have to be performed according to DIN EN ISO 10993-5 issued by the *European committee for standardization* (CEN) [184]. DIN EN ISO 10993-5 serves rather to define a test scheme requiring successive decisions than to define an individual test procedure. The test scheme should result in the best suited test procedure. Thus, a variety of different methods can be applied to determine the cytotoxicity of medical products (e.g., the following cytotoxicity tests: absorption of toluylene red [185], cell colony formation [184], test using MTT [186], test using XTT [186]). Application of these methods allows determining the biological reaction of mammalian cells to medical products *in vitro* based on suitable biological parameters.

Three classes of test procedures can be distinguished depending on the type of sample, the place of application and the type of application: (i) testing of extracts, (ii) testing with direct contact between cell and material, and (iii) testing without direct contact between cell and material. By selection of one procedure the preparation of the sample, the preparation of the cultured cells as well as the kind of exposure of the cells to the sample (or to the extract of the sample) is provided by the ISO norm.

At the end of each test procedure the qualitative and/or quantitative grade of cytotoxicity is determined. Assessing the cytotoxicity can be performed according to the following criteria: (i) evaluation of cell damage due to morphological changes, (ii) measurement of cell damage, (iii) measurement of cell growth, and (iv) measurement of certain aspects of the cell metabolism.

Different analytical methods can be applied to estimate the cytotoxicity. Among them, there are especially microscopic examinations of the cells (often after staining the cells) or photometric measurements allowing the determination of different parameters for cell vitality and metabolic activity of the cells.

3 Experimental

3.1 Chemicals

All chemicals used were of p.a. quality and ultrapure water was used for all solutions (arium® 611 UV, Sartorius, Germany). Ammonium iron(II) sulphate hexahydrate, hydrogen peroxide (30%), glacial acetic acid, sodium acetate trihydrate, nitric acid (65%) and gold standard solution (CertiPur®, $c = 1000 \text{ mg L}^{-1}$) were purchased from Merck (Germany). Disodium ethylenediaminetetraacetate dihydrate was from Fisher Scientific (USA). Ethanol and acetone were purchased from Walter CMP (Germany). Diethyl ether was from Roth (Germany) and isopropanol was purchased from Merck.

3.2 The impact of $\cdot\text{OH}$ radicals on gold implants

3.2.1 Gold preparation

Gold foils of 0.1 mm and 0.05 mm thickness were cut into small pieces. The gold surfaces were mechanically polished with $1 \mu\text{m}$ and $0.3 \mu\text{m}$ alumina (Bühler®, Germany) on a wet pad. Afterwards, the gold pieces were rinsed with ultrapure water and ultrasonicated in ultrapure water for 5 minutes to remove residual alumina particles.

Some of the mechanically polished gold pieces were treated with Fenton solutions: The mechanically polished gold pieces were introduced to a freshly prepared solution of ammonium iron(II) sulphate hexahydrate (1 mM), disodium ethylenediaminetetraacetate dihydrate (1 mM) and acetate buffer (10 mM, pH 4.7). The Fenton reaction was started by addition of hydrogen peroxide, and the gold pieces were exposed to this solution for 5 minutes. This procedure was repeated 12 times so that the total exposure time was 1 h. The molar ratio of hydrogen peroxide to ferrous ions was 10 to 1. To stop the Fenton reaction, the gold pieces were removed from the Fenton solutions and carefully rinsed with ultrapure water.

3.2.2 Implantation of the gold pieces

Rectangular pieces of gold were implanted into the peritoneal cavity of C57BL/6 wild type mice and into the peritoneal cavity of C57BL/6 gp91^{phox} knock-out mice by B. T. Tran of the group of Prof. Jack (Institute of Immunology and Transfusion Medicine, Greifswald University). The C57BL/6 gp91^{phox} knock-out mouse is a congenic strain of the C57BL/6 wild type mouse, in which the gene coding for the gp91^{phox} subunit of the NADPH oxidase is deficient.

After removing the gold from the mice, the gold was cleaned (a) by immersing the gold pieces into a 1%-ic sodium dodecyl sulphate (SDS) solution at 50 °C for 10 minutes, or (b) by washing the gold pieces in a solution of 5 mM EDTA in phosphate buffered saline (PBS) followed by immersing the gold pieces into a mixture of collagenase D (2 mg L⁻¹) and deoxyribonuclease I (DNase I) (2 mg L⁻¹) in PBS at 37 °C for 30 minutes. Then, the pieces were carefully rinsed with isopropanol and water. After that, the gold pieces were ultrasonicated in a mixture of isopropanol, ethanol, diethyl ether and acetone (equal volume of each component) until the gold surfaces were clean.

3.2.3 AFM measurements

AFM measurements were performed in the contact mode using a “NanoScope I” (Digital Instruments, USA) and the software “NanoScope E 4.23r3”.

3.3 Diminishing of the cytotoxicity of the FSMW by treatment with $\cdot\text{OH}$ radicals

3.3.1 Wires

For all experiments, stainless steel wires with a length of 160 mm and a diameter of 0.5 mm were used. The wires have been plated on one end (the first 20 mm) with a gold layer of 2 μm thickness. The gold layer was galvanically deposited (OTEK, Germany). The wires plated with the gold layer were obtained from GILUPI GmbH (Germany).

3.3.2 Washing of the wires

Before the gold layer of the wires was treated with $\cdot\text{OH}$ radicals, the wires were washed with (i) diethyl ether, (ii) ethanol, and (iii) ultrapure water for 5 minutes, respectively, in order to remove all potential organic and inorganic contaminations from the gold layer.

3.3.3 Treatment of the gold layer of the wires with $\cdot\text{OH}$ radicals

After washing the wires, the gold layer was exposed to $\cdot\text{OH}$ radicals immediately. The $\cdot\text{OH}$ radicals were generated in two different ways, namely (i) by Fenton solution and (ii) by UV-photolysis of hydrogen peroxide.

3.3.3.1 Fenton solutions

The Fenton solutions were made from ammonium iron(II) sulphate hexahydrate, disodium ethylenediaminetetraacetate dihydrate, acetate buffer and hydrogen peroxide.

For treatment with $\cdot\text{OH}$ radicals generated by Fenton solutions, the wires were placed in a wire holder allowing the simultaneous treatment of five wires (cf. Figure III-9).

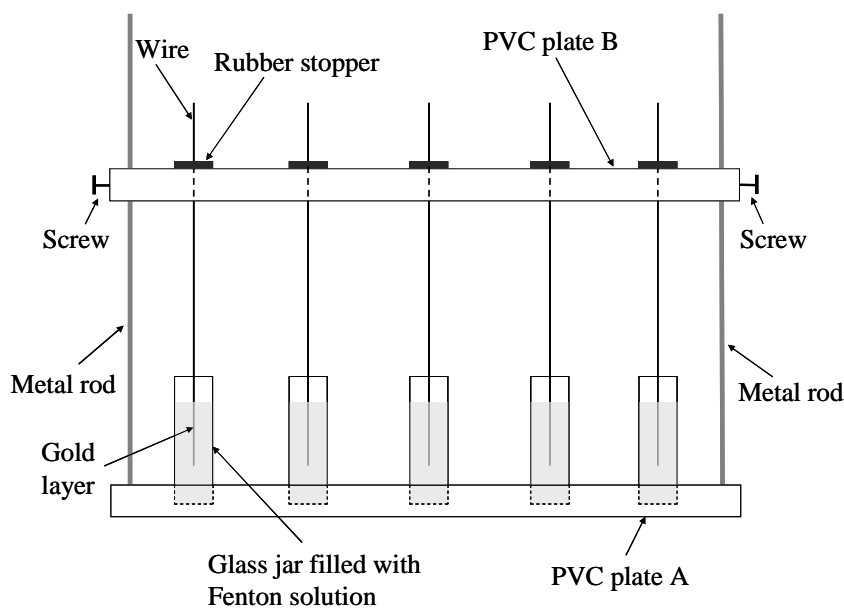


Figure III-9: Scheme of the wire holder used for the Fenton treatment.

The wire holder consisted of two PVC plates connected via two metal rods. PVC plate A had five cavities, in which the jars for the Fenton solutions were placed. PVC plate B had also five cavities in the same position, in which rubber stoppers were placed. A hole was punctured through each rubber stopper using a cannula and a wire was stuck into the hole of each rubber stopper. The wire was firmly fixed in the rubber stopper since the hole was small enough. While PVC plate A was fixed, PVC plate B was vertically removable along the metal rods by screws allowing the exchange of the jars.

For treating of the gold layer of the wires with Fenton solution, 4 mL of a freshly prepared solution (solution A) containing ammonium iron(II) sulphate hexahydrate, disodium ethylenediaminetetraacetate dihydrate and acetate buffer were filled into each jar. The jars were placed into the cavities of PVC plate A. Then, PVC plate B including the wires was moved down until the gold layers of the wires were immersed completely in the solution. To start the Fenton reaction, hydrogen peroxide was added to the solution. Then the wire holder was placed on a laboratory shaker. After a certain time, the Fenton solutions were exchanged, i.e., the wire holder was taken down from the shaker and the PVC plate B was moved up resulting in emerging the wires from the solution. New jars filled with solution A were placed in the cavities of PVC plate A and the Fenton reaction was started again. The whole procedure was repeated for a fixed number of times. To stop the Fenton reaction the wires were immersed into ultrapure water for 5 minutes. Subsequently, the wires were washed successively with (i) 0.1 mol L⁻¹ acetic acid, (ii) ultrapure water, (iii) ethanol, and (iv) ultrapure water for 5 minutes, respectively.

3.3.3.2 UV-photolysis of H₂O₂

A 705 UV Digester (Metrohm, Switzerland) was used to treat the gold layer of the wires with [•]OH radicals generated by UV-photolysis of hydrogen peroxide. In the centre of the digester a high pressure mercury lamp (radiation source power: 500 W) generated UV light. Quartz sample tubes were arranged concentrically around the UV lamp ensuring a consistent UV light exposure to all the quartz tubes (cf. Figure III-10).

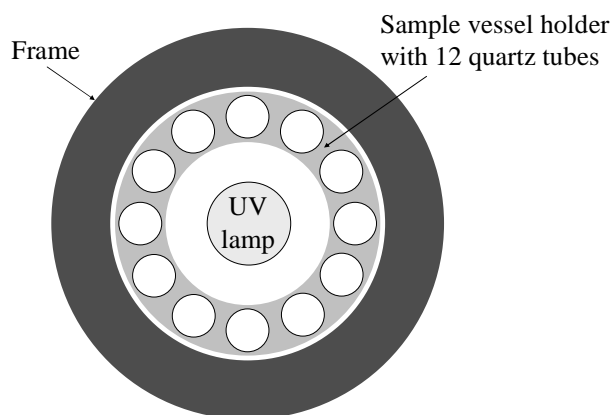


Figure III-10: Schematic assembly of the UV lamp and the quartz sample tubes in the UV digester (top view).

The temperature of the sample solutions in the quartz tubes was adjusted to approximately 65 °C by controlling the water flow rate of the continuous-flow cooler.

Four wires were treated simultaneously. Four quartz tubes were filled with ultrapure water and a certain concentration of hydrogen peroxide was added. One wire was hung into one quartz tube fixed by a rubber stopper immersing the whole gold layer of the wire in the solution of hydrogen peroxide and ultrapure water. The other quartz sample tubes were filled with ultrapure water only. After a certain exposure time, the wires were removed from the quartz sample tubes and were washed with (i) ultrapure water, (ii) ethanol and (iii) again with ultrapure water for 5 minutes, respectively.

3.3.4 Electrochemical reduction of the treated gold layer

After treatment with $\cdot\text{OH}$ radicals, the gold layer of some of the wires was electrochemically reduced at constant potential. The reduction was performed using an AUTOLAB with a PGSTAT 20 (Eco-Chemie, The Netherlands) using a three-electrode system. The gold layer of the wire served as working electrode, an Ag/AgCl electrode in 3 M KCl (Metrohm, Switzerland) with an electrode potential of $E = 207.0$ mV at 25 °C was used as reference electrode and a glassy carbon electrode was used as auxiliary electrode. As electrolyte a solution of $0.1 \text{ mol L}^{-1} \text{H}_2\text{SO}_4$ was used. The wire was immersed in the electrolyte as far as the gold layer was covered completely and a voltage of 0.5 V (vs. Ag/AgCl) was applied for 120 s. After the electrochemical reduction, the wire was removed and the gold layer was rinsed with ultrapure water.

3.3.5 ICP-AES

All solutions used for the treatment of the gold layer of the wires with $\cdot\text{OH}$ radicals were stored and analysed with respect to the gold content by ICP-AES using an ICP-Optical Emission Spectrometer Optima 2100 DV (PerkinElmer, USA). Small amounts of concentrated nitric acid were added to all solutions immediately after gold treatment to ensure that the gold remains dissolved until the ICP-AES measurements were performed. Argon of high purity (ALPHAGAZTM 1 Argon, 99.999%, Air Liquide, Germany) was used for plasma generation. For calibration, solutions of gold in a concentration range from $1\text{ }\mu\text{g L}^{-1}$ to $100\text{ }\mu\text{g L}^{-1}$ were prepared by dilution of a gold standard solution (Certipur®).

3.3.6 Gamma sterilization

The sterilization of the wires by irradiation with gamma rays was performed by BGS Beta-Gamma-Service GmbH & Co. KG (Germany) or by BBF Sterilisationsservice GmbH (Germany). Both companies use ^{60}Co as source for the gamma rays applying a radiation dose of 25 kGy.

3.3.7 Cytotoxicity test

To examine the cytotoxicity of the wires, material elution tests were performed *in vitro* by GILUPI GmbH (Germany) based on the DIN EN ISO 10933-5 [184]. The cytotoxicity was tested using normal human adult dermal fibroblasts (NHDF-cells) in a concentration of approximately $35000\text{ cells mL}^{-1}$.

For elution, the gold covered part of a wire was cut into small pieces. According to DIN EN ISO 10933-5, the conditions of elution should simulate or even exceed the conditions of the medical application to examine the toxic risk potential [184]. Thus, an eluate of the gold covered part of *one* wire was tested, as this simulates the medical application of one wire in a vein. In addition to this test, an eluate of the gold covered part of *three* wires was tested, as this amount of gold surface exceeds the normal application of *one* wire in a vein, and thus this test gives a much higher confidence with respect to the cytotoxicity risk. Therefore, the pieces of *one* wire were inserted into 1 mL of RPMI-medium and the pieces of *three* wires were inserted into 1 mL of RPMI-medium,

respectively, and incubated at 37 °C for 24 h. Additionally, eluates of reference materials (copper wire as positive control and Teflon wire as negative control) were prepared, and 1 mL RPMI-medium was incubated as further negative control. Simultaneously, the NHDF-cells in a microtiter plate (96 wells) were incubated causing an adhering of the NHDF-cells to the bottom of the wells. After 24 h of incubation, the eluates and controls were added to the NHDF-cells followed by further incubation for 48 h at 37 °C. Finally, the cytotoxicity was determined quantitatively as well as qualitatively.

A colorimetric assay based on the conversion of a yellow tetrazolium compound into an orange formazan compound due to metabolic cellular activity was used to examine quantitatively the viability of the NHDF-cells. Therefore, after 48 h of incubation of NHDF-cells with the eluates and the controls, the tetrazolium reagent (EZ4U-Kit, Cell proliferation and cytotoxicity assay, Biomedica Medizinprodukte GmbH & Co. KG, Austria) was added and the NHDF-cells were incubated for further 3 h at 37 °C. Afterwards, 50–100 µL of each sample were transferred into a new microtiter plate. The orange staining of the formazan correlates with the amount of vital cells. The colour intensity was determined in threefold replication by absorption measurements at 450 nm and additionally at 620 nm as reference using a microtiter plate reader (SPECTROstar Omega, BMG Labtech, Germany). The mean value of absorption obtained for the negative control (RPMI-medium) was defined as 100% cell vitality.

For the qualitative assessment of cytotoxic effects as, e.g., alterations of morphology, adherence or cytolysis, the same cells as used for the quantitative analysis were studied under the light microscope NIKON ECLIPSE TS100 (Nikon Instruments Europe B.V., Germany) with 20-fold magnification.

3.3.8 AFM measurements

AFM images of the gold layer of the wires were recorded in the non-contact mode using a DME DualscopeTM C-26 (DME – Danish Micro Engineering A/S, Denmark) in combination with the software DME ScanTool Version 1.4.5.3.

4 Results and Discussion

4.1 The impact of $\cdot\text{OH}$ radicals on gold implants

4.1.1 Variation of the residence time of gold implants in wild type mice and the influence of Lipopolysaccharide (LPS)

As mentioned before, Nowicka and co-workers have demonstrated that $\cdot\text{OH}$ radicals generated in Fenton solutions, smooth a polished gold surface by dissolution of gold atoms that are part of asperities on the gold surface [6, 7]. Therefore it was decided to see if $\cdot\text{OH}$ radicals generated by *in vivo* reactions induced by inflammation affect a gold surface in a similar way. A mechanically polished gold piece of 0.1 mm thickness (10 mm \times 3 mm) was implanted into the peritoneal cavity of twelve wild type mice, respectively. Into six of the mice, 5 ng LPS were injected after implantation immediately. LPS advances the inflammation in the organism and thus an enhanced release of $\cdot\text{OH}$ radicals may be induced so that an increased smoothing of the gold surface could be expected. Six of the gold pieces remained in the mice for 2 days (three with injection of LPS and three without injection of LPS) and the other six gold pieces remained in the mice for 14 days (three with injection of LPS and three without injection of LPS).

AFM measurements of the gold surfaces were performed before implantation and after removing the gold from the mice. Surprisingly, no difference was observed between the gold pieces implanted in the mice without injection of LPS and the gold pieces implanted in the mice with injection of LPS. However, Figure III-11 clearly shows that a smoothing of the gold surfaces could be observed depending on the residence time in the mice. Even after 2 days the surface is smoother. Compared with the AFM images measured before implantation (cf. Figure III-11a), especially the peaks of the asperities of the gold surface were removed (cf. Figure III-11b). The AFM images of the gold pieces, which remained inside the mice for 14 days, illustrate that the smoothing is further proceeded with increasing residence time of the gold in the mice (cf. Figure III-11c). These results clearly confirm an analogical effect between the exposure of gold to Fenton solutions and the exposure of gold to *in vivo* reactions in mice.

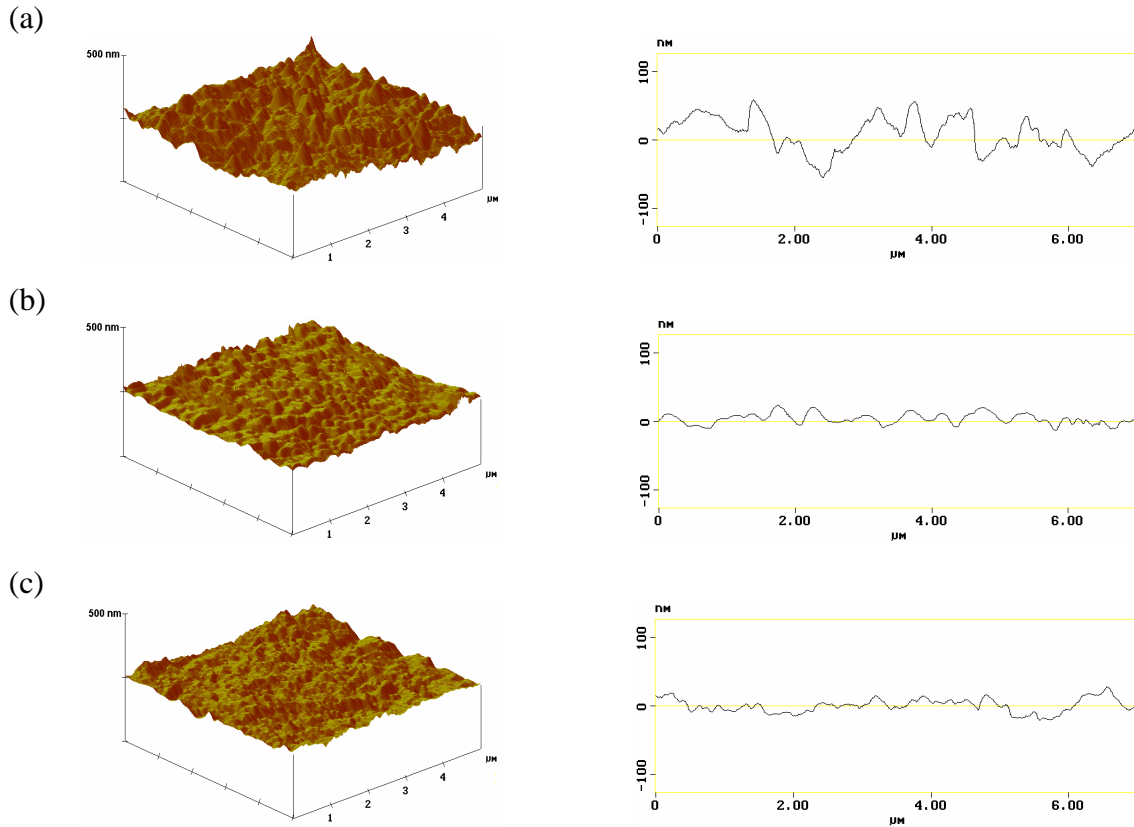


Figure III-11: Atomic force micrographs and section analysis of mechanically polished gold surfaces (a) before implantation, (b) after implantation in C57BL/6 wild type mice for 2 days, and (c) after implantation in C57BL/6 wild type mice for 14 days.

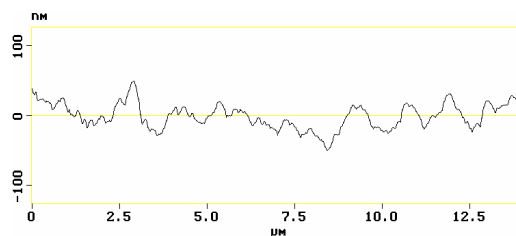
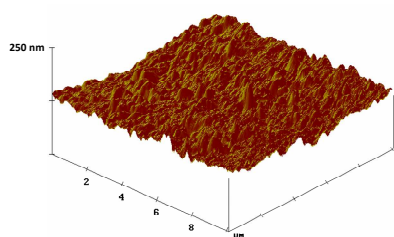
4.1.2 Implantation of mechanically polished gold and “Fenton-polished” gold plates into wild type mice and knock-out mice

Since it has been shown that the surface of gold plates was smoothed when implanted in wild type mice, in further experiments it should be investigated if the treatment of a mechanically polished gold surface with Fenton solution passivates the gold surface avoiding an alteration of the gold surface. Additionally, gold pieces were implanted into knock-out mice to examine if the smoothing of the gold surface observed after implantation into wild type mice is really provoked by $\cdot\text{OH}$ radicals generated by immune reactions.

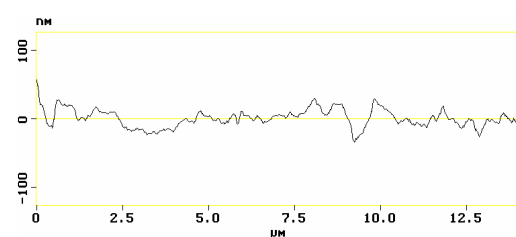
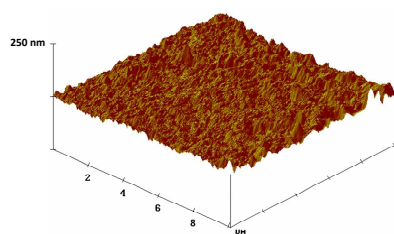
Thus, six mechanically polished and six “Fenton-polished” gold pieces of 0.05 mm thickness (15 mm \times 5 mm) were prepared for implantation. The mechanically polished gold pieces were implanted into three wild type mice and into three knock-out mice, respectively, and also the “Fenton-polished” gold pieces were implanted into three wild

type mice and into three knock-out mice, respectively. The gold pieces were implanted into the peritoneal cavity of the mice for 14 day. AFM measurements were performed before implantation and after removing the gold from the mice (cf. Figure III-12). For each case, at least 10 AFM images were recorded.

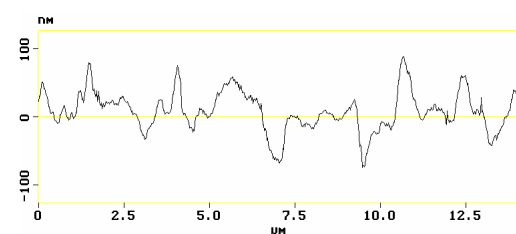
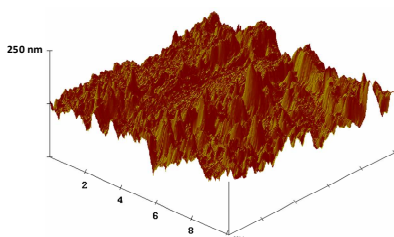
(a)



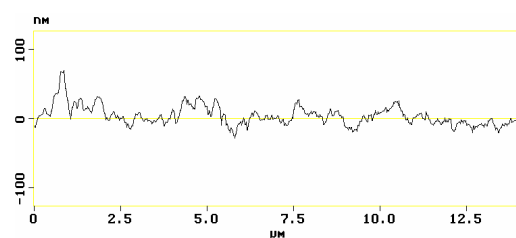
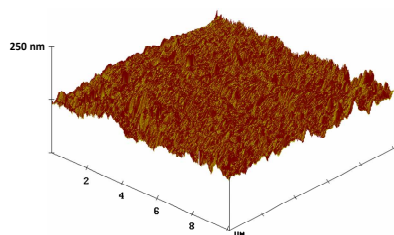
(b)



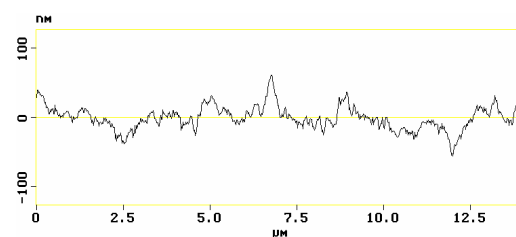
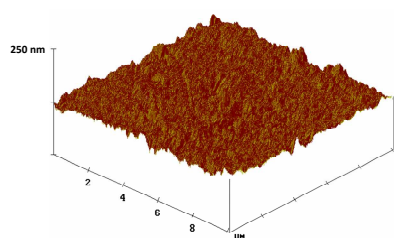
(c)



(d)



(e)



(f)

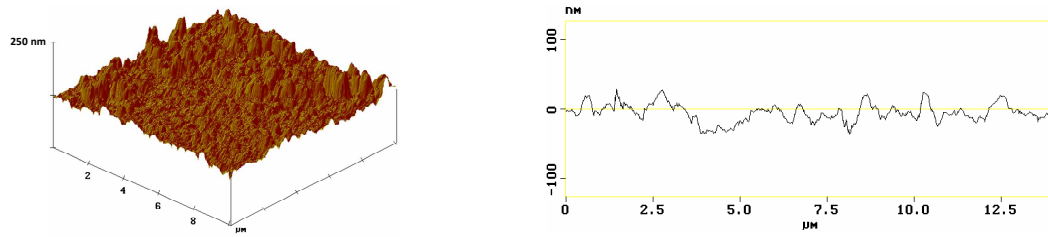


Figure III-12: Atomic force micrographs and section analysis of **(a)** a mechanically polished gold surface before implantation, **(b)** a mechanically polished gold surface after implantation in wild type mice, **(c)** a mechanically polished gold surface after implantation in knock-out mice and **(d)** a “Fenton-polished” gold surface before implantation, **(e)** a “Fenton-polished” gold surface after implantation in wild type mice, **(f)** a “Fenton-polished” gold surface after implantation in knock-out mice.

Figure III-12 clearly shows that a smoothing of the gold surface can only be observed after implantation of mechanically polished gold into the wild type mice, but not after implantation into the knock-out mice. Furthermore a roughening of the gold surface is observed after implantation of both mechanically polished and “Fenton-polished” gold pieces into knock-out mice. To confirm these results, the AFM images were analysed statistically. Therefore, the roughness factors of the gold surfaces were determined. Table III-3 shows the mean values and the standard deviations of the roughness factors obtained for mechanically polished gold and “Fenton-polished” gold before implantation, after implantation into wild type mice and after implantation into knock-out mice, respectively.

Table III-3: Mean values and standard deviations of the roughness factors calculated for the different gold surfaces.

		Roughness factor [nm]
Mechanically polished	Before implantation	14.7 ± 2.1
	After implantation into wild type mice	10.2 ± 0.5
	After implantation into knock-out mice	22.6 ± 6.8
"Fenton-polished"	Before implantation	12.6 ± 1.0
	After implantation into wild type mice	13.4 ± 1.3
	After implantation into knock-out mice	26.4 ± 12.1

Regarding the implantation of mechanically polished gold pieces into the wild type mice, the roughness factor obtained for the surface after implantation is smaller than the

roughness factor obtained for the surface before implantation. By applying a student's t -test ($p = 0.95$), it is shown that the roughness factors of the mechanically polished gold surfaces before and after implantation into the wild type mice differ significantly indicating that the gold surface is smoothed by *in vivo* reactions inside the wild type mice. Thus, the results mentioned in chapter 4.1.1 are confirmed. In contrast, the roughness factors of the "Fenton-polished" gold surfaces before implantation and after implantation into the wild type mice do not differ significantly. That means that the roughness of the "Fenton-polished" gold surface is not altered inside the wild type mice. Furthermore, the roughness factors of the mechanically polished gold surface and the "Fenton-polished" gold surface before implantation differ significantly indicating that the gold surface is made less corrosive by the Fenton-treatment. Further, it could be shown that the roughness factors obtained for the mechanically polished gold surface after implantation into the wild type mice and the "Fenton-polished" gold surface after implantation into the wild type mice differ significantly by applying the student's t -test ($p = 0.95$).

The mechanically polished gold plates and the "Fenton-polished" gold plates distinguish each other with respect to their behaviour as implants: Only the mechanically polished gold plate was smoothed during implantation in the wild type mice. As the surface of the Fenton-polished gold pieces was not altered inside the wild type mice, it is assumed that a knock-out of the highly active sites of the gold surface by $\cdot\text{OH}$ radicals generated by Fenton solution avoid the alteration of the surface of the gold implants by the attack of $\cdot\text{OH}$ radicals generated by *in vivo* reactions. Hence, it is very likely that the biocompatibility of gold implants can be improved by treating gold with Fenton solution before implantation.

Concerning the implantation of the mechanically polished and the "Fenton-polished" gold pieces into the knock-out mice, in both cases no smoothing of the gold surface can be observed; in contrast the surface becomes even rougher. Furthermore the standard deviations of the roughness factors determined for the mechanically polished gold surfaces and the "Fenton-polished" gold surfaces after removing from the knock-out mice are very high, i.e., the roughness of the surfaces differs strongly, respectively. Due to the fact that the gold surface does not become smoother during implantation into knock-out mice lacking the gp91^{phox} subunit of the NADPH oxidase, it can be concluded that a smoothing of the mechanically polished gold surfaces inside the wild type mice is caused by oxygen radicals generated *in vivo* by immune reactions catalysed by NADPH oxidase (cf. Equation III-5, Chapter 2.3.1.2).

4.1.3 Investigation of the roughening effect of the gold surface during implantation in knock-out mice

A possible explanation for the roughening effect of the gold surface in the knock-out mice could be the bending of the gold piece inside the mice caused by movements of the mice. To test this assumption, firstly an *ex vivo* experiment was performed. Therefore, a piece of mechanically polished gold was bent and atomic force micrographs were recorded before and after bending the gold (cf. Figure III-13a and b). Figure III-13b shows that “hills” occur on the surface area, where the bending has taken place. Also, the calculated roughness factors confirmed that the gold surface became rougher by bending the gold foil (cf. Table III-4). Thus, it was confirmed that the roughening of the gold surface in the knock-out mice is probably the result of bending the gold foil caused by movements of the mice. Because the roughening effect was not observed in wild type mice, it is supposed that the asperities caused by bending the gold foil are smoothed by $\cdot\text{OH}$ radicals produced in the wild type mice. To prove this assumption, the bended gold foil was exposed to Fenton solution and AFM images were recorded again. As can be seen in Figure III-13c, the asperities are dissolved and the surface become smoother compared to the bended surface (cf. Table III-4).

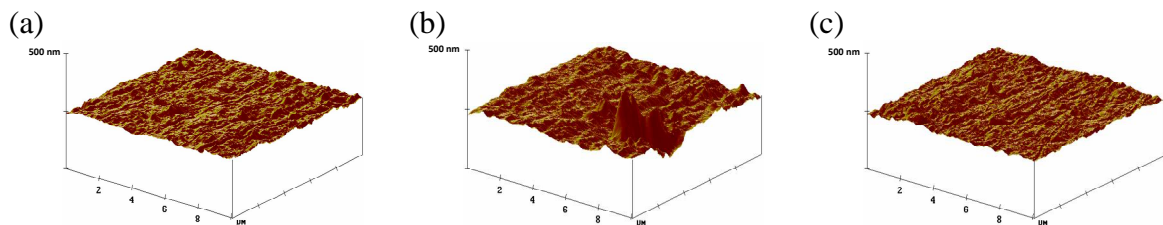


Figure III-13: Atomic force micrographs of a gold surface (a) before bending, (b) after bending, and (c) after bending and “Fenton-polishing”.

Table III-4: Mean values and standard deviations of the roughness factors calculated for the gold surfaces before bending, after bending, and after bending and “Fenton-polishing”.

	Roughness factor [nm]
Before bending	8.6 ± 1.0
After bending	12.5 ± 3.5
After bending and "Fenton-polishing"	9.8 ± 1.0

That indicates that the gold surface is affected by two opposed-acting processes in the wild type mice. On one hand the gold foil is bended caused by the movement of the mice resulting in a roughening of the surface. On the other hand $\cdot\text{OH}$ radicals are produced in the wild type mice smoothing the gold surface. Since a smoothing of the gold surface inside the wild type mice was observed by AFM, the effect of $\cdot\text{OH}$ radicals exceeds the effect of the bending process. In contrast, the knock-out mice are not able to produce $\cdot\text{OH}$ radicals, so that the surface cannot be smoothed. That means that in the knock-out mice only the bending process takes place, and thus the gold surface was roughened.

Additionally, an *in vivo* experiment was performed to test the drawn conclusions. A gold foil (thickness: 0.05 mm) was glued on a piece of PVC (dimensions: 12 mm \times 4 mm \times 2 mm) using 2-component adhesive (“Pattex Spezialkleber Kraft Mix Metall”, Henkel) to avoid a bending of the gold foil inside the mice. After the adhesive was hardened, the gold surface was mechanically polished and the piece was implanted into the peritoneal cavity of a knock-out mouse for 14 days. AFM images were recorded before implantation and after removing the gold from the mouse, and the corresponding roughness factors were determined. It was really found that the roughness factors of the gold surface before implantation (mean value of roughness factor: 15.6 nm) and after removing the gold from the mouse (mean value of roughness factor: 14.7 nm) did not differ distinctly. That means that the roughness of the gold surface is not altered in the knock-out mouse, if the gold is not liable to bending processes. The slight differences of the roughness factors could be ascribed to the facts that the roughness of the mechanically polished surface is not totally identical at all points of the surface and so it is impossible to measure the same locations of the gold surface before and after implantation. A statistical analysis requiring much more measurements would be essential to ensure the results definitely. However, the obtained results clearly show that the roughening of the gold pieces is caused by bending processes. If the bending is avoided, the roughness of the gold surface is similar to the mechanically polished gold surface before implantation. Thus, it is proved that the gold surface is not smoothed in the knock-out mice.

4.2 Diminishing of the cytotoxicity of the FSMW by treatment with $\cdot\text{OH}$ radicals

4.2.1 The effect of $\cdot\text{OH}$ radicals generated by Fenton solution

The treatment of the wires with Fenton solution should be optimized due to chemical consumption and expenditure of time purposing a diminishing of the cytotoxicity of the wires. Therefore, the concentrations of the ingredients of the Fenton solution, i.e., ferrous ion concentration ($c(\text{Fe}^{2+})$), hydrogen peroxide concentration ($c(\text{H}_2\text{O}_2)$), acetate buffer concentration ($c(\text{buffer})$) and disodium ethylenediaminetetraacetate concentration ($\text{Na}_2\text{-EDTA}$) were varied. Also, the total treatment time ($t(\text{total})$) as well as the time after which the Fenton solutions were renewed during one treatment procedure ($t(\text{reagent change})$) had to be optimized. As it is known from previous investigations, the gold layer is oxidized after treatment with Fenton solution [6]. Thus, some of the wires were electrochemically reduced after treatment with Fenton solutions in order to exclude an effect of the redox state to the cytotoxicity of the wires.

4.2.1.1 First experimental series

In a first experimental series the seven factors mentioned above had to be investigated considering 2 levels of each factor (cf. Table III-5).

Table III-5: Factors and their levels.

Factor	Factor description	–	+
A	$c(\text{Fe}^{2+})$	0.001 M	0.01 M
B	$c(\text{H}_2\text{O}_2)$	0.01 M	0.1 M
C	$c(\text{buffer})$	0.01 M	0.1 M
D	$c(\text{Na}_2\text{-EDTA})$	0.001 M	0.01 M
E	$t(\text{total})$	30 min	120 min
F	$t(\text{reagent change})$	5 min	10 min
G	Redox state	Oxidized	Reduced

To investigate all possible combinations of the factors, 2^7 (= 128) experiments would have been necessary. Such a high number of experiments was not feasible because

of the necessary time. Thus, a $2^{(7-3)}$ fractional factorial design containing 16 experiments was compiled using the Software Design-Expert[®] Version 8.0.7.1 Trial (cf. Table III-6). Each experiment was performed with five wires.

Table III-6: $2^{(7-3)}$ fractional factorial design of experiment.

No.	$c(\text{Fe}^{2+})$	$c(\text{H}_2\text{O}_2)$	$c(\text{buffer})$	$c(\text{Na}_2\text{-EDTA})$	$t(\text{total})$	$t(\text{reagent change})$	Redox state
1	+	+	–	+	–	–	–
2	+	+	–	–	–	+	+
3	+	+	+	+	+	+	+
4	+	+	+	–	+	–	–
5	+	–	+	+	–	–	+
6	–	–	+	–	+	+	+
7	–	+	–	–	+	+	–
8	–	+	–	+	+	–	+
9	+	–	+	–	–	+	–
10	–	–	–	–	–	–	–
11	+	–	–	+	+	+	–
12	–	–	–	+	–	+	+
13	–	–	+	+	+	–	–
14	–	+	+	+	–	+	–
15	+	–	–	–	+	–	+
16	–	+	+	–	–	–	+

4.2.1.1.1 Cytotoxicity test

After completing all experiments of the factorial design, the wires were irradiated with gamma rays and the cytotoxicity of the wires was assessed. For the cytotoxicity test, an eluate of the gold covered part of *one* wire (to simulate the conditions of medical application) as well as an eluate of the gold covered parts of *three* wires (to exceed the conditions of medical application) were prepared and their effects on NHDF-cells were examined quantitatively and qualitatively. The determined cell vitalities are shown in Table III-7.

Table III-7: Results of the quantitative determination of the cytotoxic potential determined in case of the wires treated with different Fenton procedures according to the fractional factorial design.

No.	Relative cell vitality [%]	
	1 wire	3 wires
1	107	78
2	103	60
3	119	118
4	111	78
5	115	84
6	105	76
7	114	74
8	98	99
9	111	58
10	114	60
11	107	69
12	97	79
13	107	73
14	107	74
15	109	60
16	112	70

In case of the cytotoxicity test using the eluate of *one* wire to simulate the conditions of the medical application, the determined cell vitality is 100% for all the wires; i.e., the cytotoxic potential of the wires is zero regardless of the treatment procedure of the wires. However, that means that from these results no conclusions could be drawn with respect to optimization of the Fenton treatment. Thus, in further experiments, cytotoxicity tests with the eluate of *one* wire were not performed anymore.

In case of the cytotoxicity tests using the eluate of *three* wires (to exceed the conditions of the medical application), the cell vitalities vary between 58% and more than 100% for the wires treated with different procedures according to the fractional factorial design. The best results were obtained by treating the wires according to experiment No. 3 and experiment No. 8; here the cell vitalities are approximately 100% for both the cytotoxicity test with the eluate of *one* wire and the cytotoxicity test with the eluate of *three* wires, respectively. In both experiments, the levels of the following four factors were similar: $c(\text{Na}_2\text{-EDTA}) = 0.01 \text{ M}$, $c(\text{H}_2\text{O}_2) = 0.1 \text{ M}$, $t(\text{total}) = 120 \text{ min}$, redox state = reduced. These data suggest that these four factors of the wire treatment affect the

cytotoxic potential of the wires, and thus the cell vitality mainly. To confirm this assumption, the effects of the factors were calculated (cf. Table III-8).

Table III-8: Effects of the factors on the cell vitality calculated for the experiments with three wires.

	$c(\text{Fe}^{2+})$	$c(\text{H}_2\text{O}_2)$	$c(\text{buffer})$	$c(\text{Na}_2\text{-EDTA})$	$t(\text{total})$	$t(\text{reagent change})$	Redox state
Mean +	75.6	81.4	78.9	84.3	80.9	76	80.8
Mean –	75.6	69.9	72.4	67.0	70.4	75.3	70.5
Effect	0	11.5	6.5	17.3	10.5	0.7	10.3

As can be seen in Table III-8, the $\text{Na}_2\text{-EDTA}$ concentration has the highest effect on the cell vitality, but also the hydrogen peroxide concentration, the total treatment time and the redox state affect the cell vitality distinctly. In contrast, the buffer concentration has only a low impact on the cell vitality while the ferrous ion concentration as well as the time after that the Fenton solution was renewed has no effect on the cell vitality in the investigated range. From the calculation of the effects of the factors it follows that the cell vitality is highest, if the factors $c(\text{Na}_2\text{-EDTA})$, $c(\text{H}_2\text{O}_2)$, $c(\text{buffer})$, $t(\text{total})$ and redox state are on the positive level, i.e., $c(\text{Na}_2\text{-EDTA}) = 0.01 \text{ M}$, $c(\text{H}_2\text{O}_2) = 0.1 \text{ M}$, $c(\text{buffer}) = 0.1 \text{ M}$, $t(\text{total}) = 120 \text{ min}$ and redox state = reduced. In case of the treatment of the wires according to experiment No. 3, all these conditions are fulfilled and the highest value of cell vitality was achieved. For the wires treated according to experimental No. 8, a slightly lower value of cell vitality was determined what can be explained by the used buffer concentration of 0.01 M (negative level).

Based on these results some twofold and threefold interactions could be calculated using the Software Design-Expert[®] Version 8.0.7.1 Trial. The results are shown in Table III-9. The effects of interactions clearly indicate that the ferrous iron concentration impacts the cell vitality indirectly. Particularly, the interaction AC ($c(\text{Fe}^{2+})$ and $c(\text{buffer})$) plays an important role, but also the interactions AB ($c(\text{Fe}^{2+})$ and $c(\text{H}_2\text{O}_2)$) and AD ($c(\text{Fe}^{2+})$ and $c(\text{Na}_2\text{-EDTA})$) are relevant. All of these interaction effects are characterized by a plus sign indicating that the improvement of the cell vitality by increasing concentrations of acetate buffer, $\text{Na}_2\text{-EDTA}$ and hydrogen peroxide is enhanced by using a higher ferrous ion concentration. Furthermore, a minor interaction effect of the hydrogen peroxide concentration and $\text{Na}_2\text{-EDTA}$ concentration (BD) is observed. All other examined interactions are negligible.

Table III-9: Effects of the interactions of the factors on the cell vitality calculated for the experiments with three wires (cf. Table III-5 for factor description).

Interaction	Effect of interaction
AB	4.25
AC	11.25
AD	6.00
AF	0.5
AG	-0.5
BC	0
BD	4.5
ABD	1.25

In addition to the quantitative determination of the cytotoxic potential of the wires, the cytotoxic potential of the same wires was estimated qualitatively applying microscopic measurements. Similar to the quantitative assay, no cytotoxicity of all the wires was observed in case of using the eluate of *one* wire. However, in case of using the eluate of *three* wires respectively, it was found that the NHDF-cells of all samples except the sample prepared in experiment No. 3 are rounded and detached indicating that the eluates of these wires have a toxic effect to the cells. Only in case of the samples prepared from the wires of experiment No. 3, the NHDF-cells attain their natural oblong shape and stay attached to the bottom of the wells of the microtiter plate; i.e., these wires are not cytotoxic.

4.2.1.1.2 ICP-AES

All Fenton solutions used for the treatment of the wires were analysed by ICP-AES measurements determining the gold content. Therefore, the five solutions simultaneously used for the treatment of five wires were mixed in order to ensure sufficient sample amounts for the ICP-AES measurements. Additionally, for each experiment a blank solution was analysed. As blank solutions, the same Fenton solutions as used in the corresponding experiments but without getting in contact with gold were used. The intensity obtained for the blank solution was subtracted from the intensity obtained for the corresponding sample solutions and the concentration of gold in the sample solutions was determined. The dissolution rates relating to the geometric area of the gold surface, which amounts to 0.32 cm^2 for one wire, were calculated (cf. Figure III-14).

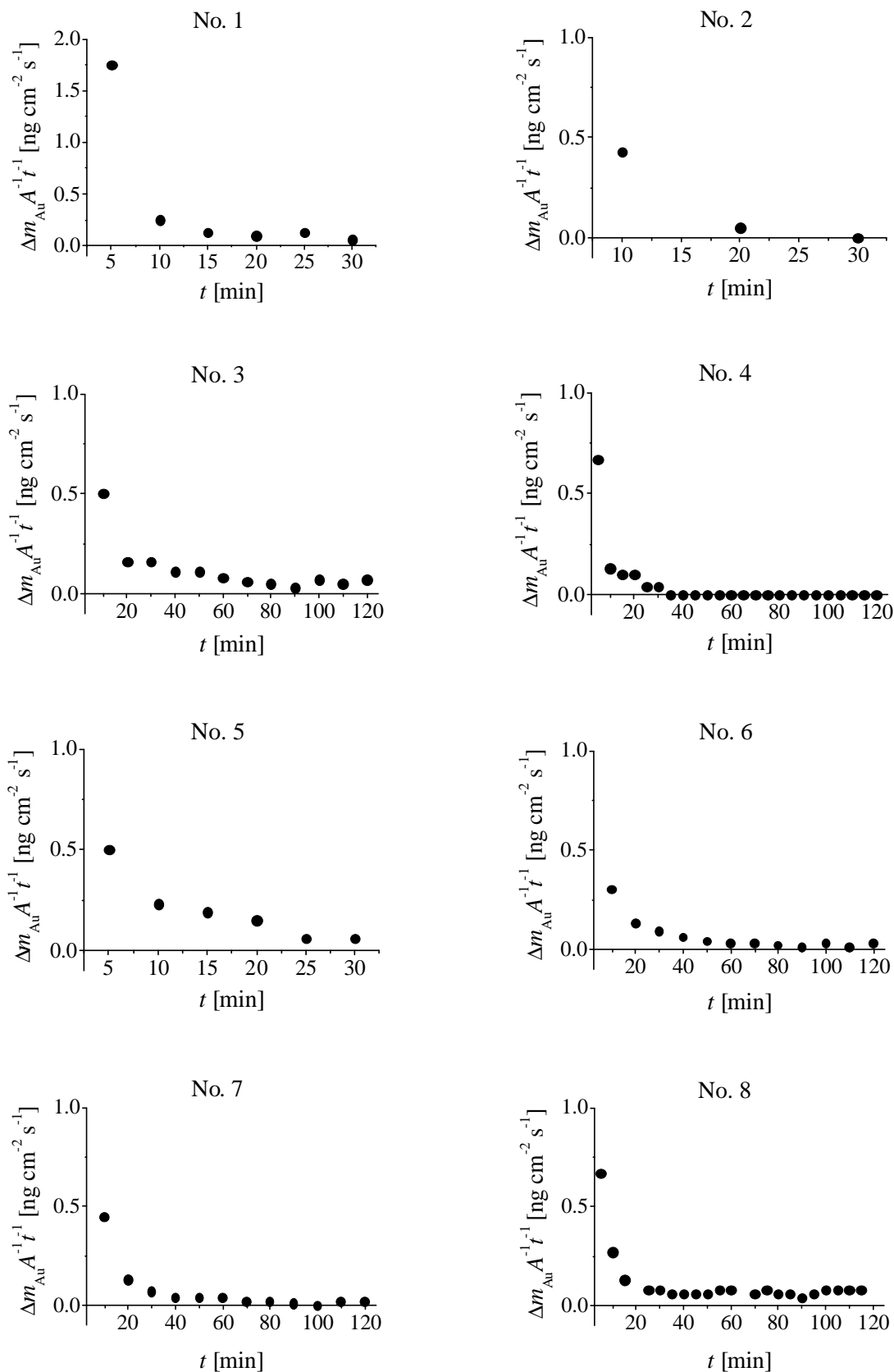


Figure III-14a: Results of ICP-AES measurements: Rate of gold dissolution from the wires as function of time obtained for experiment No. 1 to 8 of treatment with Fenton solution (overall geometric surface area of the gold layer of one wire is 0.32 cm^2).

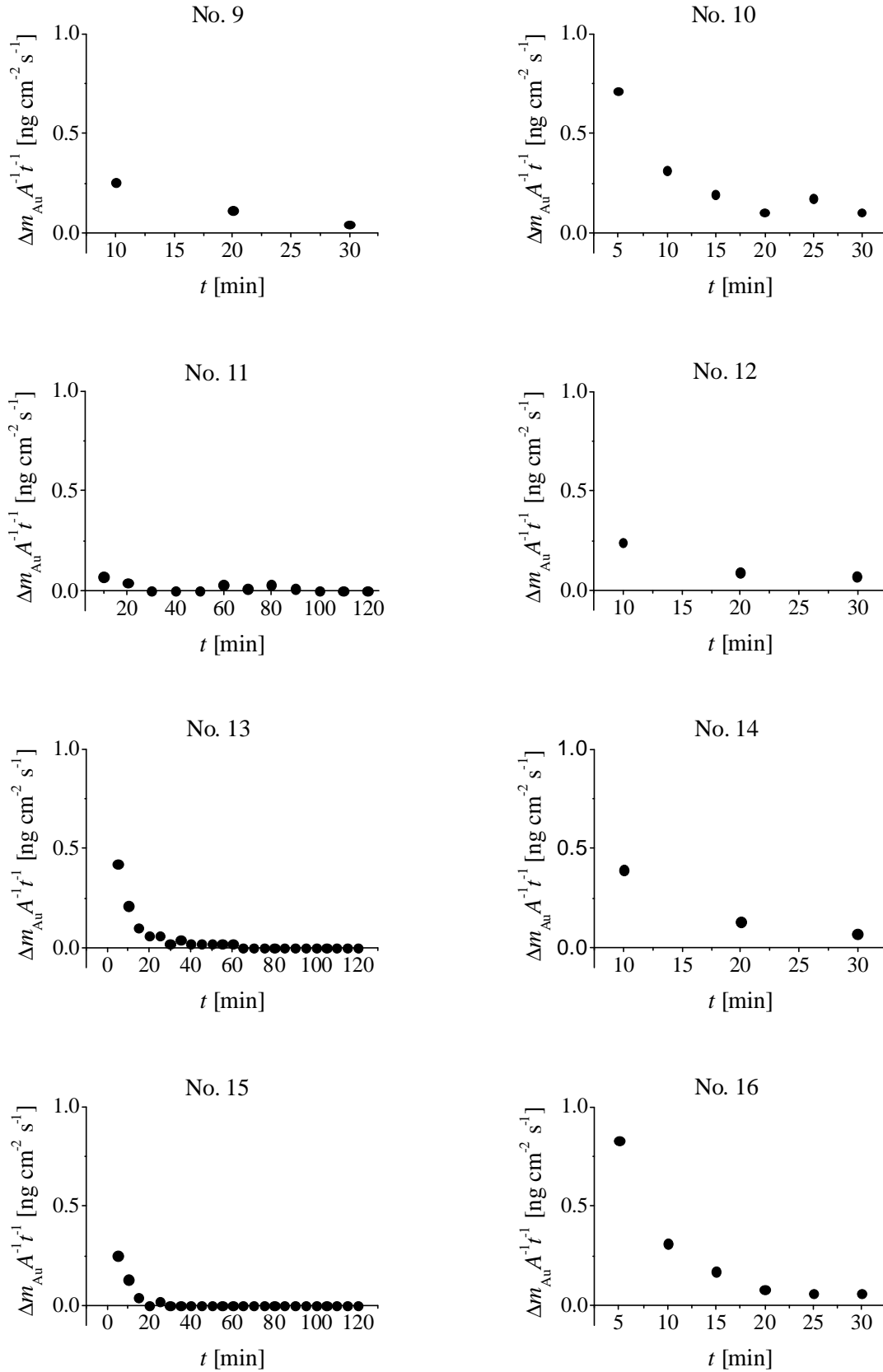


Figure III-14b: Results of ICP-AES measurements: Rate of gold dissolution from the wires as function of time obtained for experiment No. 9 to 16 of treatment with Fenton solution (overall geometric surface area of the gold layer of one wire is 0.32 cm^2).

As can be seen in Figure III-14, traces of gold were detected in the solutions of each experiment, especially in the solutions used at the beginning of the treatments. For all experiments, the largest amounts of gold were measured in the solutions used for the treatment of the wires during the first 10 to 20 minutes. Afterwards, only very small amounts of gold or even no gold were detected in the solutions. That means that most of the gold dissolution happens at the beginning of the treatment with Fenton solution. These results are in good agreement with previous investigations, in which Nowicka and co-workers have measured the same effect by treating a polished gold plate with Fenton solution [6].

Furthermore, the total amounts of gold dissolved from the five wires of one experiment during the whole treatment with Fenton solution were calculated (cf. Table III-10) and the gold amounts were correlated with the cell vitalities obtained by the cytotoxicity test (cf. Figure III-15).

Table III-10: Total amount of gold dissolved from the five wires of each experiment.

No.	$m(\text{Au})$ [μg]
1	1.16
2	0.46
3	1.41
4	0.52
5	0.57
6	0.76
7	0.83
8	1.13
9	0.39
10	0.76
11	0.19
12	0.39
13	0.49
14	0.56
15	0.21
16	0.73

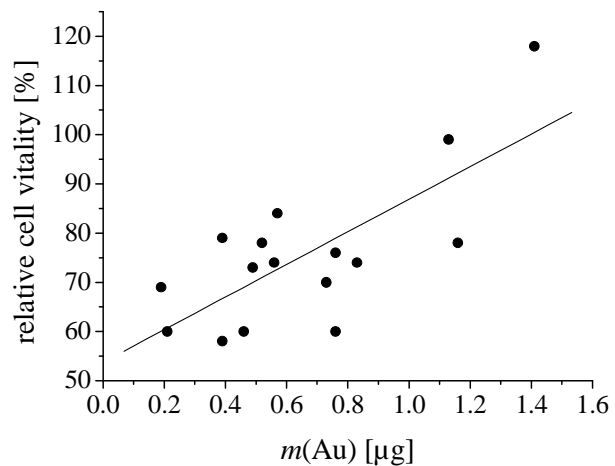


Figure III-15: Dependence of cell vitality on the total amount of gold dissolved from the wires during the whole treatment with Fenton solution.

From the data shown in Figure III-15 it can be concluded that the cell vitality and thus the cytotoxicity of the wires depends on the amount of dissolved gold. There is a clear tendency that the cell vitality increases and thus the cytotoxic potential of the wires

decreases with increasing amount of dissolved gold. This assumption is supported by the fact that the highest value of dissolved gold was obtained for the solutions of experiment No. 3. And as mentioned before, the wires treated according to experiment No. 3 result in the highest cell vitality (cf. Chapter 4.2.1.1.1). Also for experiment No. 8, high cell vitality is observed combined with a large amount of dissolved gold.

4.2.1.1.3 AFM measurements

The effect of Fenton solutions on the gold surface of the wires was also investigated by atomic force microscopy. For AFM measurements, the Fenton treatment of the wires was performed according to experiment No. 3 since this treatment procedure resulted in the highest cell vitality and largest amount of dissolved gold (cf. Chapter 4.2.1.1.1 and 4.2.1.1.2.), and thus the largest effect on the gold surface is expected for this treatment procedure.

Atomic force micrographs of four gold surfaces prepared in different ways were recorded: (i) a gold surface without Fenton treatment and without gamma irradiation, (ii) a gold surface without Fenton treatment and after gamma irradiation, (iii) a gold surface after Fenton treatment and without gamma irradiation and (iv) a gold surface treated with Fenton solution and irradiated with gamma rays. For each type of gold surface, AFM images on five different locations were recorded and the roughness factors were determined. In Figure III-16 one typical AFM image of each type of gold surface is shown and in Table III-11 the mean values of the roughness factors calculated for each type of gold surface are given.

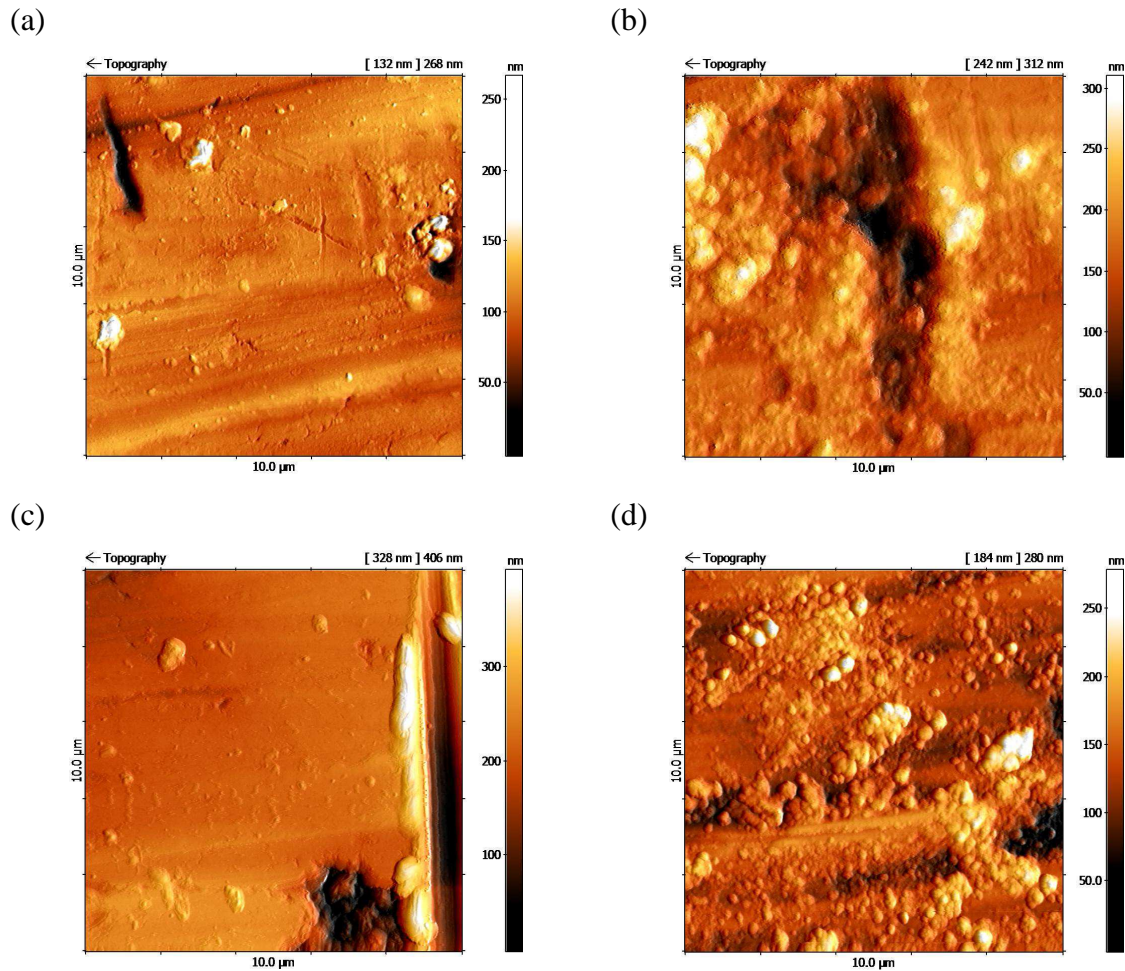


Figure III-16: Atomic force micrographs of a gold surface of the wire **(a)** without Fenton treatment and without gamma irradiation, **(b)** without Fenton treatment and after gamma irradiation, **(c)** after Fenton treatment and without gamma irradiation and **(d)** after Fenton treatment and after gamma irradiation.

Table III-11: Mean of roughness factors of atomic force micrographs.

	Roughness factor
Without Fenton treatment, without gamma irradiation	15
Without Fenton treatment, after gamma irradiation	24
After Fenton treatment, without gamma irradiation	14
After Fenton treatment, after gamma irradiation	25

As can be seen in Figure III-16a the surface of the gold layer deposited by galvanisation is quite smooth containing only a few asperities. After gamma irradiation, the surface is much rougher (cf. Figure III-16b) what is confirmed by the calculated roughness factors (cf. Table III-11). Comparing Figure III-16a and Figure III-16c, no distinct differences of the structure of the gold surface can be observed before and after Fenton

treatment. Also, the roughness factors have nearly the same values. These results are in contrast to previous investigations of Nowicka and co-workers, who observed a smoothing of a gold surface by treatment with Fenton solution [6, 7]. However, in contrast to the previous investigations, in this study an unpolished gold surface was treated with Fenton solution. Thus, no highly reactive gold atoms were generated before treatment with Fenton solution provoking that the gold surface does not alter distinctly by treating with Fenton solution. The detected gold traces in the Fenton solutions (cf. Chapter 4.2.1.1.2) indicate that minor surface alterations occur though, which cannot be detected by AFM measurements.

After irradiation with gamma rays, the Fenton treated gold surface is much rougher than before gamma irradiation. Although the roughness factor is nearly similar to the roughness factor obtained for the gamma irradiated gold surface without Fenton treatment, the structures of both gamma irradiated gold surfaces differ. In case of the Fenton treated gold surface, the gamma irradiation results in the development of a high number of small-dimensioned hills (cf. Figure III-16d), while the irradiation of a gold surface without Fenton treatment results in a large-scaled roughening of the gold surface (cf. Figure III-16b). However, in contrast to the untreated gold surface, the surface alteration of the Fenton treated gold surface caused by gamma irradiation provoke no cytotoxic effects to the wires as it was demonstrated by the cytotoxicity test.

4.2.1.2 Second experimental series

From the results of the first experimental series it follows that the Fenton solution containing the following concentrations of the ingredients is suitable to provide non-cytotoxic gold surfaces of the wires: $c(\text{Fe}^{2+}) = 0.01 \text{ M}$, $c(\text{Na}_2\text{-EDTA}) = 0.01 \text{ M}$, $c(\text{buffer}) = 0.1 \text{ M}$ and $c(\text{H}_2\text{O}_2) = 0.1 \text{ M}$. In all experiments of this second experimental series these concentrations of the ingredients were used.

The aim of the second experimental series was the further optimization of the treatment procedure of the gold layer of the wires by Fenton solution with respect to expenditure of work and time. Therefore it had to be investigated, whether the total treatment time ($t(\text{total})$) can be reduced and whether the time after which the Fenton solution has to be renewed during one treatment procedure ($t(\text{reagent change})$) can be extended. In previous studies of the Fenton reaction applying chemiluminescence measurements, it was found that even after 60 or 120 minutes the chemiluminescence and

thus the radical concentration was comparable to the chemiluminescence measured during the first minutes after starting the Fenton reaction. Thus, now it had to be tested, whether renewing the Fenton solution every 20 minutes is also sufficient to generate a gold surface, which is non-cytotoxic after gamma irradiation. It also had to be studied whether the reduction of the gold surface after Fenton treatment is really necessary. Hence, this third factor was investigated within this second experimental series. Table III-12 shows the estimated factors and their levels, and Table III-13 shows the design of experiment. Since the investigation of three factors considering two levels of each factor requires only 8 experiments, a full factorial design of experiments was compiled. Each experiment was performed twice with four wires respectively.

Table III-12: Factors and their levels.

Factor	Factor description	–	+
A	$t(\text{total})$	60 min	120 min
B	$t(\text{reagent change})$	10 min	20 min
C	Redox state	Oxidized	Reduced

Table III-13: 2^3 full factorial design of experiment.

No.	$t(\text{total})$	$t(\text{reagent change})$	Redox state
1	+	–	+
2	–	+	+
3	+	+	+
4	–	–	+
5	–	–	–
6	–	+	–
7	+	–	–
8	+	+	–

4.2.1.2.1 Cytotoxicity test

After treating the wires according to the design of experiments (cf. Table III-13), the wires were irradiated with gamma rays and the cytotoxicity of the wires was examined. For the cytotoxicity test, eluates of the gold covered part of *three* wires of one experiment were prepared only, because in the first experimental series, from the cytotoxicity test with the eluates of *one* wire no conclusions could be drawn with respect to optimizing the

parameters of Fenton treatment (cf. Chapter 4.2.1.1.1). In Table III-14, the results of the quantitative cytotoxicity test are shown.

Table III-14: Results of the quantitative determination of the cytotoxic potential obtained for the wires treated with different Fenton procedures according to the full factorial design.

No.	Relative cell vitality [%]		
	First run	Second run	Mean
1	114	74	94
2	57	49	53
3	77	90	84
4	83	68	76
5	85	60	73
6	49	31	40
7	79	69	74
8	49	93	71

Table III-14 clearly shows that the highest cell vitality was obtained with the eluates of the wires of experiment No. 1: it reached almost 100%. The treatment procedure of experiment No. 1 was similar to the procedure of experiment No. 3 of the first series of experiments, which resulted also in a cell vitality of 100% as mentioned before. Thus it is confirmed that non-cytotoxic wires were obtained by the following treatment conditions: $c(\text{Fe}^{2+}) = 0.01 \text{ M}$, $c(\text{EDTA}) = 0.01 \text{ M}$, $c(\text{buffer}) = 0.1 \text{ M}$, $c(\text{H}_2\text{O}_2) = 0.1 \text{ M}$, $t(\text{total}) = 120 \text{ min}$, $t(\text{reagent change}) = 10 \text{ min}$ and redox state = reduced.

The calculations of the effects on the cell vitality also prove these results (cf. Table III-15).

Table III-15: Effects of the factors on the relative cell vitality.

	$t(\text{total})$	$t(\text{reagent change})$	Redox state
Mean+	80.8	62.0	76.8
Mean–	60.5	79.3	64.5
Effect	20.3	–17.3	12.3

The effect of the total treatment time as well as the effect of the redox state has a positive sign indicating that a positive level of these factors improves the cell vitality, while the effect of the time of reagent change has a negative sign indicating that a negative level of this factor improves the cell vitality. That means that the highest cell vitality is obtained for a total treatment time of 120 minutes renewing the Fenton solution each 10

minutes. A decreasing of the total treatment time to 60 minutes and an extension of the time of reagent change to 20 minutes has a negative effect to the cytotoxicity of the wires. Further, the gold surface should be reduced after treating with Fenton solution to improve the cell vitality.

4.2.2 The effect of $\cdot\text{OH}$ radicals generated by UV-photolysis of hydrogen peroxide

Beside chemical generation of $\cdot\text{OH}$ radicals by Fenton solution, the method of UV-photolysis of hydrogen peroxide had to be studied for generating $\cdot\text{OH}$ radicals to treat the gold layer of the wires. The UV-photolysis of hydrogen peroxide had to be performed under different conditions to optimize the procedure of treating the gold layer of the wires for the purpose of a decrease of the cytotoxic potential of the wires. Therefore, the concentration of hydrogen peroxide ($c(\text{H}_2\text{O}_2)$) and the total treatment time ($t(\text{total})$) were varied. Further, it should be tested whether a renewing of the hydrogen peroxide solution each 15 minutes (reagent change) during the $\cdot\text{OH}$ treatment of the wires has a positive effect on the cytotoxicity of the wires. Additionally, the effect of the redox state of the gold layer of the wires after treating with $\cdot\text{OH}$ radicals had to be investigated in the same way as it was done after the Fenton treatment. These four factors were investigated considering 2 levels of each factor (cf. Table III-16).

Table III-16: Factors and their levels.

Factor	Factor description	–	+
A	$c(\text{H}_2\text{O}_2)$	0.3%	3%
B	$t(\text{total})$	30 min	120 min
C	Reagent change	No	Yes
D	Redox state	Oxidized	Reduced

A full factorial design of experiments containing 16 experiments was compiled to investigate all combinations of the factors using the Software Design-Expert[®] Version 8.0.7.1 Trial (cf. Table III-17). Each experiment was performed with four wires simultaneously.

Table III-17: 2^4 full factorial design of experiment.

No.	$c(\text{H}_2\text{O}_2)$	$t(\text{total})$	Reagent change	Redox state
1	+	–	+	+
2	+	+	–	+
3	–	+	–	+
4	–	–	–	–
5	+	+	–	–
6	+	+	+	+
7	–	+	–	–
8	–	–	+	+
9	+	+	+	–
10	–	+	+	+
11	–	–	+	–
12	–	+	+	–
13	+	–	+	–
14	+	–	–	+
15	–	–	–	+
16	+	–	–	–

4.2.2.1 Cytotoxicity test

The treated wires were irradiated with gamma rays and the cytotoxicity of the wires was examined. For the cytotoxicity test, eluates of the gold covered part of *three* wires of one experiment were prepared and their effect on NHDF-cells was examined quantitatively and qualitatively. Furthermore, the cytotoxicity of untreated wires before and after gamma irradiation was examined.

In case of all the untreated wires, the determined cell vitalities amount to around 50%; i.e., the untreated wires have cytotoxic effects on the NHDF-cells, as expected.

In Table III-18, the cell vitalities of the treated wires determined with the quantitative assay are shown. The obtained cell vitalities amount to more than 90% for all experiments. Compared to the cell vitality determined for the eluates of Teflon as negative control (80–90%), the cell vitalities determined for the eluates of all treated wires are in the same range or even higher. That means that all experiments result in wires, which are not or only marginally cytotoxic whatever the positive or the negative levels of the factors were used respectively.

Table III-18: Results of the quantitative determination of the cytotoxic potential obtained for the wires treated with different procedures according to the full factorial design.

No.	Relative cell vitality [%]
1	99
2	104
3	105
4	119
5	127
6	90
7	101
8	91
9	95
10	92
11	109
12	106
13	93
14	108
15	99
16	96

Nevertheless, the effects of the factors were calculated. As can be seen in Table III-19, the concentration of hydrogen peroxide and the total treatment time have no effect on the cell vitality in the tested ranges. In case of the redox state and the renewing of the hydrogen peroxide solution during the treatment procedure, a certain effect to the cell vitality was detectable. From these results follows that slightly higher cell vitalities are obtained by the treatment without renewing the hydrogen peroxide solution and for the oxidized surface. However for both levels the obtained cell vitalities are around 100%, and thus all treated wires are harmless relating to their cytotoxic potential determined quantitatively.

Table III-19: Effects of the factors.

	$c(\text{H}_2\text{O}_2)$	$t(\text{total})$	Reagent change	Redox state
Mean+	101.5	102.5	96.9	98.5
Mean–	102.8	101.8	107.4	105.8
Effect	–1.3	0.7	–10.5	–7.3

Additionally to the quantitative determination of the cell vitality, the vitality of the cells was estimated qualitatively. In Figure III-17, microscopic images of the cells

incubated with the eluates of (i) the controls (cf. Figure III-17a–c), (ii) the untreated wires (cf. Figure III-17d–f) and (iii) the wires treated according to experiment No. 4, 12 and 14 (cf. Figure III-17g–i) are shown.

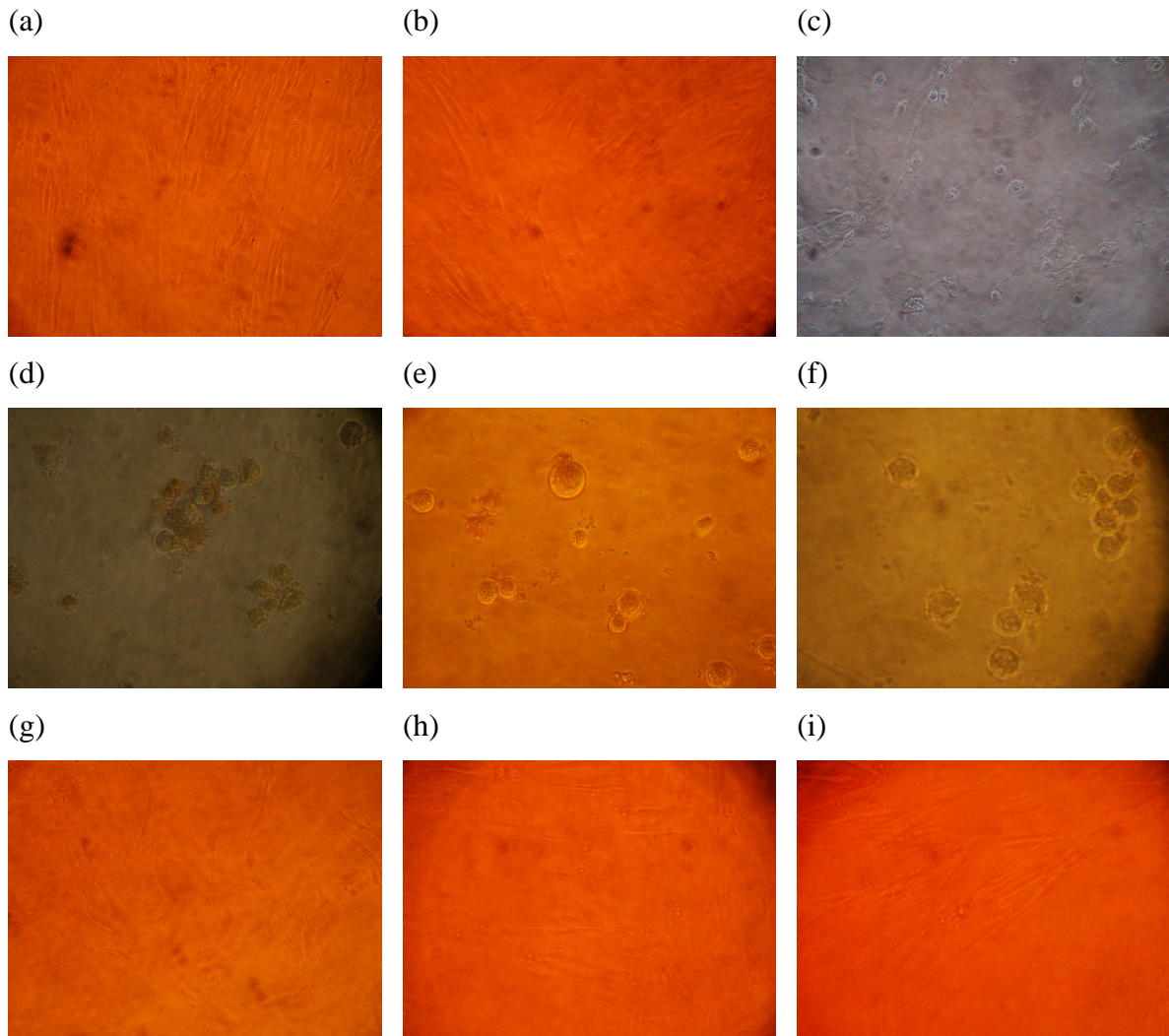


Figure III-17: Light microscopic images of the cells in the RPMI-medium of (a) negative control (only medium), (b) negative control (Teflon), (c) positive control (copper), (d) untreated and non-irradiated wires, (e) untreated and irradiated wires, (f) only washed and irradiated wires, (g) wires treated according to experiment No. 4, (h) wires treated according to experiment No. 12 and (i) wires treated according to experiment No. 14.

In case of all negative controls, vital NHDF-cells forming a confluent cell layer are observed (cf. Figure III-17a and b). In contrast, in case of the positive control the cells are rounded and detached from the bottom of the well indicating that the cells are destroyed nearly completely (cf. Figure III-17c); i.e., the eluate of copper is toxic for the NHDF-cells, as expected. All images of the cells incubated with the eluates of the treated wires

look similar; hence only a selection of three images is shown (cf. Figure III-17g–i). In comparison with the images of the negative and positive controls, the images obtained for the cells incubated with the eluates of the treated wires resemble the images of the negative controls since a confluent cell layer and only a small amount of rounded cells (less than 20%) is observed. That means that the cytotoxic potential of the treated wires is negligible. Thus the results of the qualitative estimations confirm the results of the quantitative assay. By analysing the images of the cells incubated with the eluates of the untreated wires, it is ascertained that much more cells are rounded and detached and thus more disengaged areas are observed between the cells (cf. Figure III-17d–f). That means that the untreated wires have cytotoxic effects on the NHDF-cells, as shown before by the quantitative analysis of the cell vitality.

4.2.2.2 ICP-AES

All hydrogen peroxide solutions used for the treatment of the wires were analysed by ICP-AES measurements determining the gold content. In case of all solutions, the measured intensities are in the range of the intensity obtained for ultrapure water, i.e., no gold can be detected in the hydrogen peroxide solutions used for the treatment of the gold layer of the wires. Two reasons can be discussed here: Either no gold was dissolved from the wires or the volume of the hydrogen peroxide solution required for the treatment of the wires (10 mL) was too large and thus the dissolved gold amount was too low to be detectable by ICP-AES measurements. The latter would be more convincing if it is assumed that the effect of UV-photolysis of hydrogen peroxide to gold surfaces is similar to the effect of Fenton solution (the volume of Fenton solutions was 4 mL). Of course it cannot be excluded that the UV irradiation may change the dissolution mechanism also in the way that the preliminarily dissolved gold may be quickly reduced back and deposited again on the surface, which could also decrease the cytotoxicity. This would lead to equilibration of the surface in the sense that reactive gold atoms are dissolved and this gold is then deposited to form less reactive surface sites.

4.2.2.3 AFM measurements

The effect on the gold surface caused by the treatment of the wires via UV-photolysis of hydrogen peroxide with and without subsequent gamma irradiation was investigated employing atomic force microscopy. Atomic force micrographs of four different treated gold surfaces were recorded: (i) a gold surface without treatment by UV-photolysis of H_2O_2 and without gamma irradiation, (ii) a gold surface without treatment by UV-photolysis of H_2O_2 and after gamma irradiation, (iii) a gold surface after treatment by UV-photolysis of H_2O_2 and without gamma irradiation and (iv) a gold surface treated by UV-photolysis of H_2O_2 and irradiated with gamma rays. The treatment of the wires by UV-photolysis of H_2O_2 was performed according to experiment No. 4 (cf. Table III-17). Experiment No. 4 was selected randomly since all treatment procedures resulted in high cell vitalities. For each type of gold surface, atomic force micrographs on five different positions were recorded and the roughness factors were determined. In Figure III-18 one typical AFM image of each type of gold surface is shown, respectively and in Table III-20 the means of the roughness factors calculated for each type of gold surface are given.

As can be seen in Figure III-18a and c, the treatment of the wires by UV-photolysis of hydrogen peroxide has no distinct effect to the gold surface. The calculated roughness factors confirm this results as both roughness factors are nearly the same. However, the treatment of the gold layer by UV-photolysis of hydrogen peroxide has an effect on the influence of the gamma irradiation on the gold surface. If an untreated gold surface is irradiated with gamma rays, the surface becomes rougher (cf. Figure III-18a and b). Comparing the roughness factors, the roughness increases by a factor of 1.6. In contrast, the gamma irradiation of a treated gold surface causes no distinct roughening of the surface (cf. Table III-20 and Figure III-18c and d). That means that the gold surface treated by UV-photolysis of hydrogen peroxide is passivated against gamma rays resulting in a non-cytotoxicity of the gold layer of the wires (cf. Chapter 4.2.2.1). This supports the idea expressed at the end of Chapter 4.2.2.2.

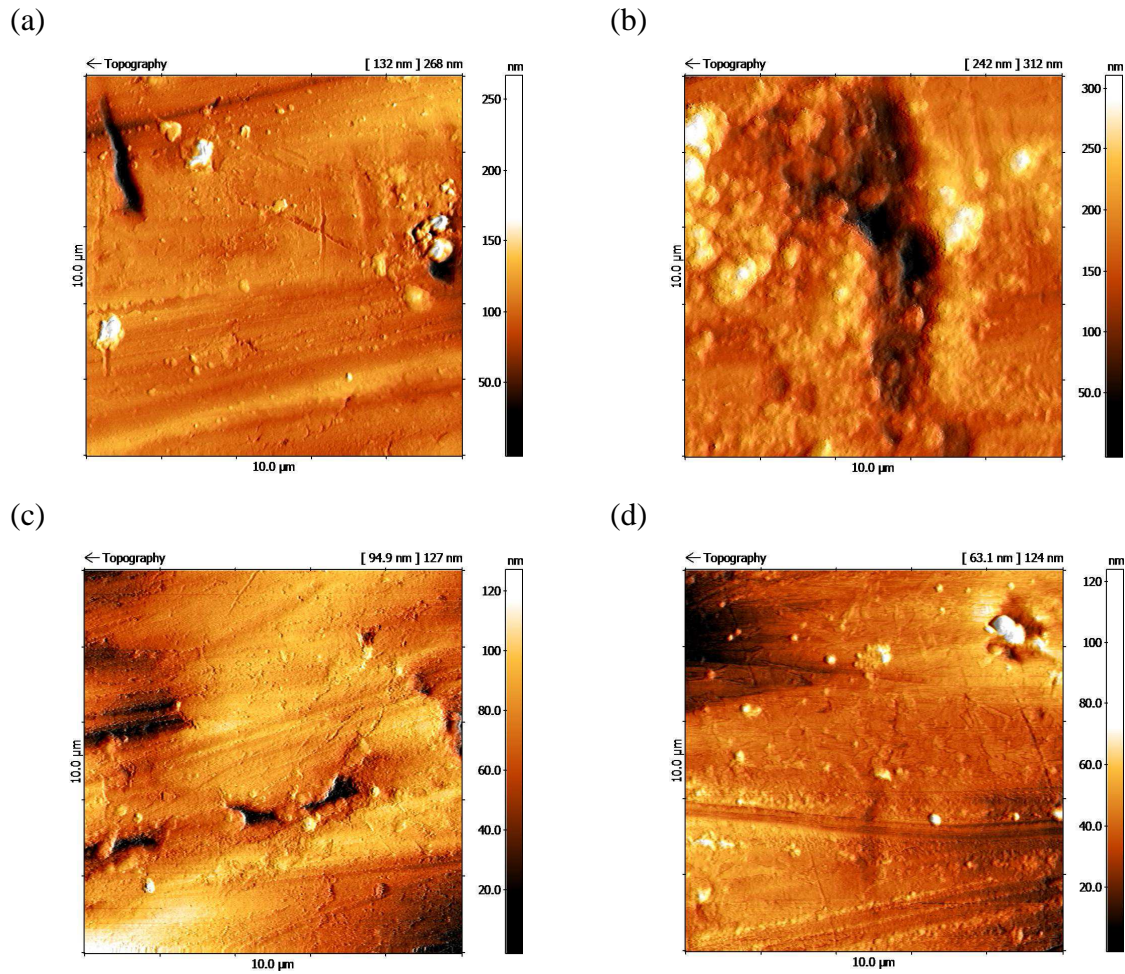


Figure III-18: Atomic force micrographs of a gold surface of the wire (a) without UV treatment and without gamma irradiation, (b) without UV treatment and after gamma irradiation, (c) after UV treatment and without gamma irradiation and (d) after UV treatment and after gamma irradiation.

Table III-20: Mean of roughness factors of atomic force micrographs.

	Roughness factor
Without UV treatment, without gamma irradiation	15
Without UV treatment, after gamma irradiation	24
After UV treatment, without gamma irradiation	14
After UV treatment, after gamma irradiation	15

4.2.3 Comparative discussion of the results obtained with both treatment methods

The gold layer of the wires was treated successfully aiming at decreasing the cytotoxic potential by applying both methods, i.e., Fenton solutions and UV-photolysis of hydrogen peroxide. Both treatment methods were optimized resulting in cell vitalities of approximately 100% indicating that the cytotoxic potential of the treated wires is zero. Thus the main aim of the study has been achieved.

In addition to the cytotoxicity test, the alterations of the gold surface caused by the radical treatment and by the subsequent gamma irradiation were investigated. After both treatment methods, i.e., with Fenton solutions and by UV-photolysis of hydrogen peroxide, no distinct smoothing of the gold surface was observed by atomic force microscopy. Nevertheless, in case of the treatment with Fenton solution, gold was detected in the treatment solutions indicating that the gold surface was changed slightly, but the alteration could not be detected by AFM measurements. In contrast, in the hydrogen peroxide solutions irradiated with UV light to generate $\cdot\text{OH}$ radicals for treating the gold surfaces no gold was detected. That means that either no net dissolution of gold happened, or the amounts of dissolved gold were too low for detection by ICP-AES measurements or by atomic force microscopy. Furthermore, it is assumed that not only the generated radicals but also the UV light and the high temperatures, to which the gold surfaces are exposed during UV-photolysis of hydrogen peroxide, affect the gold surface.

Further, it was found that the roughness of the gold surface after gamma irradiation depends on the forgoing treatment procedure. A gold surface treated with Fenton solutions gets rougher by irradiation with gamma rays, while the gamma irradiation of a gold surface treated by UV-photolysis of hydrogen peroxide causes no roughening of the gold surface. Despite these different surface roughnesses obtained after gamma irradiation, both surfaces behave similar with respect to the cytotoxicity as they are non-cytotoxic. Since an untreated gold surface is cytotoxic after gamma irradiation, it follows that the gold surface properties are changed by treating with Fenton solutions and by treating with UV-photolysis of hydrogen peroxide, although no surface alteration could be observed by atomic force microscopy.

5 Conclusions

Recently, it has been found out that $\cdot\text{OH}$ radicals generated by Fenton solution smooth mechanically polished gold surfaces by dissolution of highly reactive gold atoms. In the light of this finding, in this thesis the surfaces of medical products based on gold were investigated and modified by treating with $\cdot\text{OH}$ radicals.

The surfaces of gold implants were analysed by atomic force microscopy before implantation and after remaining the gold in the peritoneal cavity of mice for several days. It was found that there is an analogy between the exposure of mechanically polished gold to Fenton solutions and the exposure of mechanically polished gold to immune reactions as a smoothing of the gold surface is observed after implantation of gold in the peritoneal cavity of wild type mice. The effect can be ascribed to oxygen radicals formed during NADPH oxidase catalysed immune reactions, because no smoothing of the gold surface is observed after implantation into knock-out mice lacking the gp91^{phox} subunit of the NADPH oxidase. Further, an alteration of the surface of gold implants could be prevented by treating the gold surface with $\cdot\text{OH}$ radicals of Fenton solutions before implantation. This indicates that the release of gold from implants can be reduced.

In a further study, the gold layer of a recently developed nanodetector used to isolate circulating tumour cells from the blood stream of cancer patients was treated with $\cdot\text{OH}$ radicals aiming at a diminishing of the cytotoxicity of the gold after gamma irradiation. In addition to Fenton solutions, also UV-photolysis of hydrogen peroxide was used to generate $\cdot\text{OH}$ radicals. Both methods of $\cdot\text{OH}$ radical generation were optimized successfully for treating the gold layer resulting in a non-cytotoxic gold layer of the nanodetector. These results make possible an *in vivo* application of the nanodetector.

From the obtained results it follows that the properties of metallic gold for its use as medical material can be improved by treatment with oxygen radicals. Metallic gold is widely employed as implant material in medicine and dentistry, e.g., in reconstructive surgery of the middle ear [187–189], in upper eyelid implant surgery [190, 191], as coating of voice prostheses [192], in endovascular stents [193], in antitumour treatment [194], in drug delivery microchips [195] and in dental prostheses like inlays, onlays, crowns, and bridges [116]. Although gold is widely accepted as biocompatible implant material, some undesired negative effects of gold implants have been reported, e.g., rejection reactions, formation of granuloma and allergy to gold [188, 190, 193, 196, 197]. Such complications

can possibly be attributed to material properties [196] causing a dissolution of gold from the implants. Thus, it is easily conceivable that several undesired effects of gold implants can be reduced by a pre-treatment of the gold with oxygen radicals. By treating the gold with oxygen radicals before implantation, the release of gold from implants can be reduced, and a potential cytotoxicity of gold can be decreased. Thus, the biocompatibility of gold implants can be further improved.

IV Summary

Surface and electrode modifications allow the alteration of surface and electrode properties required for certain applications.

In the first part of this thesis, a pH sensitive graphite/quinhydrone composite electrode for FIA systems was optimized by using polysiloxane as binder material. This allows an easier handling of the electrode. Furthermore, new applications of the FIA system in conjunction with the pH sensitive detection system were developed.

The electrode used here in conjunction with a common reference electrode proved to be a very useful potentiometric detector for FIA acid-base titrations of aqueous solutions. Even acid-base titrations in buffered solutions were performed successfully with the FIA system allowing the determination of activities of enzymes, which catalyse reactions with increasing or decreasing proton concentrations.

A FIA system was applied to measure calcium and magnesium ions in different water samples by measuring the hydronium ion release during the complexometric reaction between EDTA and calcium or magnesium ions.

A method was established to determine sequentially the titratable acidity and the pH of different wine samples. The new FIA method fulfils the official requirements of the *Organisation Internationale de la Vigne et du Vin* with respect to reproducibility and repeatability and can be easily adjusted to the legal requirements in USA and Europe.

In summary, the first part of this thesis shows that the FIA system in conjunction with the graphite/quinhydrone/polysiloxane composite electrode is very well suited for simple, rapid and automatic determinations of small sample volumes in the areas of water analysis, food analysis or even biochemical analysis, provided that hydronium ions are involved. For all applications, one and the same measuring device without changing the detection system is used. Only different carrier solutions are necessary, which can be provided by a proper stream selector.

The second part of this thesis is focused on the modification of gold surfaces of medical devices by treatment with $\cdot\text{OH}$ radicals. These investigations are based on previous studies of the impact of $\cdot\text{OH}$ radicals on mechanically polished gold surfaces resulting in a smoothing of the surface by dissolution of highly reactive gold atoms.

In this thesis, the effect of $\cdot\text{OH}$ radicals, generated either *ex vivo* by Fenton solutions or *in vivo* by immune reactions, on gold implants was analysed using atomic force microscopy. It was found that there is an analogy between the exposure of gold to Fenton solutions and the exposure of gold to immune reactions. The pre-treatment of gold implants with $\cdot\text{OH}$ radicals of Fenton solution prevents surface alterations of the gold implants *in vivo*. This indicates that the *in vivo* release of gold from implants can be reduced by exposing the gold implants to Fenton solution before implantation.

Finally, the modification of gold surfaces by $\cdot\text{OH}$ radicals was applied to a medical nanodetector, which is coated with a gold layer and functionalized with antibodies, for isolating CTCs from the blood stream of cancer patients. By treating the gold layer of the nanodetector with $\cdot\text{OH}$ radicals generated by Fenton solution or by UV-photolysis of hydrogen peroxide, the cytotoxicity of the gold layer after gamma irradiation was reduced to almost zero. This modification of the gold surface with $\cdot\text{OH}$ radicals allows applying the nanodetector for *in vivo* applications.

V List of references

- [1] F. Scholz, H. Düssel, B. Meyer, *Fresenius J. Anal. Chem.*, 347 (1993) 458.
- [2] H. Düssel, Š. Komorsky-Lovrić, F. Scholz, *Electroanalysis*, 7 (1995) 889.
- [3] H. Kahlert, J.R. Pörksen, J. Behnert, F. Scholz, *Anal. Bioanal. Chem.*, 382 (2005) 1981.
- [4] H. Kahlert, J.R. Pörksen, I. Isildak, M. Andac, M. Yolcu, J. Behnert, F. Scholz, *Electroanalysis*, 17 (2005) 1085.
- [5] K. Cammann, *Instrumentelle Analytische Chemie*, Spektrum Akademischer Verlag, Heidelberg, Berlin, 2001.
- [6] A.M. Nowicka, U. Hasse, M. Hermes, F. Scholz, *Angew. Chem. Int. Ed.*, 49 (2010) 1061.
- [7] A.M. Nowicka, U. Hasse, G. Sievers, M. Donten, Z. Stojek, S. Fletcher, F. Scholz, *Angew. Chem. Int. Ed.*, 49 (2010) 3006.
- [8] G. Danscher, *Histochem. Cell. Biol.*, 117 (2002) 447.
- [9] A. Larsen, M. Stoltenberg, G. Danscher, *Histochem. Cell. Biol.*, 128 (2007) 1.
- [10] N. Saucedo-Zeni, S. Mewes, R. Niestroj, L. Gasiorowski, D. Murawa, P. Nowaczyk, T. Tomasi, E. Weber, G. Dworacki, N.G. Morgenthaler, H. Jansen, C. Propping, K. Sterzynska, W. Dyszkiewicz, M. Zabel, M. Kiechle, U. Reuning, M. Schmitt, K. Lücke, *Int. J. Oncol.* (2012).
- [11] M. Alunni-Fabbroni, M.T. Sandri, *Methods*, 50 (2010) 289.
- [12] J.D. O'Flaherty, S. Gray, D. Richard, D. Fennell, J.J. O'Leary, F.H. Blackhall, K.J. O'Byrne, *Lung Cancer*, 76 (2012) 19.
- [13] S. Sleijfer, J.-W. Gratama, A.M. Sieuwerts, J. Kraan, J.W.M. Martens, J.A. Foekens, *Eur. J. Cancer*, 43 (2007) 2645.
- [14] E. Dotan, S.J. Cohen, K.R. Alpaugh, N.J. Meropol, *Oncologist*, 14 (2009) 1070.

- [15] W. Buchberger, *Elektrochemische Analyseverfahren*, Spektrum Akademischer Verlag, Heidelberg, Berlin, 1998.
- [16] C. Colombo, T. Kappes, P.C. Hauser, *Anal. Chim. Acta*, 412 (2000) 69.
- [17] M. Gratzl, C. Yi, *Anal. Chem.*, 65 (1993) 2085.
- [18] O.T. Guenat, W.E. Morf, B.H. van der Schoot, N.F. de Rooij, *Anal. Chim. Acta*, 361 (1998) 261.
- [19] F. Sagara, T. Kobayashi, T. Tajima, H. Ijyuin, I. Yoshida, D. Ishii, K. Ueno, *Anal. Chim. Acta*, 261 (1992) 505.
- [20] C. Yi, M. Gratzl, *Anal. Chem.*, 66 (1994) 1976.
- [21] J. Ružička, E.H. Hansen, *Flow Injection Analysis*, 2nd ed., Wiley, New York, 1988.
- [22] B. Karlberg, G.E. Pacey, *Flow Injection Analysis: A Practical Guide*, Elsevier, Amsterdam, 1989.
- [23] K. Cammann, *Fresenius Z. Anal. Chem.*, 329 (1988) 691.
- [24] K. Vahl, H. Kahlert, D. Böttcher, R. Wardenga, Š. Komorsky-Lovrić, U. Bornscheuer, F. Scholz, *Anal. Chim. Acta*, 610 (2008) 44.
- [25] M. Lovrić, Š. Komorsky-Lovrić, H. Kahlert, F. Scholz, *Anal. Chim. Acta*, 602 (2007) 75.
- [26] T. Steinhardt, *Entwicklung von Festkörper-Chinhydron-Elektroden und deren Anwendung als pH-Sensoren*, Dissertation, Ernst-Moritz-Arndt-Universität Greifswald, 2007.
- [27] G. Schwarzenbach, W. Biedermann, F. Bangerter, *Helv. Chim. Acta*, 29 (1946) 811.
- [28] G. Schwarzenbach, W. Biedermann, *Helv. Chim. Acta*, 31 (1948) 459.
- [29] E. Pungor, Z. Fehér, G. Nagy, K. Tóth, W.J. Blaedel, *Crit. Rev. Anal. Chem.*, 14 (1983) 175.

- [30] J. Růžicka, E.H. Hansen, *Anal. Chim. Acta*, 78 (1975) 145.
- [31] J. Möller, Flow injection analysis, in: R. Borsdorf, W. Fresenius, H. Günzler, W. Huber, H. Keller, I. Lüderwald, G. Tölg, H. Wissner (Eds.), *Analytiker-Taschenbuch Band 7*, Akademie-Verlag Berlin, Berlin, 1987.
- [32] M. Otto, *Analytische Chemie*, 4th ed., Wiley-VCH, Weinheim, 2011.
- [33] D.A. Skoog, J.J. Leary, *Instrumentelle Analytik*, Springer, Berlin, Heidelberg, 1996.
- [34] W. Frenzel, Methodische Möglichkeiten der Fließinjektionsanalyse, in: H. Günzler (Ed.), *Analytiker Taschenbuch 20*, Springer, Berlin, Heidelberg, 1999.
- [35] R. Kellner, J.-M. Mermet, M. Otto, M. Valcárcel, H.M. Widmer (Eds.), *Analytical Chemistry: A Modern Approach to Analytical Science*, 2nd ed., Wiley-VCH, Weinheim, 2004.
- [36] G. Schwedt, *Taschenatlas der Analytik*, 3rd ed., Wiley-VCH, Weinheim, 2007.
- [37] J. Strähle, E. Schweda, Jander-Blasius Einführung in das anorganisch-chemische Praktikum, S. Hirzel Verlag, Stuttgart, 1995.
- [38] D.C. Harris, *Lehrbuch der Quantitativen Analyse*, Vieweg, Braunschweig, 1998.
- [39] J. Růžicka, E.H. Hansen, H. Mosbaek, *Anal. Chim. Acta*, 92 (1977) 235.
- [40] A.U. Ramsing, J. Růžicka, E.H. Hansen, *Anal. Chim. Acta*, 129 (1981) 1.
- [41] H. Kahlert, Potentiometry, in: F. Scholz (Ed.), *Electroanalytical Methods: Guide to Experiments and Applications*, 2nd ed., Springer, Berlin, Heidelberg, 2010.
- [42] H. Galster, pH Measurement: Fundamentals, Methods, Applications, Instrumentation, VCH, Weinheim, 1991.
- [43] C.H. Hamann, W. Vielstich, *Elektrochemie*, 4th ed., Wiley-VCH, Weinheim, 2005.
- [44] E. Biilmann, *Ann. Chim.*, 15 (1921) 109.
- [45] H. Kahlert, Quinhydrone electrode, in: A.J. Bard, G. Inzelt, F. Scholz (Eds.), *Electrochemical Dictionary*, Springer, Berlin, Heidelberg, 2008.

- [46] H. Kahlert, Reference Electrodes, in: F. Scholz (Ed.), *Electroanalytical Methods: Guide to Experiments and Applications*, 2nd ed., Springer, Berlin, Heidelberg, 2010.
- [47] F. Hovorka, W.C. Dearing, *J. Am. Chem. Soc.*, 57 (1935) 446.
- [48] J.L. Gabbard, *J. Am. Chem. Soc.*, 69 (1947) 533.
- [49] H. Kahlert, T. Steinhardt, J. Behnert, F. Scholz, *Electroanalysis*, 16 (2004) 2058.
- [50] T.E. Edmonds, G. Coutts, *Analyst*, 108 (1983) 1013.
- [51] C. Hongbo, E.H. Hansen, J. Růžicka, *Anal. Chim. Acta*, 169 (1985) 209.
- [52] F.R. del Mundo, T.J. Cardwell, R.W. Cattrall, P.J. Iles, I.C. Hamilton, *Electroanalysis*, 1 (1989) 353.
- [53] S. Böhm, W. Olthuis, P. Bergveld, *Mikrochim. Acta*, 134 (2000) 237.
- [54] S.A.M. Marzouk, *Anal. Chem.*, 75 (2003) 1258.
- [55] S. Alegret, J. Alonso, J. Bartroli, J. Domenech, N. Jaffrezic-Renault, Y. Duvault-Herrera, *Anal. Chim. Acta*, 222 (1989) 373.
- [56] B.H. van der Schoot, H.H. van den Vlekkert, N.F. de Rooij, A. van den Berg, A. Grisel, *Sensors and Actuators B*, 4 (1991) 239.
- [57] C.G. Zampronio, J.J.R. Rohwedder, R.J. Poppi, *Talanta*, 51 (2000) 1163.
- [58] APHA, AWWA, WEF, *Standard Methods for the Examination of Water and Wastewater*, 21st ed., American Public Health Association, American Water Works Association and Water Environment Federation, Washington DC, 2005.
- [59] C. Bliefert, *Umweltchemie*, 3rd ed., Wiley-VCH, Weinheim, 2002.
- [60] G. Jander, K.F. Jahr, *Maßanalyse*, 17th ed., Walther de Gruyter, Berlin, 2009.
- [61] E. Riedel, C. Janiak, *Anorganische Chemie*, 5th ed., Walter de Gruyter, Berlin, New York, 2002.
- [62] Wasch- und Reinigungsmittelgesetz vom 29.4.2007 (BGBl. I S. 600), <http://www.gesetze-im-internet.de/wrmg/BJNR060000007.html>.

- [63] <http://www.dvgw.de/wasser/informationen-fuer-verbraucher/wasserhaerte/>.
- [64] G. Jander, E. Blasius, Einführung in das anorgansich-chemische Praktikum, S. Hirzel Verlag, Stuttgart, 1995.
- [65] <http://www.macherey-nagel.de/tabid/10489/Default.aspx>.
- [66] http://www.serim.com/product_detail.aspx?pid=29.
- [67] M. Angel de la Fuente, M. Juárez, Analyst, 120 (1995) 107.
- [68] M. Angel de la Fuente, F. Montes, G. Guerrero, M. Juárez, Food Chemistry, 80 (2003) 573.
- [69] A. Asfaw, G. Wibetoe, Anal. Bioanal. Chem., 382 (2005) 173.
- [70] N. Kovachev, B. Almagro, M.Á. Aguirre, M. Hildago, A.M. Gañán-Calvo, A. Canals, J. Anal. At. Spectrom, 24 (2009) 1213.
- [71] M.C. Cheney, D.J. Curran, K.S. Fletcher, Anal. Chem., 52 (1980) 942.
- [72] J.-H. Kim, J.-H. Lee, J. Chromatogr. A, 782 (1997) 140.
- [73] A. Bellomo, A. de Robertis, C. D'Arrigo, Anal. Chim. Acta, 149 (1983) 401.
- [74] L.F. Capitán-Vallvey, M.D. Fernández-Ramos, P. Alvarez de Cienfuegos. Gálvez, F. Santoyo-González, Anal. Chim. Acta, 481 (2003) 139.
- [75] E. Gómez, J.M. Estela, V. Cerdà, Anal. Chim. Acta, 249 (1991) 513.
- [76] T.M. Lerga, C.K. O'Sullivan, Anal. Chim. Acta, 610 (2008) 105.
- [77] K. Suzuki, K. Tohda, Y. Tanda, H. Ohzora, S. Nishihama, H. Inoue, T. Shirai, Anal. Chem., 61 (1989) 382.
- [78] S. Rondinini, P.R. Mussini, A. Vertova, A. Bortoluzzi, L. Bono, P. Longhi, Sensors and Actuators B, 23 (1995) 27.
- [79] M. Numata, K. Baba, A. Hemmi, H. Hachiya, S. Ito, T. Masadome, Y. Asano, S. Ohkubo, T. Gomi, T. Imato, T. Hobo, Talanta, 55 (2001) 449.

- [80] P.C. Meier, D. Erne, Z. Cimerman, D. Ammann, W. Simon, *Mikrochim. Acta*, 1 (1980) 317.
- [81] M. Maj-Zurawska, M. Rouilly, W.E. Morf, W. Simon, *Anal. Chim. Acta*, 218 (1989) 47.
- [82] J. Saurina, E. López-Aviles, A.L. Moal, S. Hernández-Cassou, *Anal. Chim. Acta*, 464 (2002) 89.
- [83] R.A.C. Lima, S.R.B. Santos, R.S. Costa, G.P.S. Marccone, R.S. Honorato, V.B. Nascimento, M.C.U. Araujo, *Anal. Chim. Acta*, 518 (2004) 25.
- [84] R.J. Foster, D. Diamond, *Anal. Chem.*, 64 (1992) 1721.
- [85] O. Hernández, F. Jiménez, A.I. Jiménez, J.J. Arias, J. Havel, *Anal. Chim. Acta*, 320 (1996) 177.
- [86] R.A.S. Lapa, J.L.F.C. Lima, J.L.M. Santos, *Food Chem.*, 55 (1996) 397.
- [87] M. Blanco, J. Coello, J. Gené, H. Iturriaga, S. MasPOCH, *Anal. Chim. Acta*, 224 (1989) 23.
- [88] M.B. Petrovich, V.R.A. Filho, J.A.G. Neto, *Ecl. Quim.*, 32 (2007) 25.
- [89] N.A. Chaniotakis, J.K. Tsagatakis, E.A. Moschou, S.J. West, X. Wen, *Anal. Chim. Acta*, 356 (1997) 105.
- [90] J. Robinson, *Das Oxford Weinlexikon*, Hallwag, Bern, 1995.
- [91] C.S. Ough, M.A. Amerine, *Methods for analysis of must and wines*, 2nd ed., John Wiley & Sons New York, 1988.
- [92] B.W. Zoecklein, K.C. Fugelsang, B.H. Gump, F.S. Nury, *Wine analysis and production*, Chapman & Hall, New York, 1995.
- [93] OIV, *Compendium of International Methods of Wine and Must Analysis*, International Organisation of Vine and Wine, Paris, 2011.
- [94] O.Y. Berezin, Y.I. Tur'Yan, I. Kuselman, A. Shenhar, *Talanta*, 42 (1995) 507.

- [95] E.A. Zakharova, M.L. Moskaleva, Y.A. Akeneev, E.S. Moiseeva, G.B. Slepchenko, N.P. Pikula, *Russ. J. Anal. Chem.*, 66 (2011) 848.
- [96] M.A. Baldo, S. Daniele, G.A. Mazzocchin, *Anal. Chim. Acta*, 272 (1993) 151.
- [97] S. Ohtsuki, N. Kunimatsu, K. Takamura, F. Kusu, *Electroanalysis*, 13 (2001) 404.
- [98] A.R. Tôrres, W. da Silva Lyra, S.I.E. de Andrade, R.A.N. Andrade, E.C. da Silva, M.C.U. Araújo, E. da Nóbrega Gaião, *Talanta*, 84 (2011) 601.
- [99] M. Peris-Tortajada, A. Maquieira, R. Puchades, *Am. J. Enol. Vitic.*, 44 (1993) 118.
- [100] R.S. Honorato, M.C.U. Araújo, R.A.C. Lima, E.A.G. Zagatto, R.A.S. Lapa, J.L.F.C. Lima, *Anal. Chim. Acta*, 396 (1999) 91.
- [101] A.J.C. Garcia, B.F. Reis, *J. Autom. Methods Manage. Chem.*, 2006 (2006) 1.
- [102] E. Mataix, M.D. Luque de Castro, *Anal. Chim. Acta*, 381 (1999) 23.
- [103] J. Marcos, A. Ríos, M. Valcárcel, *Anal. Chim. Acta*, 261 (1992) 489.
- [104] E.N. Gaião, R.S. Honorato, S.R.B. Santos, M.C.U. Araújo, *Analyst*, 124 (1999) 1727.
- [105] T.J. Cardwell, R.W. Catrall, G.J. Cross, G.R. O'Connell, J.D. Petty, G.R. Scollary, *Analyst*, 116 (1991) 1051.
- [106] A.O.S.S. Rangel, I.V. Tóth, *Analyst*, 123 (1998) 661.
- [107] A. Ruland, Küster-Thiel Rechentafeln für die chemische Analytik, 103rd ed., Walter de Gruyter, Berlin, 1985.
- [108] E. Fluck, M. Becke-Goehring, Einführung in die Theorie der quantitativen Analyse, 7th ed., Steinkopff Verlag, Darmstadt, 1990.
- [109] U.R. Kunze, G. Schwedt, Grundlagen der quantitativen Analyse, 6th ed., Wiley-VCH, Weinheim, 2009.
- [110] Hydroxybernsteinsäure, Römpp Online Version 3.25, Thieme, Stuttgart, 2012.

- [111] U.T. Bornscheuer, R.J. Kazlauskas, *Hydrolases in Organic Synthesis: Regio- and Stereoselective Biotransformations*, Wiley-VCH, Weinheim, 1999.
- [112] F. Theil, *Enzyme in der organischen Synthese*, Spektrum Akademischer Verlag, Heidelberg, Berlin, Oxford, 1997.
- [113] A.E. Martell, R.M. Smith, *Critical Stability Constants*, Vol. 1: Amino Acids, Plenum Press, New York, London, 1974.
- [114] T.A. Green, *Gold Bull.*, 40 (2007) 105.
- [115] Z. Huang, D. Zhu, F. Lou, W. Zhou, *Appl. Surf. Sci.*, 255 (2008) 2619.
- [116] E.T.K. Demann, P.S. Stein, J.E. Haubenreich, J. Long-Term Eff. Med. Implants, 15 (2005) 687.
- [117] D.E. Tallman, Electrode materials, in: A.J. Bard, G. Inzelt, F. Scholz (Eds.), *Electrochemical Dictionary*, Springer, Berlin, Heidelberg, 2008.
- [118] M. Orlik, Z. Galus, Electrochemistry of Gold, Silver, and Mercury, in: A.J. Bard, M. Stratmann, F. Scholz, C.J. Pickett (Eds.), *Encyclopedia of Electrochemistry*, Vol. 7b, Wiley-VCH, Weinheim, 2006.
- [119] F. Scholz, G. López de Lara Gonzáles, L. Machado de Carvalho, M. Hilgemann, K.Z. Brainina, H. Kahlert, R.S. Jack, D.T. Minh, *Angew. Chem. Int. Ed.*, 46 (2007) 8079.
- [120] M. Hilgemann, F. Scholz, H. Kahlert, L. Machado de Carvalho, M. Barcellos da Rosa, U. Lindequist, M. Wurster, P.C. do Nascimento, D. Bohrer, *Electroanalysis*, 22 (2010) 406.
- [121] B. Halliwell, J.M.C. Gutteridge, *Free radicals in biology and medicine*, 3rd ed., Oxford University Press, New York, 1999.
- [122] M. Tarr, F. Samson, *Oxygen free radicals in tissue damage*, Birkhäuser, Boston, 1993.
- [123] W.A. Pryor, *Einführung in die Radikalchemie*, Verlag Chemie, Weinheim, 1974.
- [124] K. Müller, *Pharmazie in unserer Zeit*, 17 (1988) 71.

- [125] I. Kruk, Environmental toxicology and chemistry of oxygen species, Springer, Berlin, Heidelberg, 1998.
- [126] E. Cadenas, Mechanisms of oxygen activation and reactive oxygen species detoxification, in: S. Ahmad (Ed.), Oxidative stress and antioxidant defenses in biology, Chapman & Hall, New York, 1995.
- [127] E.F. Elstner, Der Sauerstoff: Biochemie, Biologie, Medizin, BI-Wissenschaftsverlag, Mannheim, Wien, Zürich, 1990.
- [128] J.A. Imlay, Annu. Rev. Microbiol., 57 (2003) 395.
- [129] K. Chen, S.R. Thomas, J.F. Keany, Free Radic. Biol. Med., 35 (2003) 117.
- [130] E. Cadenas, K.J.A. Davies, Free Radic. Biol. Med., 29 (2000) 222.
- [131] M.P. Murphy, Biochem. J., 417 (2009) 1.
- [132] P.G. Winyard, D.R. Blake, C.H. Evans, Free radicals and inflammation, Birkhäuser, Berlin, 2000.
- [133] B.M. Babior, J.D. Lambeth, W. Nauseef, Arch. Biochem. Biophys., 397 (2002) 342.
- [134] H.J.H. Fenton, J. Chem. Soc. Trans., 65 (1894) 899.
- [135] F. Haber, R. Willstätter, Ber. Dtsch. Chem. Ges. (A und B Series), 64 (1931) 2844.
- [136] F. Haber, J. Weiss, Naturwissenschaften, 20 (1932) 948.
- [137] J.A. Imlay, I. Fridovich, J. Biol. Chem., 266 (1991) 6957.
- [138] G.V. Buxton, C.L. Greenstock, W.P. Helman, A.B. Ross, J. Phys. Chem. Ref. Data, 17 (1988) 513.
- [139] S. Goldstein, D. Aschengrau, Y. Diamant, J. Rabani, Environ. Sci. Technol., 41 (2007) 7486.
- [140] H. Rink, Chem. Unserer Zeit, 5 (1971) 90.

- [141] S. Goldstein, G. Czapski, Superoxide dismutase, in: N.A. PUNCHARD, F.J. KELLY (Eds.), *Free Radicals: A Practical Approach*, Oxford University Press, New York, 1996.
- [142] I. Fridovich, Xanthine oxidase, in: R.A. Greenwald (Ed.), *CRC Handbook of Methods for Oxygen Radical Research*, CRC Press, Boca Raton, 1985.
- [143] G.Z. Chen, *Angew. Chem. Int. Ed.*, 49 (2010) 5413.
- [144] G. Sievers, U. Hasse, F. Scholz, *J. Solid State Electrochem.*, 16 (2012) 1663.
- [145] G. Dutta, H. Yang, *Electrochem. Commun.*, 13 (2011) 1328.
- [146] G. Feng, T. Niu, X. You, Z. Wan, Q. Kong, S. Bi, *Analyst*, 136 (2011) 5058.
- [147] A.M. Nowicka, U. Hasse, M. Donten, M. Hermes, Z.J. Stojek, F. Scholz, *J. Solid State Electrochem.*, 15 (2011) 2141.
- [148] T. Rapecki, A.M. Nowicka, M. Donten, F. Scholz, Z. Stojek, *Electrochem. Commun.*, 12 (2010) 1531.
- [149] R.A. Ghossein, S. Bhattacharya, J. Rosai, *Clin. Cancer Res.*, 5 (1999) 1950.
- [150] Y.-F. Sun, X.-R. Yang, J. Zhou, S.-J. Qui, J. Fan, Y. Xu, *J. Cancer Res. Clin. Oncol.*, 137 (2011) 1151.
- [151] S. Paget, *Cancer Metastasis Rev.*, 8 (1989) 98.
- [152] I.J. Fidler, *Nat. Rev. Cancer*, 3 (2003) 1.
- [153] M.G. Krebs, J.-M. Hou, T.H. Ward, F.H. Blackhall, C. Dive, *Ther. Adv. Med. Oncol.*, 2 (2010) 351.
- [154] M. Cristofanilli, G.T. Budd, M.J. Ellis, A. Stopeck, J. Matera, M.C. Miller, J.M. Reuben, G.V. Doyle, W.J. Allard, L.W.M.M. Terstappen, D.F. Hayes, *N. Engl. J. Med.*, 351 (2004) 781.
- [155] P. Bossolasco, C. Ricci, G. Farina, D. Soligo, D. Pedretti, A. Scanni, G.L. Deliliers, *Cancer Detect. Prev.*, 26 (2002) 60.
- [156] V.V. Iakovlev, R.S. Goswami, J. Vecchiarelli, N.C.R. Arneson, S.J. Done, *Breast Cancer Res. Treat.*, 107 (2008) 145.

- [157] N. Xenidis, M. Perraki, M. Kafousi, S. Apostolaki, I. Bolonaki, A. Stathopoulou, K. Kalbakis, N. Androulakis, C. Kouroussis, T. Pallis, C. Christophylakis, K. Argyraki, E.S. Lianidou, S. Stathopoulos, V. Georgoulis, D. Mavroudis, *J. Clin. Oncol.*, 24 (2006) 3756.
- [158] A.E. Ring, L. Zabaglo, M.G. Ormerod, I.E. Smith, M. Dowsett, *Br. J. Cancer*, 92 (2005) 906.
- [159] T.E. Witzig, B. Bossy, T. Kimlinger, *Clin. Cancer Res.*, 8 (2002) 1085.
- [160] K. Pachmann, P. Heiß, U. Demel, G. Tilz, *Clin. Chem. Lab. Med.*, 39 (2001) 811.
- [161] P.D. Beitsch, E. Clifford, *Am. J. Surg.*, 180 (2000) 446.
- [162] E. Racila, D. Euhus, A.J. Weiss, C. Rao, J. McConnell, L.W.M.M. Terstappen, J.W. Uhr, *Proc. Natl. Acad. Sci. USA*, 95 (1998) 4589.
- [163] S. Nagrath, L.V. Sequist, S. Maheswaran, D.W. Bell, D. Irimia, L. Ulkus, M.R. Smith, E.L. Kwak, S. Digumarthy, A. Muzikansky, P. Ryan, U.J. Balis, R.G. Tompkins, D.A. Haber, M. Toner, *Nature*, 450 (2007) 1235.
- [164] S.J. Cohen, C.J.A. Punt, N. Iannotti, B.H. Saidman, K.D. Sabbath, N.Y. Gabrail, J. Picus, M. Morse, E. Mitchell, M.C. Miller, G.V. Doyle, H. Tissing, L.W.M.M. Terstappen, N.J. Meropol, *J. Clin. Oncol.*, 26 (2008) 3213.
- [165] S. Riethdorf, H. Fritsche, V. Müller, T. Rau, C. Schindlbeck, B. Rack, W. Janni, C. Coith, K. Beck, F. Jänicke, S. Jackson, T. Gornet, M. Cristofanilli, K. Pantel, *Clin. Cancer Res.*, 13 (2007) 920.
- [166] J.S. de Bono, H.I. Scher, R.B. Montgomery, C. Parker, M.C. Miller, H. Tissing, G.V. Doyle, L.W.W.M. Terstappen, K.J. Pienta, D. Raghavan, *Clin. Cancer Res.*, 14 (2008) 6302.
- [167] M. Cristofanilli, D.F. Hayes, G.T. Budd, M.J. Ellis, A. Stopeck, J.M. Reuben, G.V. Doyle, J. Matera, W.J. Allard, M.C. Miller, H.A. Fritsche, G.N. Hortobagyi, L.W.M.M. Terstappen, *J. Clin. Oncol.*, 23 (2005) 1420.
- [168] D.A. Nedosekin, M. Sarimollaoglu, J.-H. Ye, E.I. Galanzha, V.P. Zharov, *Cytometry A*, 79A (2011) 825.

- [169] E.I. Galanzha, E.V. Shashkov, P.M. Spring, J.Y. Suen, V.P. Zharov, *Cancer Res.*, 69 (2009) 7926.
- [170] I. Georgakoudi, N. Solban, J. Novak, W.L. Rice, X. Wei, T. Hasan, C.P. Lin, *Cancer Res.*, 64 (2004) 5044.
- [171] W. He, H. Wang, L.C. Hartmann, J.-X. Cheng, P.S. Low, *Proc. Natl. Acad. Sci. USA*, 104 (2007) 11760.
- [172] S.I. Seldinger, *Acta radiol.*, 39 (1953) 368.
- [173] Z.C.J. Higgs, D.A.L. Macafee, B.D. Braithwaite, C.A. Maxwell-Armstrong, *Lancet*, 366 (2005) 1407.
- [174] A.W.B. Stanton, B. Holroyd, J.W. Northfield, J.R. Levick, P.S. Mortimer, *Vascular Med.*, 3 (1998) 3.
- [175] X. Zhe, M.L. Cher, R.D. Bonfil, *Am. J. Cancer Res.*, 1 (2011) 740.
- [176] A. van de Stolpe, K. Pantel, S. Sleijfer, L.W. Terstappen, J.M.J. den Toonder, *Cancer Res.*, 71 (2011) 1.
- [177] A.G.J. Tibbe, M.C. Miller, L.W.M.M. Terstappen, *Cytometry A*, 71A (2007) 154.
- [178] F.J. Giessibl, *Rev. Mod. Phys.*, 75 (2003) 949.
- [179] G. Binnig, C.F. Quate, C. Gerber, *Phys. Rev. Letters*, 56 (1986) 930.
- [180] S.N. Magonov, M.-H. Whangbo, *Surface analysis with STM and AFM: Experimental and theoretical aspects of image analysis*, VCH, Weinheim, 1996.
- [181] H.-J. Butt, *Biophys. J.*, 60 (1991) 1438.
- [182] D.A. Bonnell, B.D. Huey, *Basic principles of scanning probe microscopy*, in: D.A. Bonnell (Ed.), *Scanning probe microscopy and spectroscopy: Theory, techniques, and applications*, 2nd ed., Wiley-VCH, New York, 2001.
- [183] N. Jalili, K. Laxminarayana, *Mechatronics*, 14 (2004) 907.

- [184] CEN, Biologische Beurteilung von Medizinprodukten – Teil 5: Prüfungen auf In-vitro-Zytotoxizität (ISO 10993-5:2009), Europäisches Komitee für Normung, Brüssel, 2009.
- [185] Guidance document on using in vitro data to estimate in vivo starting doses for acute toxicity, NIH Publication No. 01-4500, 2001 (http://iccvam.niehs.nih.gov/docs/acutetox_docs/guidance0801/iv_guide.pdf).
- [186] D.A. Scudiero, R.H. Shoemaker, K.D. Paull, A. Monks, S. Tierney, T.H. Nofziger, M.J. Currens, D. Seniff, M.R. Boyd, *Cancer Res.*, 48 (1988) 4827.
- [187] M. Gjurić, S. Schagerl, *Am. J. Otol.*, 19 (1998) 273.
- [188] K. Schneider, R. Hagen, *Laryngo-Rhino-Otol.*, 82 (2003) 486.
- [189] P. Dost, *Laryngo-Rhino-Otol.*, 79 [Suppl.] (2000) S53.
- [190] A. Berghaus, K. Neumann, T. Schrom, *Arch. Facial Plast. Surg.*, 5 (2003) 166.
- [191] T.E. Linder, V.E. Pike, C.J. Linstrom, *Laryngoscope*, 106 (1996) 1115.
- [192] D. Arweiler-Harbeck, A. Sanders, M. Held, M. Jerman, H. Ehrich, K. Jahnke, *Acta Otolaryngol.*, 121 (2001) 643.
- [193] E.R. Edelman, P. Seifert, A. Groothuis, A. Morss, D. Bornstein, C. Rogers, *Circulation*, 103 (2001) 429.
- [194] D. Choy, J.S.T. Sham, W.I. Wei, C.M. Ho, P.M. Wu, *Int. J. Radiat. Oncol. Biol. Phys.*, 25 (1993) 505.
- [195] J.T. Santini, M.J. Cima, R. Langer, *Nature*, 397 (1999) 335.
- [196] T. Schrom, C. Taege, G. Wolf, A. Reinhardt, H. Scherer, *HNO*, 54 (2006) 591.
- [197] H. Möller, *Contact Dermatit.*, 47 (2002) 63.

VI List of abbreviations

A_p	Peak area
a_x	Activity of “X”
AAS	Atomic absorption spectroscopy
ADP	Adenosine diphosphate
AES	Atomic emission spectroscopy
AFM	Atomic force microscopy
AuNP	Gold nanoparticle
c	Concentration
CEN	European committee for standardization
CoA	Coenzyme A
CTC	Circulating tumour cell
D	Dispersion coefficient
DNA	Deoxyribonucleic acid
DNase I	Deoxyribonuclease I
ΔE_p	Peak height of potentiometric peak in FIA measurement
E	Electrode potential
$E_C^{\ominus'}$	Formal potential
E^{\ominus}	Standard potential
E_{redox}	Redox potential
e^-	Electron
EDTA	Ethylenediaminetetraacetic acid (H_4Y)
EMT	Epithelial-mesenchymal transition
EP	Equivalence point
EpCAM	Epithelial cell adhesion molecule
F	Faraday constant
FIA	Flow-Injection-Analysis
FSMW	Functionalized and structured medical wire
HF	High frequency
HQ^-	Anion of hydroquinone
H_2Q	Hydroquinone
I	Ionic strength

ICP	Inductively coupled plasma
ISE	Ion selective electrode
ISFET	Ion sensitive field-effect transistor
K	Equilibrium constant
K_a	Acidity constant
K_b	Basicity constant
k_s	Electron transfer rate
KCl_{sat}	Saturated potassium chloride solution
LOD	Lowest detection limit
LPS	Lipopolysaccharide
MET	Mesenchymal-epithelial transition
MTT	3-(4,5-Dimethylthiazol-2-yl)-2,5-diphenyltetrazolium bromide
n	Amount of substance
$NADP^+/NADPH$	Nicotinamide adenine dinucleotide phosphate
Na_2 -EDTA	Disodium salt of ethylenediaminetetraacetic acid (Na_2H_2Y)
NHDF-cell	Normal human adult dermal fibroblast
OIV	Organisation Internationale de la Vigne et du Vin
Ox	Oxidant
p.a.	For analysis
PBS	Phosphate buffered saline
PCR	Polymerase chain reaction
PMMA	Poly(methyl methacrylate)
PVC	Polyvinyl chloride
Q	Flow rate
Q	Quinone
Q^{2-}	Dianion of hydroquinone
R	universal gas constant
Red	Reductant
RPMI-medium	Roswell Park Memorial Institute medium
SPM	Scanning probe microscopy
ROS	Reactive oxygen species
S	Sensitive surface
S_v	Sample volume
SAM	Self-assembled monolayer

SDS	Sodium dodecyl sulphate
t	Time
T	Absolute temperature
UV	Ultraviolet
UV/VIS	Ultraviolet–visible spectroscopy
$V(\text{H}_2\text{O})_{\text{add}}$	Added water volume
WRMG	“Wasch- und Reinigungsmittelgesetz” “Gesetz über die Umweltverträglichkeit von Wasch- und Reinigungsmitteln”, i.e., law on the environmental compatibility of washing and cleaning agents
XOD	Xanthine oxidase
XTT	2,3-bis-(2-methoxy-4-nitro-5-sulfophenyl)-2H-tetrazolium-5-carboxanilide
z	Number of transferred electrons
λ	Wavelength

Erklärung

Hiermit erkläre ich, dass diese Arbeit bisher von mir weder an der Mathematisch-Naturwissenschaftlichen Fakultät der Ernst-Moritz-Arndt-Universität Greifswald noch einer anderen wissenschaftlichen Einrichtung zum Zwecke der Promotion eingereicht wurde.

Ferner erkläre ich, dass ich diese Arbeit selbständig verfasst und keine anderen als die darin angegebenen Hilfsmittel und Hilfen benutzt und keine Textabschnitte eines Dritten ohne Kennzeichnung übernommen habe.

Curriculum vitae

Katja Vahl

Mühlenweg 23
17489 Greifswald

Date and place of birth: 2nd of February 1983 in Greifswald, Germany

Education

- | | |
|-----------------|--|
| From 11/2007 | Ph.D. studies at the University of Greifswald
Under supervision of Prof. Dr. F. Scholz, Institute of Biochemistry |
| 10/2002–05/2007 | Studies of Environmental Sciences at the University of Greifswald
Final grade: 1.3
Diploma thesis: „Anwendung der FIA-Titration auf die Kinetik enzymatischer Reaktionen“ |
| 06/2002 | Abitur at the Friedrich-Ludwig-Jahn-Gymnasium, Greifswald
Final grade: 1.4 |

Grants

- | | |
|-----------------|---|
| 06/2009–05/2011 | Scholarship of the Alfried-Krupp-Wissenschaftskolleg Greifswald
Via the interdisciplinary graduate school „Studies of the interaction of free oxygen radicals with molecules at electrodes and applications to biochemical and medical systems” |
| 09/2008–11/2008 | Scholarship of the DAAD
For research stay at Hanoi University of Science / CETASD, Vietnam |

External research experience

- | | |
|-----------------|--|
| 05/2011–06/2011 | Institute of Pharmacology, Århus University, Denmark |
| 09/2008–11/2008 | Hanoi University of Science / CETASD, Vietnam |

Languages

German:	Native
English:	Fluent
Latin:	Latin proficiency certificate

Scientific publications

1. Katja Vahl, Heike Kahlert, Dominique Böttcher, Rainer Wardenga, Šeojka Komorsky-Lovrić, Uwe Bornscheuer, Fritz Scholz, A potential high-throughput method for the determination of lipase activity by potentiometric flow injection titrations, *Anal. Chim. Acta* 610 (2008) 44–49.
2. Katja Vahl, Heike Kahlert, Fritz Scholz, Rapid automatic determination of calcium and magnesium in aqueous solutions by FIA using potentiometric detection, *Electroanalysis* 22 (2010) 2172–2178.
3. Katja Vahl, Heike Kahlert, Lisandro von Mühlen, Anja Albrecht, Gabriele Meyer, Jürgen Behnert, Determination of the titratable acidity and the pH of wine based on potentiometric Flow-Injection-Analysis, *Talanta* 111 (2013) 134–139.

Acknowledgement

First of all, I would like to thank Prof. Dr. Fritz Scholz for giving me the opportunity to work on most interesting projects in his group. I greatly appreciate his supervision and his continuous interest on the progress of this thesis including the several stimulating discussions.

I also would like to thank PD Dr. Heike Kahlert for having always an open ear for the problems occurred throughout my entire Ph.D. studies. I am very grateful to all her advices and discussions, which have strongly contributed to the success of this thesis.

I am obliged to Dr. Ulrich Hasse for his assistance with the AFM measurements and his helpful suggestions.

Moreover, I sincerely like to thank all members of the group of Analytical and Environmental Chemistry for the very pleasant working atmosphere. I am particularly thankful to Anja Albrecht and Gabriele Meyer for their experimental help and for sharing many nice moments with me, in and outside the laboratory.

I also would like to thank all co-operation partners for every kind of assistance. I am very grateful to the GILUPI GmbH and its staff members for giving me the opportunity to work together on the FSMW, for the performance of the cytotoxicity tests and for the financial support. I also thank Prof. Dr. Robert Jack and Dr. Bich Thu Tran from the Institute of Immunology and Transfusion Medicine, Greifswald University, for the gold implantation into mice. Furthermore, I am very thankful to Prof. Dr. Agnete Larsen from the Århus University, Denmark, and to Prof. Dr. Pham Hung Viet from the Hanoi University of Science / CETASD, Vietnam, for their kind hospitality and their support in and outside the laboratory as well as for the many chemical and personal experiences I could gain during my research stays in their groups.

I am very grateful to the Alfried-Krupp-Wissenschaftskolleg Greifswald for the financial support by a fellowship including a research stay at the Århus University, Denmark, and for giving me the opportunity to join the interdisciplinary graduate school „Studies of the interaction of free oxygen radicals with molecules at electrodes and applications to biochemical and medical systems”.

I strongly appreciate the financial support by the DAAD enabling me a two-month research stay at the Hanoi University of Science / CETASD, Vietnam.

With all my heart, I would like to thank my parents for their inexhaustible support in every respect.

Last but not least, I particularly thank Martin for his unconditional support, his boundless patience and his words of encouragement during all phases of this thesis.